University of Nevada, Reno

Investigation of Atmospheric Mercury Concentrations and Dry Deposition Rates Using Established and Novel Methods

A dissertation submitted in partial fulfillment of the
requirements for the degree of Doctor of Philosophy in
Environmental Science and Health

by

Seth Neeley Lyman

Dr. Mae Sexauer Gustin/Dissertation Advisor

August, 2009

University of Nevada, Reno
Statewide • Worldwide

THE GRADUATE SCHOOL

We recommend that the dissertation
prepared under our supervision by

SETH NEELEY LYMAN

entitled

Investigation of Atmospheric Mercury Concentrations and Dry Deposition Rates Using Established and Novel Methods

be accepted in partial fulfillment of the
requirements for the degree of

DOCTOR OF PHILOSOPHY

Mae Sexauer Gustin, Ph.D, Advisor

Alan W. Gertler, Ph.D, Committee Member

Glenn C. Miller, Ph.D, Committee Member

Eric M. Prestbo, Ph.D, Committee Member

W. Patrick Arnott, Ph.D, Graduate School Representative

Marsha H. Read, Ph. D., Associate Dean, Graduate School

August, 2009

Abstract

This work presents new methods for and measurements of concentrations and dry deposition of atmospheric mercury. Chapter 2 reports on measurements of gaseous elemental mercury (GEM), gaseous oxidized mercury (GOM), and mercury bound to particles (PBM), mercury soil flux, and mercury in precipitation at two locations in northern Nevada, U.S.A. Concentrations of GEM were influenced by both local substrate emission and transport from regional source areas. Concentrations of GOM and PBM were within ranges reported for other rural sites, and mercury wet deposition rates were similar to other sites in the arid West. In Chapter 3, multiple methods were used simultaneously at the same sites to estimate dry deposition of atmospheric mercury. The ratio of dry to wet deposition was between 10 and 90%, and varied with season and with the methods used for dry deposition approximations.

Chapter 4 reports on two years of measurements of atmospheric mercury fractions in Reno, Nevada. Concentrations of GEM and PBM were influenced by emission from local sources and meteorological conditions. Concentrations of GOM were higher during periods with higher temperature and lower dew point, confirming the findings of others that warm, dry air from the free troposphere is a source of GOM to the surface. Chapter 5 details work focused on development of a surrogate surface for estimating GOM dry deposition. Deposition of mercury to surfaces was well correlated with GOM concentrations ($r^2 = 0.84$, $p < 0.01$, $n = 326$) and was not significantly influenced by temperature, humidity, or ozone concentrations. The surrogate surface is not able to mimic natural surface variability, but it is useful to measure the maximum potential for

and spatial and temporal trends of GOM dry deposition. Chapter 6 reports on the development of a passive sampler for characterizing GOM concentrations. Uptake of Hg by the passive sampler was correlated with measured air GOM concentration ($r^2 = 0.89$, $p < 0.01$, $n = 22$), and did not appear to be significantly affected by changes in temperature, humidity, or ozone concentration, but sampler performance did appear to be slightly dependent on wind speed. The detection limit for a 14 day sample was ~5 pg m^{-3}.

TABLE OF CONTENTS

LIST OF TABLES

LIST OF FIGURES

Chapter 1: Introduction

Mercury is ubiquitous in all compartments of the environment (c.f. Watras and Huckabee, 1994), but most toxic exposure of humans and wildlife to mercury is through consumption of methylmercury in fish (Myers et al., 2000; Mergler et al., 2007). Mercury in water is typically present at concentrations below the threshold for direct toxicity (Ullrich et al., 2001; WHO, 2005), and water consumption is usually a minor contributor to the total mercury burden of humans (WHO, 2005). However, bacteria, especially sulfate-reducing bacteria in wetlands and submerged sediments, can methylate inorganic mercury (Gilmour et al., 1992; Morel et al., 1998; Grigal, 2002), increasing its toxicity and bioavailability and allowing it to biomagnify in aquatic food chains (Morel et al., 1998).

Many of the biochemical mechanisms of methylmercury toxicity are poorly understood, but symptoms of poisoning include numbness, loss of motor skills and sensory perception, and death (from nervous system failure; Clarkson and Magos, 2006). Fetuses and children are thought to be especially susceptible to permanent neurological damage from methylmercury exposure, and a number of studies show an association between methylmercury loadings from fish consumption by pregnant mothers and young children and adverse health outcomes (Mergler et al., 2007), though contradictory data exist (e.g. Myers et al., 2003).

Methylmercury production in aquatic systems depends on environmental and chemical characteristics of the system and on input of inorganic mercury to the system (Ullrich et al., 2001). What is more, since deposition of mercury from the atmosphere

comprises a major source of inorganic mercury to aquatic systems (Fitzgerald et al., 1998), knowledge of mercury dynamics in the atmosphere, not just knowledge of aquatic cycling and chemistry, is important and necessary to mitigate mercury contamination problems in aquatic systems. Moreover, atmospheric deposition rates and processes for mercury are species-dependent (Schroeder and Munthe, 1998), so understanding the speciation and chemistry of mercury in the atmosphere is as critical as understanding deposition processes.

Mercury in the Atmosphere. Mercury exists in the atmosphere as gaseous elemental mercury (GEM), as particle-bound mercury (PBM), and as gaseous oxidized mercury compounds (GOM; Schroeder and Munthe, 1998). Elemental mercury has a relatively high vapor pressure (0.18 Pa at 20°C) and is only slightly soluble (Henry's Law Coefficient of 729 Pa m^3 mol^{-1} at 20°C, Schroeder and Munthe, 1998). The average global atmospheric lifetime of GEM is thought to be between six months and two years (Lin and Pehkonen, 1999), though some speculate that it may be lower (Gustin et al., 2008).

Particle-bound mercury has been shown to consist both of elemental mercury and oxidized mercury compounds (Feng et al., 2004). The lifetime of PBM in the atmosphere depends on particle size (Zhang et al., 2001), though few measurements of the size distribution of PBM have been made. One study in urban Detroit showed that PBM existed primarily in the fine mode (0.68 μm average fine mode diameter; Keeler et al., 1995).

The chemical species that make up GOM are not known, since the technology to measure individual GOM compounds in the ambient atmosphere doesn't yet exist.

Gaseous oxidized mercury has been hypothesized to consist of compounds such as $HgCl_2$, $HgBr_2$, HgO, $Hg(OH)_2$, and/or HgBrOH (Lindberg and Stratton, 1998; Lin and Pehkonen, 1999; Holmes et al., 2006). Among these compounds, $HgCl_2$ and HgO are the best characterized, and both are semivolatile (vapor pressures of 8.99×10^{-3} Pa for $HgCl_2$ at 20°C and between 2.53×10^{-6} and 9.20×10^{-12} Pa for HgO; Lin et al., 2006) and water soluble (Henry's law coefficients of 3.69×10^{-5} and 3.76×10^{-11} Pa m^3 mol^{-1} for $HgCl_2$ and HgO at 20°C and 25°C, respectively; Schroeder and Munthe, 1998). Because of these properties, GOM has a short atmospheric lifetime (about 2 weeks; Selin et al., 2007).

Sources of Atmospheric Mercury. Mercury is emitted to the atmosphere from natural and anthropogenic sources. It is often assumed that natural emissions of mercury are mostly GEM (Schroeder and Munthe, 1998), but emission of dimethyl mercury from oceans has been reported (Kirk et al., 2008), as has emission of GOM from soils (Engle et al., 2005). Active volcanic and geothermal activity are important sources of mercury to the atmosphere (Gustin, 2003; Nriagu and Becker, 2003; Engle et al., 2006), and mercury is also emitted from geologically mercury-enriched soils (Gustin, 2003). Unenriched soils (Ericksen et al., 2006; Gustin et al., 2006), vegetation (Lindberg et al., 1998), oceans (Fitzgerald et al., 1984; Gardfeldt et al., 2003) and fresh water (Schroeder et al., 1992; Vette et al., 2002) can emit mercury to the atmosphere, but each of these environmental compartments can take up mercury also (Gustin et al., 2006; Ericksen et al., 2003; Mason and Sheu, 2002; Vette et al., 2002). Indeed, a significant component of mercury emitted from natural surfaces is thought to be re-emission of previously deposited mercury (Lin et al., 2006). The net mercury flux direction for many unenriched natural surfaces is unclear, since emission and deposition processes happen

simultaneously and can be extremely dynamic, making generalization difficult (Vette et al., 2002; Gustin et al., 2006). Vegetation as a whole appears to be a net mercury sink, not a source (Gustin et al., 2008), but wildfires have been shown to release sequestered plant mercury back into the atmosphere (Friedli et al., 2003; Turetsky et al., 2006).

Burning of fossil fuels, especially coal, releases mercury that was sequestered by vegetation in the ancient past (Joensuu, 1971), and coal-fired power plants are the world's largest anthropogenic source of mercury to the atmosphere (Pacyna et al., 2006). Other major anthropogenic mercury sources include cement production, waste incineration, mining and metals processing, and various industrial processes (Schroeder and Munthe, 1998; Pacyna et al., 2006). Many anthropogenic sources release GEM, PBM, and GOM. Significant fractions of emissions from coal-fired power plants, ore processing, waste incineration, and cement production are known to be GOM (Pacyna and Pacyna, 2002; Nevada, 2007; Pacyna et al, 2001; Carpi, 1997). Overall, emissions of mercury to the atmosphere are estimated to be between 6600 and 7000 Mg yr^{-1}, and between 36 and 57% are primary emissions from anthropogenic sources (Lindberg et al., 2007)

Atmospheric Mercury Transformations. The chemical and physical transformations of mercury in the atmosphere are somewhat poorly understood. Gaseous elemental mercury can be oxidized to GOM, but the oxidizing compounds involved and the reaction products are not known definitively. Reactions with ozone (Pal and Ariya, 2004a), OH radical (Pal and Ariya 2004b), nitrate radical, hydrogen peroxide (Lin and Pehkonen, 1999), and halogen radicals (Lindberg et al., 2002; Hedgecock and Pirrone, 2004; Holmes et al., 2009) have been proposed and/or investigated. Measurements show that

the upper atmosphere can have high GOM concentrations (Swartzendruber et al., 2006; Sillman et al., 2007), and halogen radicals and OH radical have both been implicated as potential oxidizers of GEM there (Sillman et al., 2007; Holmes et al., 2006). Gaseous oxidized mercury is thought to build up in the upper atmosphere because of the relative paucity of removal processes there (Selin et al., 2007; Sillman et al., 2007). Since different oxidants of GEM are likely to produce different GOM compounds (Lin and Pehkonen, 1999), definitive answers about GOM production pathways may prove elusive until a method to measure individual GOM species in the atmosphere is developed.

Some evidence suggests that GOM may be reduced to GEM in power plant plumes (Edgerton et al., 2006), and SO_2 is hypothesized to be the reducing agent (Lohman et al., 2006). Reduction of oxidized mercury also occurs within cloud droplets, with various mechanisms proposed (Lin et al., 2006), and GOM taken up by cloud water may quickly be converted to (less soluble) GEM and released back into the gas phase (Sillman et al., 2007). Like other semivolatiles, GOM can partition dynamically to and from the particle phase (Rutter and Schauer, 2007). Gas-particle partitioning depends on the available surface area of particulate matter, the vapor pressure of the compound of interest, and the ambient temperature (Finlayson-Pitts and Pitts, 1999).

Methods to Measure Atmospheric Mercury. While several methods exist to measure mercury fractions in the atmosphere (Ebinghaus et al., 1999; Munthe et al., 2001), the Tekran 2537A/1130/1135 system is the most widely used. In this system, ambient air passes through an elutriator and particle impactor to remove large particles, then passes through a KCl-coated quartz annular denuder, which collects GOM compounds but allows fine particles and GEM to pass through (Landis et al., 2002). After removal of

GOM by the denuder, the airstream passes through a particulate filter assembly to remove fine PBM. Next the airstream (which now contains only GEM) is pulled into a mercury analyzer, where mercury is collected on dual traps containing gold beads. At regular intervals the traps are heated to volatilize captured mercury, which is then passed into an analytical cell and analyzed by cold vapor atomic fluorescence spectrometry. The system alternates between this sampling mode and a desorption mode, wherein the denuder and particulate filter assembly are flushed with mercury-free air and heated sequentially to thermally desorb the mercury they contain, and the desorbed mercury is pulled into the analyzer to quantify GOM and PBM.

Some custom-built atmospheric mercury measurement systems exist, but most are methodologically similar to the Tekran system (Ebinghaus et al., 1999; Munthe et al., 2001). An automated atomic absorption spectrometer (manufactured by Ohio Lumex Co.) has been used to measure total mercury in ambient air (Kim et al., 2006), but the detection limit is too high for atmospheric mercury measurements in air unimpacted by sources, and the system doesn't differentiate between GEM and GOM (http://www.ohiolumex.com). Alternative methods for GOM measurement include collection on cation-exchange membranes (Ebinghaus et al., 1999) and KCl-coated quartz fiber filters (Rutter et al., 2008), though neither of these methods is widely used.

Concentrations of GEM or total gaseous mercury (TGM; GEM + GOM) measured by the Tekran system in Northern Hemispheric air that is not impacted by local sources range from 1.32 to 2.35 ng m^{-3}, fine mode PBM concentrations in unimpacted air range from 0 to 42 pg m^{-3}, and GOM concentrations in unimpacted air range from 2 to 24 pg m^{-3} (Valente et al., 2007).

Atmospheric Deposition of Mercury. Multiple deposition pathways exist for GEM, GOM, and PBM. All three fractions may be taken up by cloud or rainwater and removed from the atmosphere as a component of rainfall. Though GEM is only slightly soluble, aqueous oxidation pathways exist by which it may be converted to a more soluble form after dissolution in cloud water (Lin and Pehkonen, 1999). Since GOM is extremely soluble, it is expected to be easily removed by clouds or rain (Bullock, 2000; Seigneur et al., 2004). Particulate matter is also efficiently scrubbed from the atmosphere by rainfall, and PBM has been shown to be a major component of mercury in rainwater (Mason et al., 1997). Deposition of mercury in precipitation (wet deposition) is measured by collecting precipitation in trace-cleaned containers and analyzing it for mercury content (Vermette et al., 1995), and wet deposition of mercury is measured at more than 100 sites throughout North America by the National Atmospheric Deposition Program's Mercury Deposition Network (MDN; http://nadp.sws.uiuc.edu/mdn/). Low-volume rain events or the first part of rain events tend to have the highest mercury concentrations in rainwater (Glass et al., 1991), and mercury in rainfall can originate from local or regional anthropogenic sources (Keeler et al., 2006) or from oxidation of GEM from the global mercury pool (Selin and Jacob, 2008). About 10% of oxidized mercury in wet deposition may be rapidly reemitted to the atmosphere after reaching the surface (Hintelmann et al., 2002; Ericksen et al., 2005).

In addition to wet removal, GEM, GOM, and PBM may be taken up by surfaces via dry chemical and physical processes (i.e. dry deposition). Gaseous elemental mercury undergoes dynamic two-way exchange with many surfaces. For soils, the direction and magnitude of this exchange depends on soil mercury concentration, solar

radiation, temperature, atmospheric turbulence, soil moisture, and precipitation (Carpi and Lindberg, 1998; Engle et al., 2001; Gustin, 2003; Gustin et al., 2003; Gustin and Stamenkovic, 2005; Lindberg et al., 1999). Uptake of GEM by vegetation is traditionally thought to occur primarily via the stomatal pathway, but research has shown that GEM may also be taken up by leaf cuticular surfaces (Stamenkovic and Gustin, 2009). Some modeling studies have neglected GEM surface exchange (Lin et al., 2006), but even if the net GEM flux to or from vegetation and soils is small, it may prove significant at regional and continental scales (Gustin et al., 2006).

As is true for particulate matter in general, mechanisms and rates of PBM dry deposition depend on particle size (Schroeder and Munthe, 1998; Zhang et al., 2001). Large particles deposit relatively quickly because they are strongly influenced by gravitational settling, and ultrafine particles can deposit quickly because they are small enough to be efficiently transported by Brownian diffusion (Seinfeld and Pandis, 1998). Particles of 0.1-1 μm in size, in contrast, are thought to have relatively low deposition velocities because they are not strongly influenced by either forcing mechanism (Seinfeld and Pandis, 1998). Unfortunately, research on PBM size distribution is sparse. In urban settings PBM may exist primarily in the fine mode (Keeler et al., 1995), and some research points to coarse sea salt aerosols as reservoirs for oxidized mercury formed in marine air (Engle et al., 2008; Holmes et al., 2009). Direct measurements of PBM dry deposition are even rarer, with only one study to date (Poissant et al., 2004).

Because GOM is soluble and reactive, it is expected to deposit rapidly and irreversibly, though measurements of GOM emissions have been reported (Engle et al., 2005; Skov et al., 2006). Also, dry deposition of soluble and reactive gases is expected to

depend mostly on the turbulent transfer rate of the atmosphere and not (primarily) on the chemical properties of the surface to which the gas deposits (Wesely, 1989). Only a few direct measurements of GOM dry deposition have been published (Lindberg and Stratton, 1998; Poissant et al., 2004; Skov et al., 2006), and these measurements utilized either Modified Bowen Ratio or Relaxed Eddy Accumulation methodology, both of which require precise measurement of the difference between GOM concentrations in two separate but nearby air streams. The precision of GOM measurements is relatively weak (relative percent difference between replicate denuders is about 15%; Landis et al., 2002), calling into question the statistical significance of the unreplicated GOM gradients reported (see Duyzer et al. (1992) for more discussion of this problem).

In the absence of reliable data, modelers use dry deposition modules or values that are largely unverified by measurements, often substituting parameterizations developed for nitric acid deposition (Seigneur et al., 2004; Lin et al., 2006). Surrogate surface measurements of GOM and PBM may help bridge this knowledge gap and have been used (Sakata and Marumoto, 2005; Caldwell et al., 2006; Marsik et al., 2007), but surrogate surfaces have limitations, even for fast-depositing compounds, and surrogate surface measurements should be considered cautiously (Wesely and Hicks, 2000).

This Work. In this work, new methods to measure atmospheric mercury concentrations and deposition were developed and used along with established methods, providing tools for future studies and contributing to the body of knowledge of atmospheric mercury dynamics.

Chapter 2 describes measurements of atmospheric mercury that were collected at two rural sites in northern Nevada, where a variety of anthropogenic and natural sources

of atmospheric mercury exist. Trends among atmospheric mercury species, mercury soil flux, mercury concentrations in rain water, and meteorological parameters were analyzed to elucidate mechanisms that controlled observed mercury concentrations.

Chapter 3 details the use of a variety of measurement and modeling tools, including soil flux measurements, cation-exchange membrane surrogate surfaces, leaf surfaces, and resistance-scheme models, to estimate mercury dry deposition at three sites in northern Nevada. Dry deposition estimates were compared to wet deposition measurements to understand the relative contributions of wet and dry deposition and to estimate total mercury loading to northern Nevada ecosystems.

Chapter 4 reports on two years of atmospheric mercury measurements in Reno, Nevada and on multiple regression analyses and other statistical tools that were applied to determine sources and controlling factors for mercury in the Reno airshed.

Chapter 5 describes work to further develop the surrogate surface method utilized in Chapter 3, including determination of optimal deployment methods and characterization of its performance in a variety of environmental and chemical conditions. Surrogate surfaces were deployed at four field sites in locations throughout the United States in long term (3 months to 1 year) campaigns and were deployed in a laboratory chamber where temperature, humidity, ozone concentrations, and gaseous mercury concentrations were manipulated.

In Chapter 6, a passive concentration sampler was developed for GOM. The sampler was deployed at several sites throughout the United States and in a laboratory chamber where meteorological and chemical conditions were manipulated. Optimal

sampling techniques were determined and the overall performance of the sampler was assessed.

Chapter 7 summarizes major findings and places this research in a broader scientific context.

Chapter 2: Speciation of Atmospheric Mercury at Two Sites in Northern Nevada, U.S.A.

Seth N. Lyman* and Mae Sexauer Gustin*

*University of Nevada, Reno, Department of Natural Resources and Environmental Science/MS 370, Reno, Nevada, 89557

(Published in *Atmospheric Environment*, 2008, vol. 42, pp. 927-939*)*

Abstract. Gaseous elemental mercury (GEM), reactive gaseous mercury (GOM), and mercury bound to particles (PBM) were measured during seasonal one- or two-week data collection campaigns at two Mercury Deposition Network sites (NV02 and NV99) in northern Nevada, U.S.A. The sites are rural but are located in an area of diverse natural and anthropogenic mercury sources that include undisturbed and mining-disturbed enriched substrates, coal-fired power plants, ore processing facilities, and industrial facilities. Concentrations of GEM averaged over all campaigns were 3.0 ± 1.7 ng m^{-3} at NV02 and 2.5 ± 3.1 ng m^{-3} at NV99, higher than has been reported for other rural sites. GEM concentrations at the sites were found to be influenced by both local substrate emission and transport from regional source areas. Concentrations of GOM and PBM were within ranges reported for other rural sites (13 ± 18 pg m^{-3} and 9 ± 7 pg m^{-3} at NV02, 7 ± 8 pg m^{-3} and 13 ± 12 pg m^{-3} at NV99, respectively). Mercury wet deposition rates measured over three years (2003-2005) were similar to other sites in the arid West (3.0 ± 0.7 µg m^{-2} yr^{-1} at NV02, 3.9 ± 0.4 µg m^{-2} yr^{-1} at NV99).

Introduction

Mercury exists in the atmosphere as three major forms: gaseous elemental mercury (GEM), reactive gaseous mercury (GOM), and particle-bound mercury (PBM) (Shroeder and Munthe, 1998). Measurement of air mercury speciation is necessary to understand the overall transport and fate of atmospheric mercury, and speciated mercury concentrations have been measured in a variety of settings (e.g. Temme et al., 2003; Weiss-Penzias et al. 2003; Lynam et al., 2005; Poissant et al., 2005; Caldwell et al., 2006; Hall et al., 2006; Liu et al., 2007; Valente et al., 2007).

A number of measurements of total gaseous mercury (TGM) have been made in Nevada, U.S.A. (e.g. Gustin et al., 1996; Nacht et al., 2004; Ericksen et al., 2005; Stamenkovic et al., 2007), and average concentrations ranged from 1.3 to 2.5 ng m^{-3} for sites remote from sources (note that these measurements were made at different heights). Speciated mercury measurements for rural sites in the inland western United States have been reported by Hall et al. (2006), who collected data at Yellowstone National Park for 10 days in summer 2003 (GEM range: 0.7 to 2.5 ng m^{-3}; GOM range: <d.l. to 5 pg m^{-3}; PBM range: <d.l. to 30 pg m^{-3}), and Caldwell et al. (2006), who made limited measurements in southern New Mexico in 2001-2002 (GEM range: 1.1 to 2.3 ng m^{-3}; GOM range: 2 to 25 pg m^{-3}; PBM range: 1 to 7 pg m^{-3}). Additionally, Engle et al. (2006) measured GOM concentrations as high as 261 pg m^{-3} at geothermal areas in Yellowstone National Park.

This paper reports on concentrations of GEM, GOM, and PBM collected in northern Nevada, U.S.A. Northern Nevada contains a variety of mercury sources, including undisturbed and mining-disturbed enriched substrates, extensive geothermal activity, a

coal-fired power plant, and gold ore processing facilities (Figure 2-1). Among these potential sources, naturally enriched substrates occur primarily in zones of hydrothermal alteration, which make up about 7% of the surface area of Nevada (Zehner and Gustin, 2002). Zehner and Gustin (2002) estimated an area average mercury flux for Nevada (enriched and unenriched areas) to be 4.2 ± 1.4 ng m^{-2} hr^{-1} (mean ± standard deviation), or about 10 000 kg yr^{-1}, though in a subsequent paper Gustin et al. (2008) reduced that estimate to 3600 kg yr^{-1} based on evidence that the flux applied to unenriched soils was too high (a value of 3.5 ng m^{-2} hr^{-1} was used by Zehner and Gustin for unenriched soils and was revised to 0.5 ng m^{-2} hr^{-1} by Gustin et al.). Engle et al. (2001) measured soil fluxes at the Ivanhoe Mining District in Nevada, an area of mercury enrichment and historical mercury mining, and calculated an average flux of 17.1 ng m^{-2} hr^{-1}, or 87 kg yr^{-1} for the 586 km^2 area. The average flux from the open pit of one historic mercury mine in the district was 27 600 ng m^{-2} hr^{-1}. Mercury emissions have been estimated for other mercury-enriched areas in the region, including but not limited to Flowery Peak, Nevada (37 kg yr^{-1} from a 251 km^2 area), and Peavine Peak, Nevada (10 kg yr^{-1} from a 108 km^2 area) (Engle and Gustin, 2002).

Active geothermal areas are often enriched in mercury and may also be sites of atmospheric mercury emission (Varekamp and Buseck, 1986, Engle et al., 2006). Mercury emissions from geothermal areas in northern Nevada and the surrounding region were measured by Coolbaugh et al. (2002) at the Steamboat Springs geothermal area near Reno, Nevada (estimate of 12 kg yr^{-1} from an 8 km^2 area), Engle et al. (2006) at the Dixie Valley geothermal area in Nevada (estimate of 0.3-0.4 kg yr^{-1} from an 84 km^2 area), and

Engle and Gustin (2002) at the Long Valley Caldera in California (estimate of 110 kg yr^{-1} from the 946 km^2 area).

Mercury emitted from enriched substrates is mostly GEM (Gustin, 2002), and emissions tend to increase with increasing temperature, sunlight, atmospheric turbulence, soil moisture, and substrate mercury concentration (Carpi and Lindberg, 1998; Engle et al., 2001; Gustin, 2002; Gustin et al., 2003; Gustin and Stamenkovic, 2005). Wetting of dry soils tends to significantly enhance mercury emission (Lindberg et al., 1999; Gillis and Miller, 2000; Engle et al, 2001; Gustin and Stamenkovic, 2005).

Anthropogenic mercury sources also exist in the region, including coal-fired power plants, mining operations, waste storage facilities, and various industrial sources (Figure 2-1). Notable among these are sixteen gold mining facilities in northern and central Nevada, which reported total fugitive air emissions of 38 kg (includes emissions from equipment leaks, evaporative losses, and losses from ventilation systems) and total point source air emissions of 2086 kg for year 2005 (U.S. Environmental Protection Agency (EPA) Toxics Release Inventory, http://www.epa.gov/triexplorer/). A 2006 study of gold ore processing facilities (Nevada, 2007) showed that emitted mercury is 72 ± 30% GEM, 27 ± 29% GOM, and 1 ± 2% PBM, with significant variability among processing units and facilities tested. Mine tailings and waste rock constitute another source of mercury to the atmosphere, and it is hypothesized that emission from these sources would be controlled by the same factors as other enriched substrates.

Additionally, Valmy Generating Station, a 530 MW coal-fired power plant, is located about 80 km southeast of Mercury Deposition Network (MDN) site NV02 (Figure 2-1). According to the EPA Toxics Release Inventory, Valmy Generating Station

released 5 kg of mercury into the atmosphere in 2005. Mercury emissions from coal-fired power plant exhaust streams have been reported to be 20-75% GEM, 25-80% GOM, and 2-10% PBM, and speciation depends on the type of coal used, combustion characteristics, and control technologies in place (Chu and Porcella, 1995; Carpi, 1997; Senior et al., 2000; Pacyna and Pacyna, 2002; Edgerton et al., 2006).

This study included short term (one or two weeks) seasonal data collection campaigns conducted in 2005 and 2006 at NV02 and NV99, two National Mercury Deposition Network (MDN) sites (http://nadp.sws.uiuc.edu/mdn) in northern Nevada. Atmospheric mercury species, meteorological parameters, and mercury soil flux were measured during each campaign. Precipitation was collected on a weekly basis throughout the study period at both sites and analyzed for mercury content as part of the MDN network. Trends among atmospheric mercury species, mercury soil flux, mercury wet deposition, and meteorological parameters were analyzed. HYSPLIT, an atmospheric transport model (http://www.arl.noaa.gov/ready/hysplit4.html), was used to further elucidate atmospheric mercury behavior.

Methods

Mercury speciation and meteorological data were collected simultaneously at NV02 and NV99 in spring (29 Mar – 4 Apr), summer (26 Jul – 8 Aug), and fall (22 – 28 Oct) 2005, and at NV02 only in winter (24 – 30 Jan) 2006 due to limitations in availability of sampling equipment. Mercury soil flux was measured during all campaigns except NV02 in spring and was not measured simultaneously at both sites.

Site descriptions. NV02 (41.50°N, 117.50°W, 1388 m) is located at Lesperance Ranch, 70 km north of Winnemucca, Nevada in a broad, rural desert valley surrounded on three sides by mountains. A historical mercury mine and several known mercury occurrences exist in the valley. Soil mercury concentration at NV02 was 56 ± 53 ng g^{-1}. NV99 (41.55°N, 115.21°W, 1806 m) is located at Gibbs Ranch, 80 km northwest of Wells, Nevada in a narrow, remote river valley on the southeast end of the Jarbidge Mountains. Soil mercury concentration at NV99 was 32 ± 13 ng g^{-1}.

Atmospheric mercury speciation. Mercury speciation was measured using the Tekran 2537A/1130/1135 system described by Landis et al. (2002), which sequentially collects GOM on a KCl-coated quartz denuder, PBM (<3 µm) in a regenerable filter assembly, and GEM on gold traps within a Model 2537A Mercury Vapor Analyzer. The Model 2537A flow rate was 1 L min^{-1}, and the total flow through the denuder and particulate filter assembly was 7 L min^{-1}. At this flow rate, the particle impactor on the system inlet had a cut point of 3.0 µm. The sampling time was 5 min for GEM and 2 hr for GOM and PBM. Fresh denuders and clean particulate filters were installed at the beginning of each sampling campaign. Sample train glassware and tubing were trace-metal cleaned as needed. The Model 2537A was calibrated every 24 hr using its internal permeation source. Sampling heights were 3 m and 1.5 m at NV02 and NV99, respectively, during the spring, summer, and fall campaigns, and was 1.5 m at NV02 during the winter campaign.

At the beginning and end of each field campaign, standard additions were performed to check instrument calibration and gold trap efficiency by injecting a known amount of GEM into ambient air being sampled by the 2537A. Also at the beginning and

end of each field campaign, all 2537A analyzers were set to sample the same air for several days to determine inter-system precision. These precision checks included the 2537A analyzer used to measure mercury soil flux, and this analyzer was also used to monitor inter-system precision for short periods (2-4 hr) in the field. Additionally, inter-system precision checks of complete 2537A/1130/1135 speciation systems were performed before and after the fall and winter campaigns. Relative instrument drift during campaigns was assessed based on these tests, and data were adjusted using the percent change. Relative percent difference for TGM was 7.0 ± 5.3% (n = 19 comparative periods) and relative percent differences for GOM and PBM in fall were 7.2 ± 37.7% and 41.4 ± 62.1% , respectively (2 hr samples, n = 19). Measured GOM and PBM concentrations were both consistently 0 pg m^{-3} during the winter comparative tests.

Blanks for the 2537A were measured during each internal calibration cycle and were consistently 0 ng m^{-3}, regardless of season, preventing the calculation of a detection limit. The manufacturer's reported detection limit for 5 minute samples measured with the 2537A is <0.1 ng m^{-3} (http://www.tekran.com/). During the summer campaign, the detection limit for GOM and PBM, calculated as 3 times the standard deviation of the 1130/1135 system blank, was 5 pg m^{-3}. During other campaigns system blank measurements were consistently 0 pg m^{-3} and detection limits could not be calculated. Thus, the level of quantitation for the instruments varied with season. Detection limits for similar speciation systems were reported by Hall et al. (2006) and Weiss-Penzias et al. (2003) as 0.88 and 1.6 pg m^{-3}, respectively.

Dynamic flux chambers. Field measurements of TGM soil flux were made with a cylindrical polycarbonate chamber of 10 cm radius, 1 L volume, and 1.5 L min^{-1} flow rate

(Engle et al., 2001). Inlet and outlet chamber air concentrations were measured at 10 min intervals with a Tekran Model 2537A and a Model 1110 Synchronized Two Port Sampling System. Flux (F) was calculated in ng m^{-2} hr^{-1} as:

$$F = \Delta C*Q/A,$$

where ΔC is the difference in mercury concentrations in outlet versus inlet air in ng m^{-3}, Q is the flow of air through the chamber in m^3 hr^{-1}, and A is the surface area exposed to the chamber in m^2. Flux chamber blanks were measured before and after field campaigns by placing the chamber on a clean polycarbonate plate during daylight for at least 3 hr. Blank ΔC values were 0.04 ± 0.03 ng m^{-3}. Fluxes were not blank-corrected.

Meteorology. Wind speed and direction (Young Model 05103-5), solar radiation (Li-Cor Model LI200X), and relative humidity and temperature (Vaisala Model HMP45AC) were measured and recorded as 5 min averages using a Campbell Scientific data logger. Weekly total precipitation was measured at NV02 and NV99 as part of the MDN network, and daily area precipitation was assessed using data from the following sites of the RAWS Climate Archive: Sho-Pai, Morey Creek, Antelope Lake, Stag Mountain, and Rock Spring Creek (http://www.raws.dri.edu/index.html).

Soil mercury analysis. At NV02 and NV99, soil samples were collected at the center of the study area (where all atmospheric measurements were made) and at 25 m and 50 m from the center of the study area in the 4 cardinal and 4 ordinal directions (n = 17 per site). Samples were analyzed for total mercury content using a Milestone DMA-80 analyzer (EPA method 7473).

HYSPLIT wind trajectories. The HYSPLIT trajectory model was used to compute 24 hr back-trajectories of air transport to the study sites for each 2 hr mercury speciation

sampling period during field campaigns (n = 410). The Eta Data Assimilation System 40 km (EDAS40) dataset, which is composed of successive 3 hr meteorological forecasts interpolated on a 40 km grid, was used as the model input (http://www.arl.noaa.gov/ss/transport/edas40.html). The start height for trajectories was 500 m, and a subset of trajectories were computed at 100 m and 1000 m start heights for comparison with the 500 m trajectories (n = 52 for each alternative start height).

Trajectories from the 100 m and 1000 m subsets were considered to be similar to the 500 m trajectories (thus confirming that use of a constant 500 m start height is adequate to represent average transport conditions) if the majority of a 100 m or 1000 m trajectory path and the majority of the corresponding 500 m trajectory path fell within the bounds of two rays angled 30° from each other with origin at NV02 or NV99. In cases where the majority of a 500 m trajectory was not bounded by 30 directional degrees, 100 m and 1000 m trajectories were considered similar to corresponding 500 m trajectories if at least 80% of their trajectory paths were within 40 km of the 500 m trajectory path. Of the 100 m and 1000 m trajectories, 90% were found to be similar to the 500 m trajectories.

For purposes of analysis, trajectories were organized geographically by assigning each trajectory to the directional quadrant in which the majority of its path fell (northeast quadrant is 0 to 90 directional degrees with NV02 or NV99 as center, southeast quadrant is 90 to 180 directional degrees, southwest quadrant is 180 to 270 directional degrees, and northwest quadrant is 270 to 360 directional degrees). This quadrant method of trajectory analysis admittedly provides low-resolution results and may ignore smaller scale phenomena. However, mercury sources in this region exist over broad areas, and a

variety of source types often occur within the same area, rendering problematic any detailed analysis of the contributions of each source or source type based on these data. Therefore, a low-resolution analysis of trajectory results that indicated potential source areas rather than specific sources was thought to be most prudent.

Statistical analyses. Data were processed using Intercooled STATA 8.0 and Microsoft Office Excel 2003. Summary statistics were computed using Microsoft Office Excel 2003. Correlation analyses (Pearson product moment) were conducted using NCSS 2004. Correlation analyses were first conducted using data from each seasonal data collection period at each site, then all seasonal datasets were combined for each site and correlation analyses were again performed. HYSPLIT trajectories were processed and analyzed using ArcGIS 9.1.

Results and Discussion

Atmospheric mercury concentrations at NV02 and NV99 exhibited different patterns and variability across seasons and sites. It should be noted that these data comprise limited snapshots in time, and observed trends may not fully represent average conditions. During most seasons average GEM concentrations (Table 2-1) were higher than has been reported for other rural North American sites, but GOM and PBM concentrations were within the range of other rural sites (Valente et al., 2007). Average GEM concentrations were highest in summer at both sites, and average PBM concentrations were highest in spring. Median GOM concentrations were highest at both sites in summer, but average GOM was highest in fall at NV02, where the GOM dataset was dominated by a few large peaks. Large spikes in GEM were often observed at both sites, as were periods of

sustained elevated GEM concentrations (Figure 2-2).

GOM showed more diurnal variability at NV02 relative to NV99 (Figure 2-3). At both sites GOM was correlated with temperature ($r = 0.50$, $p < 0.01$ at NV02; $r = 0.54$, $p < 0.01$ at NV99 for combined datasets) and solar radiation ($r = 0.39$, $p < 0.01$ at NV02; $r = 0.24$, $p < 0.01$ at NV99) and negatively correlated with relative humidity ($r = -0.57$, $p < 0.01$ at NV02; $r = -0.43$, $p < 0.01$ at NV99). GOM concentrations tended to be higher during the afternoon, which could be indicative of production via photooxidation (Liu et al., 2007) or may be due to entrainment of GOM from the upper atmosphere as mixing layer height increases during the day. GOM concentrations are thought to increase with height in the atmosphere (Swartzendruber et al, 2006).

GOM and PBM concentrations were correlated with GEM concentrations at both sites ($r = 0.19$ for GOM, 0.23 for PBM at NV02; $r = 0.43$ for GOM, 0.26 for PBM at NV99; using combined datasets, $p < 0.01$ for all). Atmospheric mercury species composition did not change significantly during periods with elevated GEM concentrations (concentrations >2 standard deviations above the mean). On average at NV02, atmospheric mercury was 99.2 ± 0.7% GEM, 0.5 ± 0.6% GOM, and 0.3 ± 0.4% PBM. For periods with elevated GEM concentrations the composition was not statistically different, with 99.5 ± 0.5% GEM, 0.3 ± 0.6% GOM, and 0.2 ± 0.1% PBM. At NV99, atmospheric mercury was 99.2 ± 0.5% GEM, 0.3 ± 0.2% GOM, and 0.5 ± 0.5% PBM on average, and 99.5 ± 0.2% GEM, 0.2 ± 0.1% GOM, and 0.2 ± 0.1% PBM for periods with elevated GEM concentrations. Concurrent peaks in GEM, GOM, and PBM may indicate simultaneous release of all species from a source or may be due to secondary production of GOM and PBM from GEM.

In summer at both sites, sustained episodes of elevated GEM concentrations corresponded with periods of thunderstorm activity (Figure 2-4). This trend was observed in summer at NV02 in spite of the fact that no precipitation fell at the immediate study site, but only in the surrounding areas. Elevated GEM concentrations during these periods may have been caused by enhanced mercury emission from enriched substrates in the region following rainfall (Lindberg et al., 1999; Gillis and Miller, 2000; Engle et al, 2001). Also, higher relative humidity during periods of thunderstorm activity may have enhanced mercury emission from soils (Figure 2-4). Retention of volatile organic pesticides by dry soils with low organic matter content has been shown to decrease with increasing relative humidity due to the displacement of volatile organics by H_2O on mineral surfaces (Chiou and Shoup, 1985; Goss, 1993), and GEM may behave similarly. Finally, lower atmospheric pressure associated with the thunderstorms may have caused some flow of GEM-enriched interstitial air from the soil into the atmosphere.

Wildfires have been shown to be sources of mercury to the atmosphere in the form of GEM and PBM (Friedli et al., 2003; Engle et al., 2006). Several small (<900 ha), short (<24 hr) fires burned in the region during the first half of the summer field campaign (Western, 2005). However, concentrations of GEM and PBM were not uniquely high during periods when fires burned, and HYSPLIT analysis showed that trajectories which passed through wildfire areas were not consistently associated with higher GEM or PBM concentrations (data not shown). Thus, wildfires are not thought to have contributed significantly to atmospheric mercury concentrations measured at NV02 and NV99.

Soil flux. Mean flux of mercury from soil was always positive when measured at NV02

(Table 2-1). At NV99, however, the mean flux direction was positive during summer but negative during spring and fall (Lyman et al., 2007). At NV99, soil flux and GEM concentrations were positively associated during some seasons. For example, soil was frozen and partly snow-covered during the first three days of the spring campaign at NV99 and mean mercury soil flux was negative, but when temperatures increased rapidly and the soil thawed soil flux and GEM concentrations both increased (Gustin et al., 2006). Also, mercury soil fluxes and GEM concentrations both consistently peaked at midday during the second half of the summer campaign at NV99 (Figure 2-4). Although a similar trend was not observed in fall, this suggests that local substrate emission may influence GEM concentrations at NV99.

In contrast, soil flux at NV02 was inversely correlated with GEM during the summer and fall campaigns ($r = -0.42$, $p < 0.01$ in summer ; $r = -0.43$, $p = 0.10$ in fall), with maximum soil fluxes occurring at midday and maximum GEM concentrations tending to occur around midnight (Figure 2-4). The nighttime increase in GEM concentrations was observed only during the summer and fall campaigns. This trend may have been caused by a buildup of emitted GEM in the shallow nighttime surface layer followed by dissipation during the day when the boundary layer was well mixed. Soil fluxes measured at the study site during summer and fall were low (Table 2-1) and may have been outpaced by much greater emission fluxes from enriched substrates in the area (an abandoned mercury mine is located 18 km from NV02 on the southern end of the same valley). These patterns suggest that local substrate emission may influence GEM concentrations measured at NV02.

HYSPLIT analysis. No consistent relationships between HYSPLIT trajectory path and

concentrations of GOM or PBM were observed at either study site. Higher GEM concentrations, however, did tend to be associated with trajectories that passed over certain regions, and Figure 2-5 shows trajectories categorized by 2 hr average GEM concentration. Some GEM peaks observable in Figure 2-2 appear to correspond with transport over certain regions (e.g. NV02 in winter).

During the spring campaign, air arrived at both sites either from the northwest or southwest quadrants, and GEM concentrations were similar regardless of trajectory direction (Table 2-2; note that mean GEM concentrations in spring were greater at NV99). In summer at NV02 GEM concentrations tended to be high regardless of wind trajectory path. Potential sources of mercury to the atmosphere (historical mercury mines and enriched substrates) exist <20 km from NV02, much closer than the 40 km resolution of the EDAS dataset used to compute HYSPLIT trajectories, and may have confounded results. Also, trajectory paths were more convoluted in summer, making quadrant analysis less useful. In spite of this, trajectories at NV02 that fell within the northwest quadrant corresponded with periods of significantly higher GEM concentrations relative to the remainder of the summer dataset (using an unpaired t-test, $p = 0.01$). About 60 km northwest of NV02 is a region of mercury enrichment with five historical mercury mines which together produced >1 000 000 kg mercury (Rytuba, 2003). Warm conditions with frequent thunderstorms during summer may have favored emissions from enriched substrates in this area. Trajectories that fell within the southeast quadrant during summer at NV02 corresponded with GEM concentrations that were significantly lower than others ($p < 0.01$). Conversely, in fall and winter at NV02 the southeast quadrant corresponded with significantly higher GEM concentrations ($p = 0.01$ for fall, $p < 0.01$

for winter). The southeast quadrant for NV02 contains a variety of mercury sources, including gold mines, a coal-fired power plant, and enriched substrates.

In summer and fall at NV99 trajectories from the southwest quadrant corresponded with significantly higher GEM concentrations ($p = 0.07$ in summer, $p < 0.01$ in fall). The southwest quadrant at NV99 contains the same potential sources of mercury as the southeast quadrant at NV02 (listed above). It is not known why this area appeared not to contribute to atmospheric mercury concentrations observed at NV02 in summer or NV99 in spring, but did appear to have an influence during other seasonal campaigns.

During two periods of the study (8/2-8/3/2005 and 10/23-10/24/2005) 24 hr trajectories were oriented such that the end point of a trajectory at one site corresponded both temporally and geographically with the start point of a trajectory at the other site, making possible an analysis of the change in GEM concentration as the modeled air parcel traveled from one site to the other (Figure 2-6). Trajectory direction was west to east during the first period and east to west during the second, but both periods show that GEM concentrations increased as the air parcel traveled between the sites, implying that the area between the sites is a source of atmospheric mercury.

Wet deposition. Wet deposition of atmospheric mercury has been monitored at NV02 and NV99 since February 2003 as part of the MDN (Table 2-3). In 2003 and 2005 total deposition was 43% and 69% higher, respectively, at NV99 than at NV02 but was slightly lower at NV99 in 2004. Total precipitation was also higher at NV99 in 2003 and 2005 but was similar at both sites in 2004, and the observed differences between the two sites may be largely due to precipitation amount.

Wet deposition at these sites is similar to other MDN sites in the inland western United States. For comparison, the average for other inland western sites is 5.1 ± 1.7 µg m^{-2} yr^{-1} (using available 2003-2005 data from NM10, CO97, CO99, WY08, and MT05). Although concentrations of GEM are higher at NV02 and NV99 relative to other rural sites (Valente et al., 2007), it is possible that the observed elevated GEM concentrations do not have a significant effect on local wet deposition, since GOM and PBM are thought to dominate depositional processes (Bullock, 2000; Seigneur et al., 2004). In a related paper that utilized the dataset from this study, Lyman et al. (2007) reported a likely annual total atmospheric deposition (wet + dry) range at NV02 to be 5.0-13.5 µg m^{-2}.

Log of mercury concentration in precipitation was negatively correlated with log of precipitation amount at both sites (see Figure 2-7; $r = -0.57$, $p < 0.01$ at NV02; $r = -0.40$, $p < 0.01$ at NV99), as has been found in other studies (e.g. Glass et al., 1991; Lamborg et al., 1995; Mason et al., 1997). Studies wherein precipitation was sampled sequentially during rain events have found that mercury concentrations are usually highest at the beginning of an event and then decrease over time as the event continues (e.g. Ferrara et al., 1986; Bloom and Watras, 1989; Glass et al., 1991). This "washout effect" is attributed to scavenging of PBM and gaseous species (especially GOM) (Poissant and Pilote, 1998; Schroeder and Munthe, 1998). Mercury concentration in rainwater is high at NV02 and NV99 (Table 2-3) and at other arid sites (e.g. average from 2003-2005 (excluding dry weeks) for NM10 is 28.2 ± 40.9 ng L^{-1}), which may be because average precipitation amount is low (6.8 ± 7.8 and 9.1 ± 9.3 mm per week (excluding dry weeks) at NV02 and NV99, respectively) and washed-out mercury in collected precipitation is not diluted by continued rainfall.

Summary

Northern Nevada contains a variety of atmospheric mercury sources, and the dynamic behavior of mercury at NV02 and NV99 is the result of complex interactions among local and regional sources and meteorology. While GOM concentrations appeared to depend mostly on meteorological conditions, GEM concentrations at the sites depended both on meteorological influences, which mobilize mercury from local and regional enriched substrates, and on transport from various regional source areas. Enriched substrates in the region appeared to be larger sources of mercury to the sites during warmer months when meteorological conditions would promote emission, and local soil emission appeared to influence GEM concentrations during some seasons at both sites. Also, though GEM concentrations were higher at these sites than is common at other rural sites in North America (Valente et al., 2007), mercury wet deposition was low and similar to other inland western sites.

Acknowledgements

This project was funded by a HATCH grant from the University of Nevada, Reno (UNR) College of Agriculture, Biotechnology and Natural Resources, by the UNR Environmental Sciences and Health Graduate Program, and by EPA STAR Grant 82980001. Equipment was borrowed from Oak Ridge National Laboratory and EPA Region IX Lab. The authors thank the owners and operators of Lesperance Ranch and Gibbs Ranch and Steve Lindberg of Oak Ridge National Laboratory for their support of

this research, Julide Koracin of the Desert Research Institute for help with setup of the HYSPLIT model, and Jelena Stamenkovic of UNR for providing a critical review of the manuscript.

Tables and Figures

Table 2-1. Statistical summary of parameters measured at NV02 and NV99 during seasonal campaigns.

			GEM	GOM	PBM	Hg Soil Flux	Temp-erature	Humid-ity	Solar Rad.	Wind Speed
			ng m^{-3}	pg m^{-3}	pg m^{-3}	ng m^{-2} hr^{-1}	℃	%	W m^{-2}	m s^{-1}
Spring	**NV02**	Mean	1.7	5	16		4.3	56	207	3.3
29 Mar - 4 Apr		Median	1.6	4	14		3.6	54	18	2.7
2005		Max	3.7	25	39		16.8	100	1080	12.2
		St. Dev.	0.3	4	8		5.0	22	302	2.3
	NV99	Mean	2.2	2	27	-0.02	1.8	60	181	1.8
		Median	2.2	1	26	-0.05	0.8	66	2	1.5
		Max	4.4	15	65	2.11	14.9	94	1095	6.4
		St. Dev.	0.6	3	15	0.60	6.6	23	295	1.6
Summer	**NV02**	Mean	3.8	17	9	0.32	23.7	33	304	2.1
26 Jul - 8 Aug		Median	3.5	13	8	0.23	24.6	28	78	1.8
2005		Max	11.2	72	39	2.26	36.1	85	1125	11.0
		St. Dev.	1.5	12	7	0.59	7.3	17	363	1.3
	NV99	Mean	2.9	10	12	0.47	21.2	42	217	1.2
		Median	2.2	9	11	0.29	20.8	35	19	0.9
		Max	106.0	74	49	5.50	35.5	95	1287	7.8
		St. Dev.	4.2	8	7	0.77	7.8	25	336	1.1
Fall	**NV02**	Mean	2.5	24	5	0.15	10.7	56	128	1.7
22 - 28 Oct		Median	2.2	12	4	0.10	9.1	54	0	1.4
2005		Max	16.0	150	16	1.69	25.9	100	732	8.1
		St. Dev.	1.6	30	3	0.43	6.9	25	210	1.3
	NV99	Mean	2.0	4	3	-0.22	8.3	56	85	1.0
		Median	1.7	3	1	-0.25	6.1	59	0	0.5
		Max	5.3	14	19	1.03	22.9	94	757	4.7
		St. Dev.	0.8	4	4	0.33	7.2	25	176	1.1
Winter	**NV02**	Mean	2.8	2	4	0.11	1.7	79	78	1.9
24 - 30 Jan		Median	1.7	0	1	0.10	1.5	83	0	1.3
2006		Max	10.7	42	23	1.31	12.8	98	691	9.4
		St. Dev.	2.1	7	6	0.20	3.6	15	144	1.7

Table 2-2. Mean concentrations of GEM for 2 hr sampling periods corresponding with HYSPLIT air back trajectories that fell within different quadrants. A trajectory was assigned to the northeast quadrant if the majority of its path fell between 0 and 90 directional degrees (with NV02 or NV99 as center), to the southeast quadrant if its path fell between 90 to 180 directional degrees, etc. N.D. indicates that < 3 trajectories fell within the specified quadrant.

	($ng\ m^{-3}$)	**Northeast**	**Southeast**	**Southwest**	**Northwest**
Spring	**NV02**	N.D.	N.D.	1.7 ± 0.3	1.7 ± 0.1
	NV99	N.D.	N.D.	2.3 ± 0.6	2.3 ± 0.2
Summer	**NV02**	3.4 ± 1.1	3.0 ± 0.6	3.8 ± 1.7	4.3 ± 1.5
	NV99	1.8 ± 0.3	2.4 ± 1.5	4.2 ± 4.0	2.3 ± 0.7
Fall	**NV02**	2.5 ± 0.4	3.2 ± 1.8	1.8 ± 0.4	N.D.
	NV99	1.8 ± 0.2	1.5 ± 0.3	2.5 ± 0.9	N.D.
Winter	**NV02**	N.D.	6.4 ± 1.4	2.2 ± 1.5	N.D.

Table 2-3. Annual precipitation, annual mercury wet deposition, and average mercury concentration in precipitation (excluding dry weeks) at NV02 and NV99.

		Total Precip.	Average Conc.	Total Deposition
		cm	ng L^{-1}	µg m^{-2}
2003	**NV02**	13.7	55.2 ± 90.1	3.0
	NV99	24.4	24.2 ± 27.2	4.3
2004	**NV02**	21.6	28.9 ± 41.2	3.7
	NV99	21.8	22.4 ± 31.5	3.5
2005	**NV02**	23.4	25.6 ± 62.9	2.3
	NV99	28.7	22.6 ± 37.5	3.9

Figure 2-1. MDN sites NV02 and NV99 and regional mercury sources. Industrial sources, coal-fired power plants, waste disposal facilities, gold mines, and other mining facilities were taken from the 2005 EPA Toxics Release Inventory.

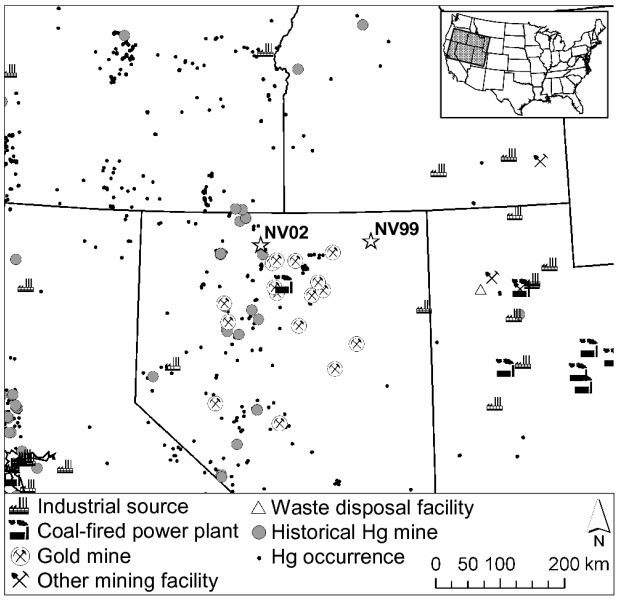

Figure 2-2. Time series of GEM measurements at NV02 and NV99 (note differences in scale).

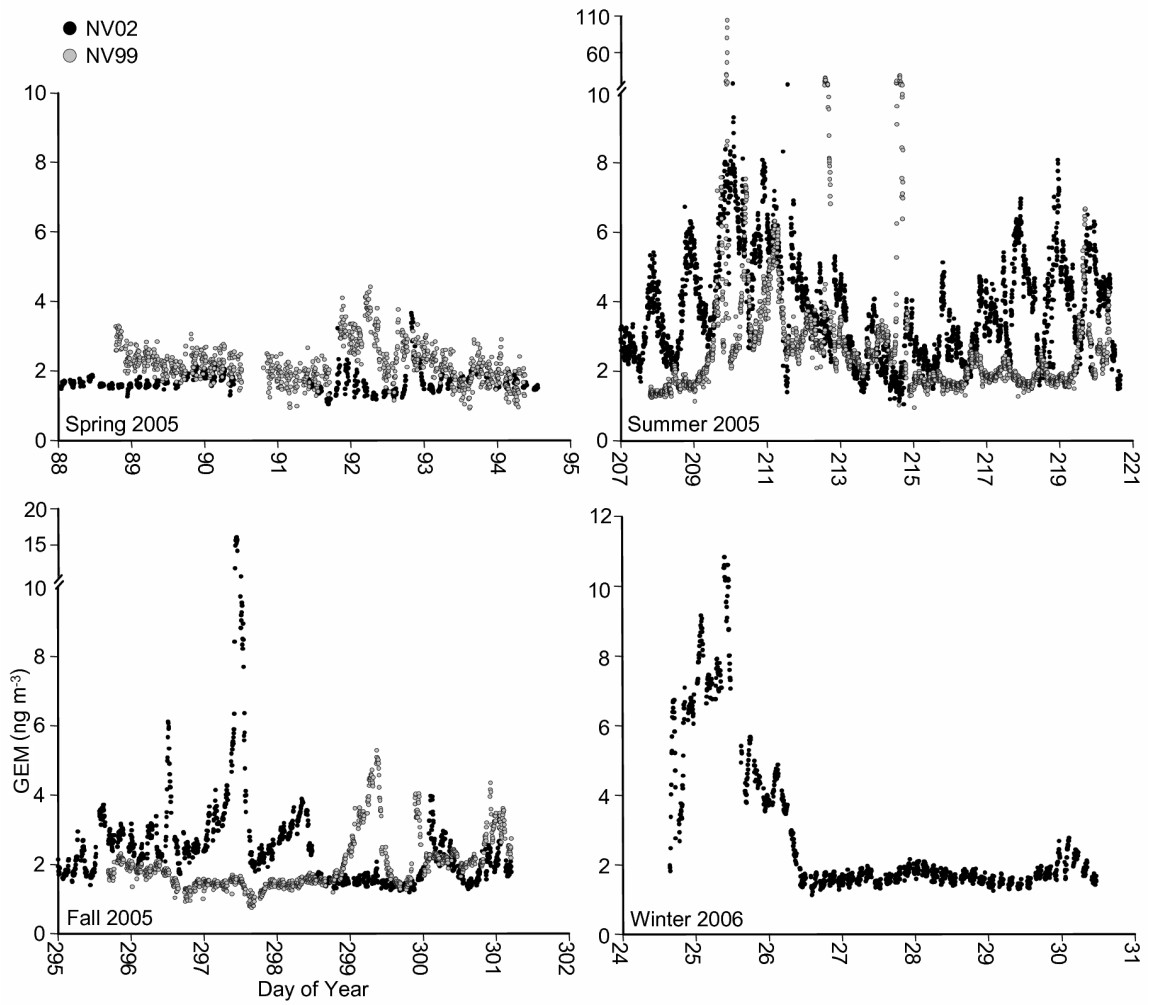

Figure 2-3. Hourly GOM and PBM at NV02 and NV99 averaged from all field campaigns. Whiskers represent standard error.

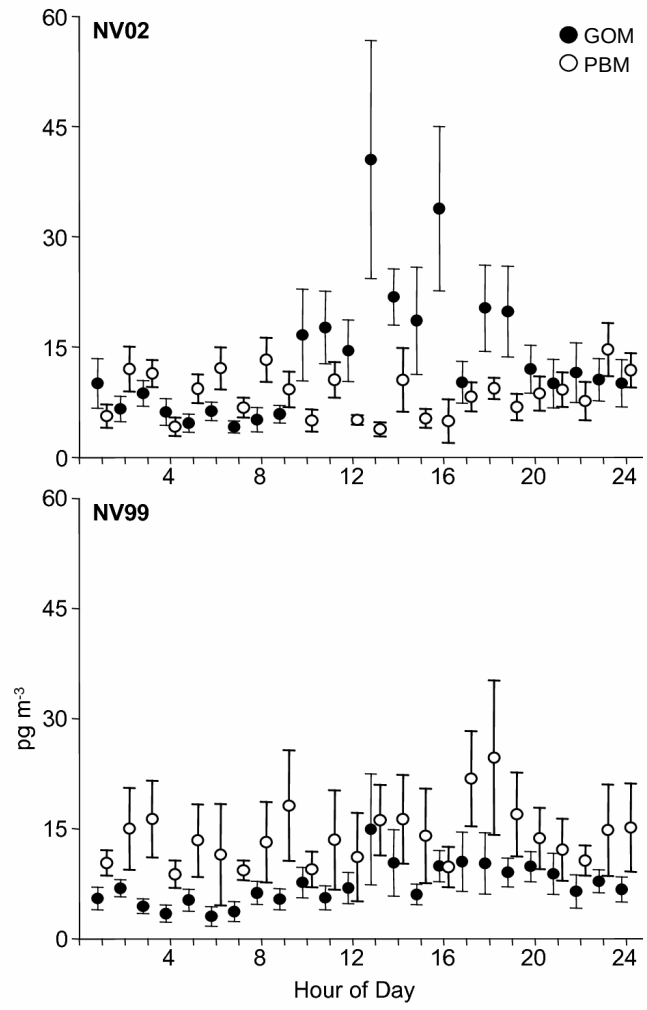

Figure 2-4. Air GEM concentration, mercury soil flux, relative humidity (running median), and days wherein area precipitation occurred at NV02 and NV99 in summer 2005. Note that GEM concentrations >10 ng m^{-3} are removed. See Figure 2-2 for the full range of GEM values.

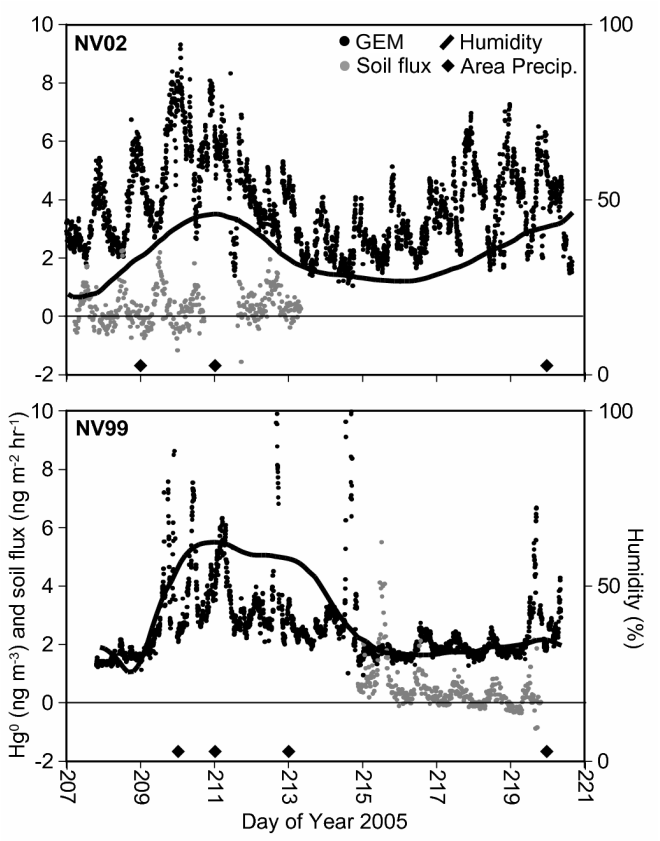

Figure 2-5. 24 hr HYSPLIT air back trajectories from field campaigns (500 m start height). Each trajectory ends at NV02 or NV99 during a 2 hr mercury speciation sampling period and is categorized on the map according to the average GEM concentration for that 2 hr period. Delineations for quadrant analysis of trajectories are shown with the Spring 2005 trajectories. Symbols are as in Figure 2-1.

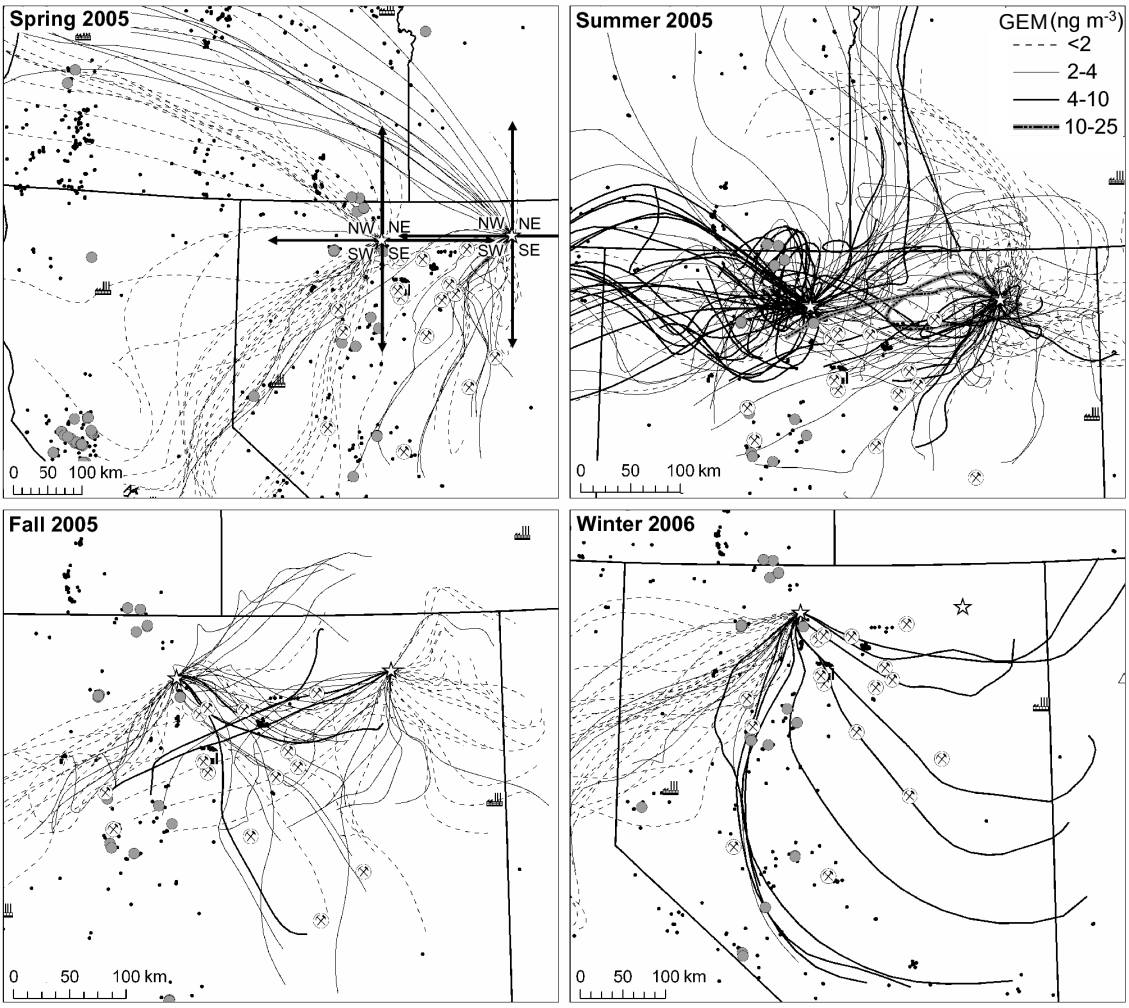

Figure 2-6. Sets of 24 hr trajectories that passed directly from NV02 to NV99 or from NV99 to NV02. Trajectories are numbered consecutively from the earliest to the latest end time. Symbols are as in Figures 1 and 5.

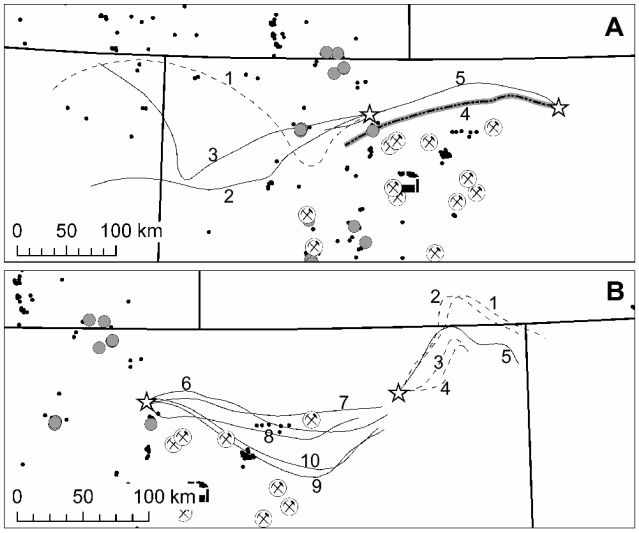

	Trajectory Numbers	End Time of Trajectories	Average GEM Conc. ng m^{-3}
A	1-3	8/2/05 15:00-22:00	2.6 ± 1.0
	4-5	8/3/05 17:00-20:00	7.8 ± 7.1
B	1-5	10/23/05 0:00-21:00	2.0 ± 0.2
	6-10	10/24/05 1:00-22:00	2.9 ± 0.6

Figure 2-7. Total mercury in precipitation (log scale) versus weekly precipitation amount (log scale) at NV02 and NV99.

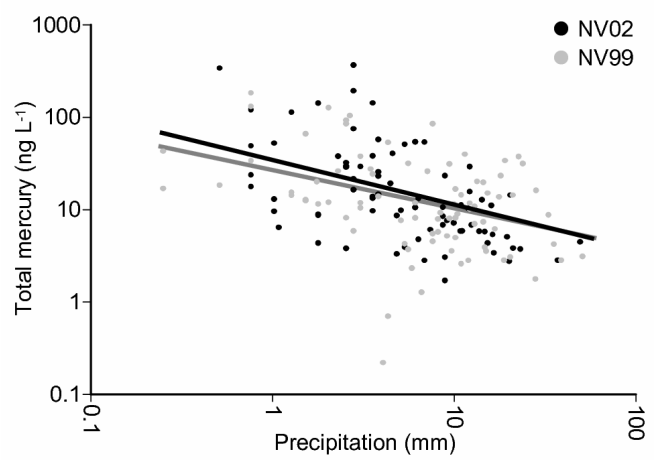

Chapter 3: Estimation of Dry Deposition of Atmospheric Mercury in Nevada by Direct and Indirect Methods

Seth N. Lyman[†], Mae Sexauer Gustin[†], Eric M. Prestbo[‡], Frank J. Marsik[§]

†University of Nevada, Reno, Department of Natural Resources and Environmental Science/MS 370, Reno, Nevada, 89557

‡Frontier Geosciences, 414 Pontius Avenue North, Seattle, Washington, 98109

§University of Michigan, Department of Atmospheric, Oceanic and Space Sciences, Ann Arbor, Michigan, 48109

(Published in *Environmental Science and Technology*, 2007, vol. 41, pp. 1970-1976)

Abstract. Atmospheric models and limited measurements indicate that dry deposition of atmospheric mercury is an important process by which mercury is input to ecosystems. To begin to fill the measurement data gap, multiple methods were used simultaneously during seasonal campaigns conducted in 2005 and 2006 to estimate dry deposition of atmospheric mercury at two Mercury Deposition Network (MDN) sites in rural Nevada, U.S.A. and in Reno, Nevada, U.S.A. Gaseous elemental mercury (GEM), reactive gaseous mercury (GOM), and particulate-bound mercury (PBM) concentrations were measured using Tekran 2537A/1130/1135 systems. These speciated measurements were combined with on-site meteorological measurements to estimate depositional fluxes of GOM and PBM using dry deposition models. Modeled fluxes were compared with more

direct measurements obtained using polysulfone cation-exchange membranes and foliar surfaces. Dynamic flux chambers were used to measure soil mercury exchange.

GOM concentrations were higher during warmer months at all sites, leading to seasonal variation in the modeled importance of GOM as a component of total depositional load. The ratio of dry to wet deposition was between 10 and 90%, and varied with season and with the methods used for dry deposition approximations. This work illustrates the variability of mercury dry deposition with location and time and highlights the need for direct dry deposition measurements.

Introduction

Atmospheric deposition is thought to be an important pathway for the input of inorganic mercury to aquatic and terrestrial environments (Fitzgerald et al., 1998). Mercury is deposited by both wet and dry processes, and wet deposition of mercury is monitored at ~90 Mercury Deposition Network (MDN) sites in North America (http://nadp.sws.uiuc.edu/mdn). Dry deposition rates depend on meteorological and surface parameters, as well as the composition of mercury species in the atmosphere. Gaseous elemental mercury (GEM) is the most abundant atmospheric mercury species, comprising greater than 90% of total atmospheric mercury. GEM is less reactive and is thought to have a longer residence time relative to other atmospheric mercury species (Schroeder and Munthe, 1998). Gaseous species of oxidized mercury are referred to collectively as reactive gaseous mercury (GOM) (Lindberg and Stratton, 1998). GOM species are highly soluble in water (e.g. $HgCl_2$ has a Henry's law coefficient of 1.4×10^6 M atm^{-1}) (Lin and Pehkonen, 1999) and are considered to have a short atmospheric residence time. Mercury bound to particles (PBM) has an intermediate residence time that depends on particle size (Schroeder and Munthe, 1998).

GEM is known to exhibit both emission and deposition (Lindberg et al., 1992; Lindberg et al., 1995; Gustin et al., 1996; Schroeder and Munthe, 1998; Lindberg and Meyers, 2001). Seigneur et al. (2004) reviewed a variety of studies of GEM deposition and noted that bi-directional model simulations resulted in an average deposition velocity (V_d) of 0.06 cm s^{-1}, but they chose 0.01 cm s^{-1} as a constant V_d for GEM in their global atmospheric mercury model, citing evidence that uptake by vegetation may occur only when atmospheric concentrations rise above a compensation point. Estimates of GOM

dry deposition obtained from vertical gradient measurements and application of the modified Bowen ratio method provided deposition velocities ranging from 0.4 to 7.6 cm s^{-1} (Lindberg and Stratton, 1998; Poissant et al., 2004). A study of mercury deposition to forest foliar surfaces resulted in an estimated V_d for GOM ranging from 0.1 to 0.5 cm s^{-1} (Rea et al., 2000). PBM depositional behavior will depend on particle mass and size distribution. Keeler et al. (1995) reported that 88% of PBM in urban Detroit was in the fine mode (<2.5 μm) and that the mean fine mode diameter was 0.68 μm. Particles of diameter less than 1 μm have V_d in the range of 0.1 to 1.0 cm s^{-1} (Zhang et al., 2001).

In this study, concentrations of atmospheric mercury species were measured and direct (soil chambers, leaf washes, surrogate surfaces) and indirect (dry deposition models) methods were used to estimate dry deposition of mercury species at two MDN sites in rural Nevada, U.S.A., and one suburban site in Reno, Nevada. Estimates of dry deposition obtained using different methods are compared and the significance of dry versus wet deposition as mechanisms of atmospheric mercury input is considered.

Methods

This study included one- to two-week intensive field campaigns at 2 MDN sites (NV02 and NV99) in Nevada, U.S.A. and long-term data collection at the Desert Research Institute (DRI) in Reno, Nevada (Figure 3-1). The short-term field campaigns were conducted in spring, summer, and fall 2005 at NV02 and NV99 simultaneously, and in winter 2006 at NV02. Each short-term field campaign included measurement of atmospheric mercury species and meteorological parameters and deployment of cation-

exchange membranes as surrogate surfaces to estimate dry deposition of GOM. Mercury soil flux was measured during most short-term field campaigns and, due to equipment limitations, was not measured at the two sites simultaneously. The summer field campaign included leaf wash measurements. In addition to seasonal field campaigns, mercury speciation and meteorological data were collected at DRI from November 2004 through February 2006, and cation-exchange membranes were deployed monthly. Mercury soil flux was measured at DRI in September 2005, and leaf washes were collected at DRI in August and September 2005.

Site Descriptions. MDN site NV02 (41.50^{o}N, 117.50^{o}W) is located at Lesperance Ranch, 70 km north of Winnemucca, Nevada. It lies on the northern end of a broad, flat desert valley. The area is rural with a mix of pastureland and sagebrush-dominated native vegetation. MDN site NV99 (41.55^{o}N, 115.21^{o}W) is located at Gibbs Ranch, 80 km northwest of Wells, Nevada. The site lies on the eastern side of a narrow river valley with irrigated native grass fields surrounded by sagebrush-dominated native vegetation. The Desert Research Institute (DRI) (39.57^{o}N, 119.80^{o}W) is located about 5 km north of downtown Reno, Nevada. The area is hilly and suburban with sage- and rabbitbrush-dominated native vegetation. Prevailing winds are from the west at DRI, and wind measurements were made on the east side of the building complex. Due to possible interference from the building complex, wind measurements at DRI may not be representative of turbulent transfer conditions, and modeled deposition results from DRI should be considered with caution. Despite this, the authors feel modeled results may be used to investigate seasonal trends in dry deposition at the site. See Supporting Information for more discussion of study sites.

Atmospheric Mercury Speciation. Tekran automated mercury speciation systems were used to measure concentrations of GEM, GOM, and PBM (<3 μm). The Tekran speciation system is described by Landis et al. (2002), and includes sequential collection of GOM on a KCl-coated quartz annular denuder, PBM on a quartz filter assembly, and GEM on gold traps within a Model 2537A Mercury Vapor Analyzer. Collected mercury is thermally desorbed and analyzed by cold vapor atomic fluorescence spectrometry. A detailed discussion of system operation and quality control procedures can be found in Supporting Information.

Dynamic Flux Chambers. In situ measurements of mercury soil flux were made using a cylindrical polycarbonate chamber with a 10 cm radius, 3.5 cm height, 1 L volume, and 1.5 L min^{-1} flow rate (Engle et al., 2001). Air entering and exiting the chamber was measured sequentially at 10 min intervals by a Tekran Model 2537A with a Tekran Model 1110 Synchronized Two Port Sampling System. Flux of Hg was calculated using the equation:

$F = \Delta C*Q/A,$

where F is the surface flux of Hg in ng m^{-2} hr^{-1}, ΔC is the difference in mercury concentrations in the outlet airstream versus the inlet airstream in ng m^{-3}, Q is the flow of air through the chamber in m^3 hr^{-1}, and A is the soil surface area exposed to the chamber in m^2. Flux chamber blanks were measured before and after field deployment by placing the chamber on a clean polycarbonate plate during daylight for at least 3 h. Blank ΔC values were 0.04 ± 0.03 ng m^{-3}. Sample flux measurements were not blank-corrected.

Meteorology. At NV02 and NV99, wind speed and direction (Young Model 05103-5), incident radiation (Li-Cor Model 190SA), and relative humidity and temperature (Vaisala

Model HMP45AC) were recorded and averaged using a Campbell Scientific data logger. At DRI, meteorological measurements were collected at a weather station operated by the Western Regional Climate Center (http://www.wrcc.dri.edu/weather/nnsc.html).

Cation-exchange Membranes. Cation-exchange membranes (Pall Corporation, P/N ICE45S3R) were deployed as surrogate surfaces for measurement of GOM deposition. The cation-exchange membrane is constructed of negatively-charged polysulfone, has a 0.45 μm pore size and 140 μm thickness, and has a non-woven polyester backing. Membranes were deployed on trace-cleaned clear acrylic plates with acrylic fasteners, and the exposed surface of mounted membranes was 107 cm^2. Membranes were handled only with PTFE-coated forceps and were deployed for six-day periods in quadruplicate at 1 m with the exposed face down to reduce contamination from large particles or precipitation and to reduce evasion of deposited mercury in conditions of high solar radiation.

At the end of each deployment period, membranes were collected into I-Chem glass jars with PTFE-coated lids. At the same time, four clean membranes were collected in jars to serve as blanks. Samples were frozen and stored for less than 30 days before analysis. Samples were digested in a 0.02 M bromine monochloride solution and digests analyzed for total mercury in solution as described in EPA Method 1631 (USEPA, 2002). In unpaired t-tests, samples were always significantly greater than blanks at $\alpha = 0.01$. Standard deviations of replicates were 6-20% of sample means. Depositional flux (D) of mercury to membranes was determined in ng m^{-2} hr^{-1} by the equation:

$D = [(S - B)/A]/T,$

where S is the total mercury recovered from a deployed sample in ng, B is the average total mercury in ng recovered from blanks, A is the exposed membrane area in m^2, and T is the time in hours the sample was deployed.

Leaf Washes. Mercury removed from leaf surfaces by rinsing was quantified for aspen (*Populus tremuloides*) and sagebrush (*Atemisia tridentata*). Aspen were used during the summer field campaign at NV02 and NV99, and aspen and sagebrush were used at DRI in August and September 2005. All plants were potted in low mercury (< 20 ppb) soils and grown in a greenhouse for several months before deployment. Immediately prior to use, foliage of each plant (5 plants per deployment) was rinsed with 1 L 18.2 $M\Omega\ cm^{-1}$ deionized water. Five sets of leaves (consisting of one leaf from each plant for aspen and three leaves from each plant for sagebrush) were collected immediately and rinsed in two 50 mL aliquots of 18.2 $M\Omega\ cm^{-1}$ deionized water (Frescholtz and Gustin, 2004). The two aliquots of rinse water were combined in Teflon bottles and acidified with 1 mL Optima HCl. At the end of the deployment period (6 days at DRI, 12 days at NV02 and NV99), five sets of leaves were again collected and rinsed in the same manner. Rinse water was analyzed for total mercury in solution as described in EPA Method 1631 (USEPA, 2002). Depositional flux (D) of water-soluble mercury to leaf surfaces was calculated in ng $m^{-2}\ hr^{-1}$ by the equation:

$$D = (S/L_S - B/L_B)/T,$$

where S is the total mercury in ng recovered from rinse water from a set of leaves collected at the end of the deployment period, B is the average total mercury in ng from rinse water from the five sets of leaves collected at the beginning of the deployment

period, L_S is the total area in m^2 of the leaves from S, L_B is the average total area in m^2 of the leaves from B, and T is the time in hr the plants were deployed.

Dry Deposition Models. GOM and PBM dry depositional fluxes were calculated based on the resistance models of Zhang et al. (2003) and Zhang et al. (2001), respectively. Most established dry deposition models assume surface flux to be unidirectional (Wesely and Hicks, 2000), and GEM dry deposition was not modeled in this study because it exhibits bi-directional surface flux. The GOM model calculates V_d for gaseous species. V_d is calculated by the equation

$$V_d = 1/(R_a + R_b + R_c)$$

where R_a, R_b, and R_c are the aerodynamic resistance, quasi-laminar sublayer resistance, and canopy resistance, respectively. The particle deposition model calculates V_d for particles based on the equation

$$V_d = V_g + 1/(R_a + R_s)$$

where V_g is the gravitational settling velocity, R_a is the aerodynamic resistance, and R_s is the surface resistance. Venkatram and Pleim (1999) noted that the resistance analogy is not appropriate for modeling particle deposition, but concede that this inconsistency may have little effect on model results. These models have been shown to produce reasonable values that are within the range of measured V_d for various gas species and for particles (Zhang et al., 2001; Zhang et al., 2003). Additional information about model design and implementation is available in Supporting Information.

Results and Discussion

Model Sensitivity Analyses. Model parameters with the most uncertainty and the greatest potential to influence results were investigated through sensitivity analyses. For the GOM model, these included the scaling parameters α and β (chemical species-dependent values used to scale ground and cuticle resistance from established values for SO_2 and O_3, respectively), stomatal resistance, standard deviation of wind direction, and land use category. The standard deviation of wind direction affects R_a, R_b, and R_c, while α and β, stomatal resistance, and land use category affect only R_c. For the PBM model, investigated parameters included particle size, particle density, standard deviation of wind direction, and land use category. Sensitivity analyses were conducted using datasets collected at NV99 in spring, NV99 and NV02 in summer, and DRI in November.

For the GOM deposition model, when the scaling parameters α and β were increased from the values applied in the model base case of $\alpha = \beta = 2$ to $\alpha = \beta = 10$ ($\alpha = \beta = 10$ is recommended by Zhang et al. (2002) for HNO_3), V_d increased by 120% (from 0.46 ± 0.16 cm s^{-1} to 1.00 ± 0.35 cm s^{-1}). When stomatal uptake was eliminated from the model GOM V_d decreased by only 1%. Due low humidity, low leaf area index, and extreme temperatures, the stomatal pathway was not important to modeled deposition rates during most seasons at these high desert sites. Because of the reduced influence of stomatal uptake and the high reactivity and solubility of GOM, modeled GOM deposition was highly dependent on R_a and friction velocity (u_*). The equations used in this study to calculate R_a and u_* depend on wind speed and standard deviation of wind direction, which serve as estimates of atmospheric turbulence. To test the sensitivity of the model to these parameters, standard deviation of wind direction was doubled, which caused u_*

to increase by 100% relative to the base case, R_a to decrease by 75%, and V_d to increase by 103% (0.93 ± 0.28 cm s^{-1}). Changing the land-use category from broadleaf evergreen shrubs to desert increased V_d by 11% (0.51 ± 0.05 cm s^{-1}) (the desert category assumes no vegetation exists). For the PBM dry deposition model, doubling the particle diameter from 0.68 μm to 1.36 μm decreased PBM V_d by 29% (from 0.12 ± 0.04 to 0.08 ± 0.03 cm s^{-1}), and changing the particle density from 1.5 to 2.5 g cm^{-3} increased PBM V_d by 1%. Doubling of standard deviation of wind direction led to a 98% increase in PBM V_d (0.24 ± 0.09 cm s^{-1}). Modeled PBM V_d did not change significantly when land use category was changed to desert.

These analyses show that model results were sensitive to environmental and meteorological conditions observed during the study periods, and application of the models to other land use categories or climatological conditions would likely yield different results. Also, these analyses show that the models were sensitive to the chemical and physical properties of gaseous species and particles, and assumptions made about these properties are likely to be an added source of uncertainty. Note that model calculations for GOM and PBM used mean concentrations, so results do not reflect measurement uncertainty, and that modeled deposition velocities for GOM are on the lower end of the range reported by others (Lindberg and Stratton, 1998; Poissant et al., 2004).

Field data. Table 3-1 summarizes results of field campaigns at NV02 and NV99 and periods of cation-exchange membrane deployment at DRI. GEM concentrations were greatest at the rural MDN sites, but DRI had consistently higher GOM concentrations. Since DRI is an urban site and is also closer to large urban areas upwind (i.e. Sacramento

and San Franciso), it is possible that the higher GOM concentrations reflect urban air pollution, which is thought to enhance GOM formation (Weiss-Penzias et al, 2003). GOM concentrations at all sites were highest in the warmer seasons, as was mercury deposition to cation-exchange membranes. Average GOM in colder months was low, though it was significantly greater than the level of quantitation (See Supporting Information). Trends in mercury soil flux varied among the study sites. Net emission was always observed at NV02, while the net direction of soil flux changed with season at NV99. Diel variation in fluxes was observed with higher flux during the day and lower flux during the night (Gustin et al., 2006).

Comparison of Methods. Mercury depositional flux calculated from cation-exchange membrane results was well correlated with mean GOM concentrations ($r^2 = 0.84$, $p < 0.001$) (Figure 3-2), and addition of wind speed, GEM concentration, or PBM concentration in a linear regression model did not improve the correlation. Calculated membrane deposition was well correlated with modeled GOM deposition ($r^2 = 0.87$, $p < 0.001$), though membrane deposition was, on average, more than five times greater than modeled GOM deposition. The difference between deposition to membranes and modeled GOM deposition was greatest at NV99, where rain or snow fell during all field campaigns. The calculated V_d of GOM to membranes that received rain was 3.24 ± 1.69 cm s^{-1}, while the V_d to membranes that did not receive rain was 1.54 ± 0.54 cm s^{-1}, indicating that contamination during rain events likely led to artificially high results. The mean V_d of membranes that did not receive rain was still greater than modeled GOM V_d by more than three times. It is thought that the reactive membrane surface presented little resistance to GOM deposition, whereas modeled GOM surface resistance was

considerable (755 ± 1050 s m^{-1}). When the GOM model was set to ignore surface resistance, modeled GOM V_d was 1.62 ± 0.73 cm s^{-1} and similar to that calculated using membranes. Because GOM may deposit to cation-exchange membranes more readily than natural surfaces a surface resistance factor could potentially be applied to membrane results to estimate deposition to natural surfaces. This hypothesis warrants exploration via collection of data in different environmental settings.

Cation-exchange membranes collected about 20 times more mercury than the surfaces of simultaneously deployed aspen leaves (Figure 3-2), and no measurable deposition of mercury to sagebrush leaves occurred. The leaf wash data is limited and differences in wash mercury concentrations for the two leaf types may reflect a difference in the surface area washed and/or leaf surface efficacy for mercury collection. Mercury collected from leaf rinses is thought to reflect mostly GOM and PBM deposition (Rea et al., 2000). Mean modeled V_d values for PBM (Table 3-2) were near a "typical" value of 0.1 cm s^{-1} for fine particles over land reported by Seigneur et al. (2004).

Relative Importance of Mercury Species. The field chamber/Tekran 2537A system only measured TGM soil flux, and the contribution of individual species to the net flux could not be determined using this method. Nevertheless, average ΔC values used to calculate flux were always greater than GOM concentrations (GOM concentrations averaged 8 ± 6% of ΔC at NV02 and 5 ± 3% at NV99), indicating that most of the difference between inlet and outlet TGM concentrations was attributable to GEM. Therefore, chamber-derived mercury soil flux is considered to reflect predominantly GEM exchange.

GOM comprised a larger component of modeled dry deposition in summer and a

smaller component in winter, whereas the inverse behavior was observed for mercury soil flux, with net soil emission observed more often during summer months (Table 3-1). Although GEM vegetative flux was not measured, modeled stomatal resistance was consistently high and thus, GEM stomatal uptake was probably low. Estimates of the relative contribution of GOM, PBM, and GEM to total dry deposition were explored using three scenarios (Table 3-3, Figure 3-3). GOM was the dominant depositing species when scenarios 1 and 2 were utilized, but GEM was dominant in scenario 3 (Figure 3-3). The relative contribution of each species was dependent not just on methods, but also on site and season. For example, at NV99 in scenario 1 PBM was responsible for ~69% of total deposition during spring while GEM was responsible for 89% of deposition during fall (Table 3-1). Figure 3-3 does not include any winter field campaign data, and it is noteworthy that total dry deposition was lowest in winter at NV02 for scenarios 1 and 2 (Table 3-4).

Wet and Dry Depositional Load. MDN mercury wet deposition data from spring 2005 through winter 2005/2006 were compared against dry deposition values for the different scenarios (Table 3-4). Rainfall at NV02 and NV99 is erratic, so wet deposition data from the one- to two-week field campaign periods alone may not adequately characterize longer-term wet deposition behavior. To compare wet and dry deposition, dry deposition values for each period of data collection were scaled up by season by multiplying average depositional fluxes from field campaigns by three months time (winter = Dec.-Feb.; summer = Jun.-Aug.; spring = Mar.-May; fall = Sep.-Nov.). These seasonal estimates of dry deposition were compared against measured wet-deposited mercury based on MDN data for each season (Table 3-4). The percent dry deposition was always higher at NV02

relative to NV99 for all scenarios, which could be due to the fact that precipitation was higher at NV99 (annual rainfall was 25.9 cm at NV02 and 31.0 cm at NV99). Overall, the relative importance of mercury dry deposition at the different locations was influenced by meteorological conditions and it must be noted that Nevada has a semi-arid climate with low precipitation (DCNR, 2006*)*. Thus, the results of this study must be considered with respect to the climatic setting.

Estimation of the percent of total deposition that was dry was highly dependent on the methods applied (Table 3-4). Scenario l, which used the net mercury soil flux for GEM deposition, resulted in the lowest calculated dry deposition percentage. Scenario 2 also used net mercury soil flux, but the high deposition rates calculated using the cation-exchange membranes led to higher estimated dry deposition. Scenario 3 resulted in the highest deposition estimates due to the application of a unidirectional deposition velocity for GEM.

As shown above, underlying all these estimates are considerable uncertainties. Sensitivity analyses showed that changes in important model parameters could change V_d by 100% or more. In addition, the dry deposition model does not account for possible reduction and subsequent re-emission of deposited GOM. Direct measurements of GOM and PBM dry deposition are needed to validate model results. Surrogate surfaces like the cation-exchange membranes may be applied for measurement of GOM deposition, but, because they are usually not chemically or physically similar to natural surfaces, data obtained might not be directly applicable to natural environments (Wesely and Hicks, 2000). The observed discrepancy between deposition velocity calculated for cation-exchange membranes and modeled values may be due to a high affinity of GOM for the

reactive membrane surface. As suggested, membrane deposition may be representative of GOM deposition in the absence of surface resistance. The discrepancy between depositional flux to foliar surfaces and membranes may have been due to differences in surface physicochemical properties, differences in surface area, or may reflect the fact that the leaves were washed with water while the membranes were digested in a BrCl solution. It is hypothesized that cation-exchange membranes may be a better surrogate for GOM deposition, for they provide a homogeneous, consistent surface, whereas leaves will vary with leaf age and species. Additionally, since dry deposition occurs to both vegetative and soil surfaces, use of leaf wash data alone to estimate GOM and PBM deposition may result in underestimation of system-level flux.

This research illustrates that the use of different methods to quantify and model dry deposition can produce different results. Further method development is needed for accurate measurement of mercury dry deposition, and direct measurements of dry deposition are needed to validate chemical models. The different methods applied showed similar seasonal and geographical variations in the depositional behavior of GEM, GOM, and PBM, and each form of mercury was found to be a component of dry deposition that needs to be considered.

Acknowledgements

This project was funded by a HATCH grant from the University of Nevada, Reno (UNR) College of Agriculture, Biotechnology and Natural Resources, by the UNR Environmental Sciences and Health Graduate Program, and by EPA STAR Grant 82980001. Equipment was loaned from Oak Ridge National Laboratory and EPA Region

IX Lab. The authors would like to thank the owners and operators of Lesperance Ranch and Gibbs Ranch and Steve Lindberg of Oak Ridge National Laboratory for their support of this research. We also would like to thank the four anonymous reviewers whose critiques helped to improve the quality of this manuscript.

Tables and Figures

Table 3-1. Twenty-four hour average temperatures, mercury concentrations, and surface fluxes of mercury species from field campaigns and from monthly six-day cation-exchange membrane deployment periods at DRI. Superscripts a, b, c, and d denote study periods wherein data were collected at two sites simultaneously (except soil flux). Superscript R denotes periods of cation-exchange membrane deployment with precipitation. Values are given as mean ± standard deviation, and negative sign indicates deposition.

Site	Month	Temp °C	GEM conc. ng m^{-3}	GOM conc. pg m^{-3}	PBM conc. pg m^{-3}	Hg Soil Flux ng m^{-2} hr^{-1}	Model GOM Flux ng m^{-2} hr^{-1}	Memb. GOM Flux ng m^{-2} hr^{-1}	Model Hg_p Flux ng m^{-2} hr^{-1}	Aspen Leaf Flux ng m^{-2} hr^{-1}
NV02	Mar 05[a]	4.2 ± 5.0	1.7 ± 0.30	5 ± 4	16 ± 8		-0.14 ± 0.11	-0.48 ± 0 .12	-0.13 ± 0.13	
	Jul 05[b]	23.5 ± 7.2	4.2 ± 1.6	15 ± 11	9 ± 7	0.32 ± 0.77	-0.34 ± 0.43	-0.81 ± 0.16	-0.05 ± 0.05	
	Aug 05[b]	24.2 ± 7.3	3.3 ± 1.3	18 ± 13	10 ± 6		-0.37 ± 0.35	-0.99 ± 0.02	-0.07 ± 0.07	
	Oct 05[c]	10.4 ± 7.0	2.5 ± 1.6	24 ± 30	5 ± 3	0.14 ± 0.43	-0.34 ± 0.29	-0.87 ± 0.18[R]	-0.02 ± 0.02	
	Jan 06[d]	1.7 ± 3.6	2.8 ± 2.1	2 ± 7	4 ± 6	0.11 ± 0.20	-0.02 ± 0.08	-0.24 ± 0.03[R]	-0.02 ± 0.03	
NV99	Mar 05[a]	1.7 ± 6.6	2.2 ± 0.6	2 ± 3	27 ± 15	-0.02 ± 0.60	-0.03 ± 0 .06	-0.41 ± 0.09[R]	-0.11 ± 0.15	
	Jul 05[b]	20.4 ± 7.8	3.5 ± 5.7	12 ± 6	12 ± 6		-0.17 ± 0.23	-1.24 ± 0.23[R]	-0.04 ± 0.04	-0.13 ± 0.08
	Aug 05[b]	21.8 ± 7.7	2.4 ± 1.7	9 ± 10	12 ± 8	0.47 ± 0.59	-0.11 ± 0 .11	-0.85 ± 0.09[R]	-0.04 ± 0.04	
	Oct 05[c]	8.2 ± 7.2	2.0 ± 0.8	4 ± 4	3 ± 4	-0.22 ± 0.33	-0.02 ± 0. 04	-0.50 ± 0.13[R]	-0.01 ± 0.01	
DRI	May 05	13.1 ± 5.3	1.8 ± 0.3	9 ± 8	4 ± 3		-0.12 ± 0.15	-0.52 ± 0.08[R]	-0.02 ± 0.03	
	Jun 05	18.7 ± 4.7	1.3 ± 0.3	43 ± 25	10 ± 21		-0.48 ± 0.60	-1.88 ± 0.47	-0.03 ± 0.06	
	Jul 05	21.9 ± 4.2	1.6 ± 1.6	64 ± 27	4 ± 3		-0.93 ± 1.15	-4.54	-0. 01 ± 0.01	
	Aug 05	24.0 ± 4.6	1.7 ± 0.5	51 ± 43	7 ± 8		-0.75 ± 1.11	-2.83 ± 0.73	-0.02 ± 0.03	-0.06 ± 0.05
	Sep 05	14.5 ± 5.6	2.0 ± 0.4	34 ± 27	6 ± 3	-0.05 ± 1.10	-0.31 ± 0.40	-0.86 ± 0.04	-0.02 ± 0.01	-0.07 ± 0.12
	Nov 05	7.7 ± 4.2	1.4 ± 0.3	6 ± 7	4 ± 3		-0.10 ± 0.14	-0.46 ± 0.1 1	-0.02 ± 0.02	
	Dec 05	-1.3 ± 1.6	2.3 ± 0.4	1 ± 1	5 ± 2		-0.02 ± 0.02	-0.10 ± 0. 06	-0.01 ± 0.01	
	Jan 06[d]	3.7 ± 3.2	1.8 ± 0.5	2 ± 5			-0.03 ± 0.09	-0.44[R]		
	Feb 06	4.2 ± 4.6	1.6 ± 0.3	13 ± 6	12 ± 4		-0.16 ± 0.12	-0.39 ± 0 .17	-0.04 ± 0.02	

Table 3-2. Modeled GOM and PBM deposition velocities and calculated deposition velocities of GOM to cation-exchange membranes and the sum of GOM and PBM to aspen foliar surfaces. Cation-exchange membranes that received rain were not used.

		Deposition Velocity (cm s^{-1})
NV02	Modeled GOM	0.78 ± 0.11
	GOM to membranes	1.72 ± 0.19
	GOM + PBM to aspen	
	Modeled PBM	0.18 ± 0.03
NV99	Modeled GOM	0.30 ± 0.10
	GOM to membranes	
	GOM + PBM to aspen	0.16 ± 0.10
	Modeled PBM	0.08 ± 0.02
DRI	Modeled GOM	0.37 ± 0.07
	GOM to membranes	1.52 ± 0.58
	GOM + PBM to aspen	0.03 ± 0.02
	Modeled PBM	0.10 ± 0.02

Table 3-3. Methods used in three scenarios to calculate total dry deposition. Dry deposition for each scenario is the sum of deposition of all mercury species. Where Hg soil flux is indicated, field chamber-derived flux was used when net deposition was observed over a study period.

Scenario	GOM	PBM	GEM
1	Modeled	Modeled	Hg soil flux
2	Membrane deposition	Modeled	Hg soil flux
3	Modeled	Modeled	V_d = 0.01 cm/s

Table 3-4. Total seasonal wet and dry mercury deposition and the percent of total deposition that was dry at NV02 and NV99 from spring 2005 through winter 2005/2006. Columns *Dry 1*, *Dry 2*, and *Dry 3* correspond with dry deposition scenarios in Table 3-3.

* Note: winter data was not included in calculation.

		Deposition (μg m^{-2})				% of total that is dry		
Site	**Season**	**Wet**	**Dry 1**	**Dry 2**	**Dry 3**	**Dry 1**	**Dry 2**	**Dry 3**
NV02	Spring	0.82	0.60	1.34	1.91	42%	62%	70%
	Summer	0.37	0.90	2.10	3.95	71%	85%	91%
	Fall	0.57	0.79	1.96	2.75	58%	77%	83%
	Winter	0.83	0.10	0.58	2.28	11%	41%	73%
	% dry of total*		**57%**	**75%**	**83%**			
NV99	Spring	1.03	0.36	1.18	2.06	26%	53%	67%
	Summer	1.80	0.39	2.37	2.70	18%	57%	60%
	Fall	0.65	0.55	1.59	1.64	46%	71%	72%
	Winter	0.57						
	% dry of total		**27%**	**60%**	**65%**			

Figure 3-1. MDN sites NV02 and NV99 and DRI in Reno, Nevada.

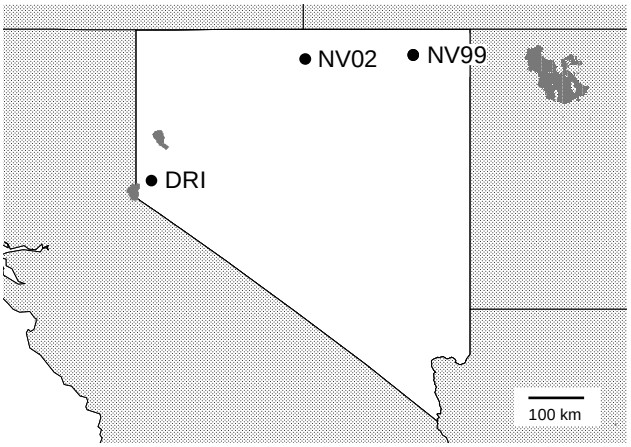

Figure 3-2. Average GOM concentrations versus measured deposition of mercury to cation-exchange membranes and foliar surfaces as well as modeled GOM deposition.

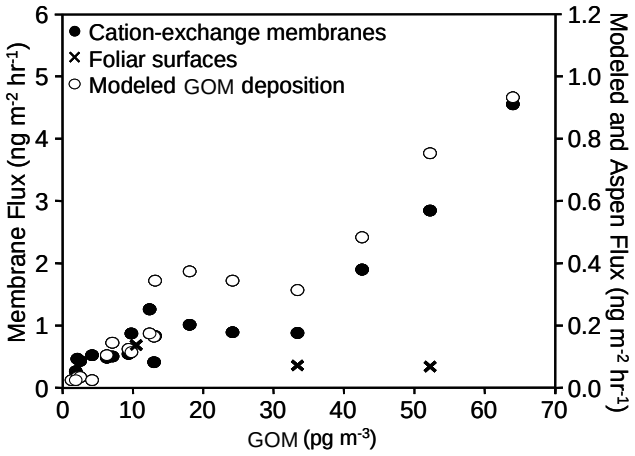

Figure 3-3. Relative contribution of GEM, GOM, and PBM to total dry deposition. Bars represent the average contribution from the spring, summer, and fall field campaigns, and whiskers indicate standard deviation. Scenarios 1, 2, and 3 correspond with scenarios 1, 2, and 3 as described in Table 3-3.

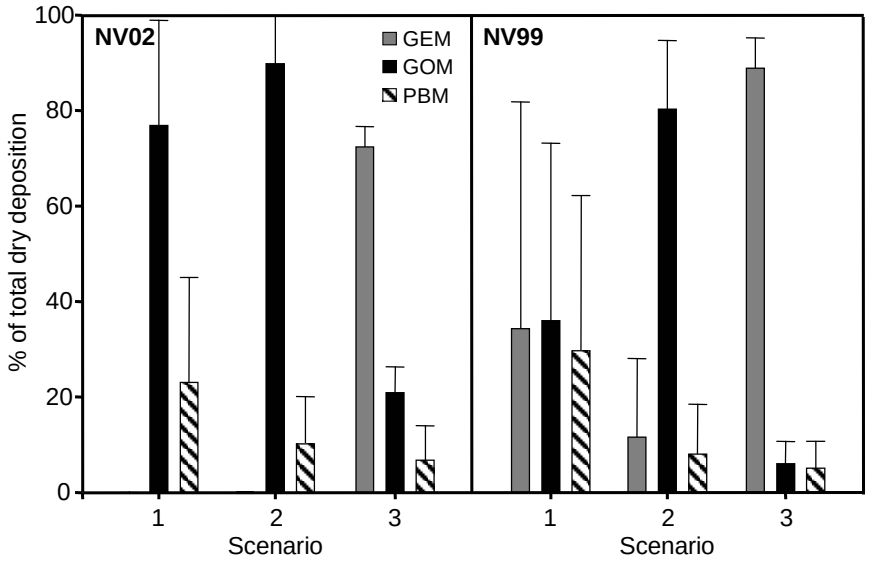

Supporting Information

Detailed Site Descriptions. *NV02*- Soil is loam with mercury concentrations of 56 ± 53 µg kg^{-1} (mean ± standard deviation). Concentrations of atmospheric mercury species were measured at 3 m during the spring, summer, and fall field campaigns and at 1.5 m during the winter field campaign due to a change in field equipment availability. Wind measurements were collected at 3 m.

NV99- Soil is loam to sandy loam with mercury concentrations of 32 ± 13 µg kg^{-1}. Concentrations of mercury species were measured at 1.5 m, and wind measurements were collected at 3 m.

DRI- Soil is stony loam with a mean mercury concentration of 78 µg kg^{-1} (average of two samples). Measurements of mercury species were collected atop a 20 m tower on the western edge of the DRI building complex. Wind measurements were collected at a developed weather station at 15 m on a rooftop at the east end of the building complex.

Details of Speciation System Operation and Quality Control Procedures. The flow rate into the Tekran Model 2537A analyzer was 1 L min^{-1}, and the total flow through the denuder and quartz filter assembly was 7 L min^{-1}. These flow rates were lower than suggested by Landis et al. (2002), and were applied at the recommendation of Tekran personnel to adjust for altitude effects on instrument mass flows. The lower flow rate does not affect denuder performance, but it does increase the aerodynamic diameter cut point of the impactor from 2.5 to 3.0 µm (Chow and Watson, 2006). Sampling time was 5 minutes for GEM and 2 hours for GOM and PBM**.** The system inlet, tubing, glassware, and other components were cleaned or replaced regularly. Quartz annular denuders were cleaned and coated with KCl as described in Landis et al. (2002), and fresh denuders

were installed at the beginning of each field campaign at NV02 and NV99 and every three weeks at DRI. Particulate filter assemblies were packed with new quartz filter disks on the same schedule. The Model 2537A was set to automatically calibrate every 24 hours using its internal mercury permeation source. Calibration checks were performed at the beginning and end of each field campaign and at least once per week at DRI by injecting a known amount of gaseous mercury into ambient air being sampled by the Model 2537A.

The 2537A analyzer quantifies total gaseous mercury (TGM) and operationally defined GEM, GOM, and PBM when the unit is operated with the speciation system, and has a detection limit of <0.1 ng m^{-3} (Tekran, 2002; Temme et al, 2003). Mercury collected by in the denuder or particulate assembly is transported into the 2537A unit in mercury free air. During summer months (June through September), the detection limit, calculated as three times the standard deviation of the speciation system blank measured before and after each GOM and PBM analysis, was 5 pg m^{-3}. During all other months the blank measurements were 0 pg m^{-3}. It is thought that the seasonal difference in blanks is due to high temperatures in the summer, which may have caused mercury to be mobilized from the sampling/analytical line. Thus the level of quantitation, or that constituent concentration that produces a signal sufficiently greater than the blank (Clesceri et al., 1998), varies according to operating and atmospheric conditions. Detection limits reported for two recent studies were 0.88 and 1.6 pg m^{-3} (Hall et al., 2006 and Weiss-Penzias et al., 2003, respectively).

Before and after each simultaneous deployment of mercury speciation systems, both systems were operated at the same location and set to sample the same air for

several days to determine inter-system precision. TGM was measured during each of the comparative experiments, and GEM, GOM, and PBM were measured in October and January. The Model 2537A used for mercury soil flux was also collocated and sampled the same air during these periods. Based on these experiments, relative instrument drift from the beginning to the end of field campaigns was quantified, and field data were adjusted using the percent change over this time. Average TGM relative percent difference among instruments during all comparative experiments was 7.0 ± 5.3%. GOM and PBM were both below instrument detection limits during the January comparative experiments, but in October relative percent difference was 7.2 ± 37.7% and 41.4 ± 62.1%, respectively (n = 19 two hour measurements). The discrepancy between replicate PBM measurements was possibly due to the low concentrations in air. In a separate comparative experiment at DRI, relative percent difference between systems for GOM was 6.1 ± 28.1% (n = 10).

Model Details. *GOM Dry Deposition Model*- GOM was modeled using the method of Zhang et al. (2003), which does not explicitly outline a technique for calculating R_a (aerodynamic resistance) or R_b (quasi-laminar sublayer resistance). In this study, R_a was calculated from measurements of wind speed and standard deviation of wind direction by the equations

$R_a = 4/[u\sigma_\theta^2]$ (neutral and stable conditions)

and

$R_a = 9/[u\sigma_\theta^2]$ (unstable conditions)

where u is wind speed and σ_θ is standard deviation of wind direction (Hicks et al., 1987). As suggested by Meyers et al. (1998), the atmosphere was assumed to be unstable when

global radiation exceeded 100 W m^{-2}. Standard deviation of wind direction was calculated by the equation

$$\sigma_\theta = \sin^{-1}(\varepsilon)[1.0 + 0.1547\varepsilon^3]$$

where

$$\varepsilon^2 = 1 - (s_a^2 + c_a^2),$$

s_a is the average sine of wind direction, and c_a is the average cosine of wind direction (Yamartino, 1984). R_b was calculated by the equation

$$R_b = (2/ku_*)(Sc/Pr)^{2/3}$$

where k is the von Karman constant (0.4), u_* is the friction velocity, Sc is the Schmidt number, and Pr is the Prandtl number for air (0.72) (Hicks et al., 1987). The Schmidt number is the kinematic viscosity of air divided by the diffusivity of a gas of interest. The diffusivity of GOM was estimated from the square root of the ratio of the molecular weights of water and $HgCl_2$ as outlined by Wesely (1989). Friction velocity (u_*) was calculated from the equation

$$u_* = (u/R_a)^{1/2}$$

as inferred from Hicks et al. (1987).

R_c was calculated as described in Zhang et al. (2003). Land use category 10 (evergreen broadleaf shrubs) was chosen because all study sites consisted predominantly of sage, rabbitbrush, and other evergreen shrub species. Leaf area index was estimated at 0.75 for NV99 and 0.50 for NV02 and DRI (NASA, 2006). Leaf angle distribution was assumed to be spherical. The model calculates R_c from the equation

$$1/R_c = (1 - W_{st})/(R_{st} + R_m) + 1/R_{ns}$$

where

$1/R_{ns} = 1/(R_{ac} + R_g) + 1/R_{cut}$

and W_{st} is a stomatal wetness parameter, R_{st} is stomatal resistance, R_m is mesophyll resistance, R_{ns} is non-stomatal resistance, R_{ac} is in-canopy aerodynamic resistance, R_g is ground resistance, and R_{cut} is cuticle resistance. R_m was given a value of zero for GOM, as suggested in Zhang et al. (2002) for species with high solubility. R_g and R_{cut} are scaled from land use category-dependent values for O_3 and SO_2 by the equation

$1/[R_x(i)] = \alpha(i)/[R_x(SO_2)] + \beta(i)/[R_x(O_3)]$

where $R_x(i)$ is R_g or R_{cut} for gaseous species *i*, $R_x(SO_2)$ is R_g or R_{cut} for SO_2, $R_x(O_3)$ is R_g or R_{cut} for O_3, and $\alpha(i)$ and $\beta(i)$ are scaling parameters for species *i*. Because of their contrasting chemical properties, O_3 and SO_2 are convenient compounds from which to scale resistances of other species (Zhang et al., 2002; Wesely, 1989). The scaling parameters α and β depend on the species being modeled, and Zhang et al. (2002) provide scaling parameters for a number of gaseous species. They also outline a method for choosing scaling parameters for any chemical species of interest based on the effective Henry's Law constant (H*) and the negative log of electron activity for half-redox reactions in neutral solutions [$pe^0(W)$]. In this study, H* for $HgCl_2$ and $Hg(OH)_2$ were calculated using available data (Lin and Pehkonen, 1999; Seigneur et al., 1994). For calculation of H* for $HgCl_2$, $[Cl^-]$ was assumed to be 0.2 mg L^{-1}, a typical value for continental rainwater (Drever et al., 1997). $pe^0(W)$ was calculated for the half-redox reaction

$Hg^{2+}_{aq} + 2e^- \leftrightarrow Hg^0_l$

using the equation

$Pe^0(W) = (1/n)[\log_{10}(K)] - 7n_H$

given in Zhang et al. (2002), where n is the number of electrons in the half-reaction, K is the equilibrium constant of the reduction half-reaction, and n_H is the number of protons exchanged per electron in the half-reaction. K was calculated from values of Gibbs free energy of formation (Stumm and Morgan, 1996). The calculated values for H* and pe^0(W) were used to compare GOM to gaseous species listed in Zhang et al. (2002), and, based on evident similarity, the scaling parameters listed for nitrous acid (HONO) were used to scale R_g and R_{cut} for GOM ($\alpha = \beta = 2$).

PBM Dry Deposition Model- The model described in Zhang et al. (2001) was used to infer PBM deposition. R_a and u_* were calculated as described above, and land use category 10 (shrubs and interrupted woodlands) was used. A particle diameter of 0.68 μm (Keeler et al., 1995) and a density of 1.5 g cm^{-3} were assumed.

Chapter 4: Determinants of Atmospheric Mercury Concentrations in Reno, Nevada, U.S.A.

Seth N. Lyman and Mae Sexauer Gustin

University of Nevada, Reno, Department of Natural Resources and Environmental Science/MS 370, 1664 North Virginia Street, Reno, Nevada, 89557

Abstract: Concentrations of gaseous elemental mercury (GEM), gaseous oxidized mercury (GOM) and particulate-bound mercury (PBM) were measured along with ancillary variables 9 km east of downtown Reno, Nevada, U.S.A. from November 2006 through March 2009. Mean two year (February 2007 through January 2009) GEM, GOM, and PBM concentrations were 2.0 ± 0.7 ng m^{-3} (± standard deviation), 18 ± 22 pg m^{-3}, and 7 ± 7 pg m^{-3}, respectively. Data collected were compared with measurements collected at another location just north of the city at 169 m higher elevation. At both locations higher concentrations of GEM and PBM occurred in periods with little atmospheric mixing, indicating that local sources were important for enhancing GEM and PBM concentrations in Reno above that considered continental background. Concentrations of GOM were higher (maximum of 177 pg m^{-3}) during periods with higher temperature and lower dew point. Higher GOM concentrations at the higher elevation site with less urban impact relative to the valley site, along with other data trends, support the hypothesis that in northern Nevada warm, dry air from the free troposphere is a source of GOM to the surface.

Introduction

The atmosphere has been identified as a major pathway by which mercury reaches and contaminates ecosystems (Fitzgerald et al., 1998). Atmospheric mercury is frequently measured as three fractions: gaseous elemental mercury (GEM), gaseous oxidized mercury (GOM, a.k.a. RGM), and particulate-bound mercury (PBM). Measurements of atmospheric mercury fractions have been made in a variety of environments throughout the world (c.f. Valente et al., 2007), but significant gaps in our understanding of the mechanisms that control mercury concentrations in the atmosphere still exist (Lin et al., 2006; Lindberg et al., 2007).

In urban or other anthropogenically impacted environments concentrations of GEM, GOM, and PBM may depend on releases from specific sources (Liu et al., 2007; Edgerton et al., 2006; Manolopoulos et al., 2007) or on oxidation of GEM by anthropogenic oxidants to produce GOM (Weiss-Penzias et al., 2003; Lynam and Keeler, 2005), though uncertainty exists regarding which oxidants play important roles (Lindberg et al., 2007; Calvert and Lindberg, 2005). Reactions with ozone and OH radical have been investigated (Pal and Ariya, 2004a; Pal and Ariya 2004b; Calvert and Lindberg, 2005; Sommar et al., 2001), as have reactions with nitrate radical and hydrogen peroxide (Lin and Pehkonen, 1999). Oxidation of GEM by halogen radicals has been shown to account for the dynamic behavior of atmospheric mercury in polar regions (Lindberg et al., 2002; Ebinghaus et al., 2002), and may contribute to formation of GOM in ocean environments (Hedgecock and Pirrone, 2004; Holmes et al., 2009) and the upper atmosphere (Holmes et al., 2006).

Northern Nevada (U.S.A.) is a region with diverse natural and anthropogenic mercury sources (c.f. Engle et al., 2001; Zehner and Gustin, 2002; Lyman and Gustin, 2008). Moreover, before measurements of GOM in northern Nevada had been published, Selin et al. (2007) predicted that high elevation deserts (like Nevada) would have high GOM concentrations due to subsidence of GOM-rich air from the free troposphere. Weiss-Penzias et al. (2009) recently reported high GOM in Nevada and showed that regional variation in GOM concentrations could be explained by air mass transport from a dry, high-altitude area of the atmosphere.

This paper presents an analysis of more than two years of atmospheric mercury measurements collected on the Reno, Nevada valley floor. It builds on the work of Weiss-Penzias et al. (2009), who report on air mercury data collected at three sites (including the location of this work) in summer 2007, as well as the works of Stamenkovic et al. (2007) and Peterson et al. (2009), who describe observations of air mercury concentrations made at 169 m above the valley floor in Reno from 2002 to 2005 and from 2005 to 2007, respectively. Detailed statistical analyses and comparison of data collected at these two closely situated locations provide the basis for discussion of the mechanisms that control atmospheric mercury concentrations in northern Nevada, with implications for the global mercury cycle.

Methods

Site Description. Data were collected from November 2006 through March 2009 at Mercury Deposition Network (http://nadp.sws.uiuc.edu/mdn) site NV98 in Reno, Nevada, U.S.A (39.51° latitude, -119.72° longitude, elevation 1340 m). This site is located on the

University of Nevada, Reno Nevada Agricultural Experiment Station approximately 9 km east of downtown Reno and 4 km southeast of downtown Sparks, Nevada (Figure 4-1). The Reno-Sparks area is urban and suburban with a population of approximately 400 000, and does not have heavy industrial facilities or any mercury sources listed on the United States Environmental Protection Agency's Toxics Release Inventory (http://www.epa.gov/triexplorer/). The metropolitan area is situated in an arid valley (average annual precipitation of 19 cm) between the Sierra Nevada and Virginia mountain ranges. This region includes some mercury enriched areas, including but not limited to Steamboat Springs (Coolbaugh et al., 2002) and Peavine Peak (Engle and Gustin, 2002).

Atmospheric Mercury. Concentrations of GEM, GOM, and PBM (fine mode) were measured with a Tekran 2537A/1130/1135 system as described by Landis et al. (2002). The flow rate through the denuder and particulate filter assembly was 7 standard L min^{-1} (standard conditions of 0°C and 100 kPa), and the flow rate through the Model 2537A was 1 standard L min^{-1}. The system alternated between 2 h sampling periods and 1 h desorption periods, and the Model 2537A was automatically calibrated using its internal permeation source every eight sampling cycles. The denuder and the 0.1 μm filter on the particulate assembly were replaced every three weeks. The particulate assembly, sample train glassware, and sample lines were removed and cleaned every six months. The accuracy of the permeation rate of the internal permeation source was checked every three months by repeated injections of a known amount of saturated mercury vapor into mercury-free air being sampled by the instrument. Calibration checks were performed weekly by injecting a known amount of saturated mercury vapor into ambient air being

sampled by the instrument. Data were only included for analysis if bracketed by calibration checks that fell within the range of 100 ± 10%.

Also, the Tekran system from this study and that from the higher elevation site in Reno reported on by Peterson et al. (2009) were compared for 10 days in February 2008. The systems were mounted side by side at the same height and were programmed and calibrated identically. The difference between GEM concentrations reported by the two systems was 11 ± 4%, while the difference between GOM and PBM concentrations were 8 ± 40% and -71 ± 41%, respectively (positive values indicate the system from this study was higher).

Ozone. Ozone concentrations were measured using a Teledyne-API Model 400E ozone analyzer. Calibration checks of the Model 400E were performed weekly using a Teledyne-API Model 700E Dynamic Dilution Calibrator equipped with an internal ozone generator. The Model 700E was checked against a NIST-traceable ozone standard every 6 months. Data were only included for analysis if bracketed by span calibration checks that fell within the range of 100 ± 10% and zero calibration checks that were within the range of 0 ± 2 ppb.

Meteorology. Wind speed and direction (Young Model 05305), humidity and temperature (Vaisala Model HMP45AC), and solar radiation (LI-COR Model LI200X) were measured and values were logged with a Campbell Scientific CR1000 data logger.

Particulate Matter. Two DustTrak Model 8520 Aerosol Monitors were used, one with a 1 μm impactor inlet and one with a 10 μm cyclone inlet, and they sampled outside air through a 1.5 m grounded copper tube. DustTrak analyzers measure particle scattering and are factory calibrated for mass concentrations using a road dust standard. These

instruments were zero checked each week, and data were only included for analysis if zero checks were within the range of 0 ± 1 μg m^{-3}. Flow rates and instrument filters and inlets were checked every three weeks, and filters and inlets were replaced or cleaned as needed.

Also, measurements of PM2.5 were obtained from the Washoe County Health District Air Quality Management Division for June-August 2007 and June-August 2008. These measurements were collected in downtown Reno on filters deployed for 24 h every third day.

Dataset Structure. The Tekran system returned one 2 h average measurement of GOM and PBM every 3 h, but GEM, ozone, and meteorological parameters were collected as 5 min averages, so 2 h composite averages of GEM and ozone concentrations and meteorological parameters were calculated for each GOM and PBM measurement period, and these composite averages were used for analysis. Composite 24 h averages were also computed for all parameters and used to elucidate and compare trends at a coarser temporal resolution.

Data Analyses. Data were processed using Microsoft Excel 2003 and SPSS 15.0. Multiple linear regression analyses and Pearson correlation coefficients were developed using SPSS. While Pearson correlation coefficients (r) allow for the assessment of the degree of linear relationship between two variables (Kutner et al., 2004), multiple regression analysis allows for assessment of the predictive value of each independent variable on a dependent variable while taking into account the effects of other independent variables in the analysis (Foster et al., 2006). In multiple regression analysis r^2 is a measure of the collective strength of all independent variables in predicting the

dependent variable, and standardized regression coefficients for individual independent variables indicate the predictive value of each independent variable on the dependent variable with the influence of the additional variables removed. Unlike metric coefficients, standardized coefficients for independent variables with different units or scales are directly comparable with respect to their effect on the dependent variable. Similar to Pearson correlation coefficients, higher standardized regression coefficients (in absolute value) indicate a better predictive value of the independent variable on the dependent variable.

Multiple regression equations were computed for entire 2 h and 24 h data sets and with data divided by season (spring = March-May; summer = June-August; fall = September-November; winter = December-February) with GEM, GOM, PBM, and ozone as dependent variables. To allow wind direction to be used in multiple regression analysis, wind direction values were categorized into four directional variables (i.e. if wind direction was between 45 and 135 directional degrees, a value of one was assigned to the East variable and a value of zero was given to the other variables, and so on). To account for periods with low wind, a value of zero was given to all variables if wind speed was less than 0.5 m s^{-1} .

Ozone was only measured from February 2007 through January 2009, and this two year period was used to compute summary statistics and to perform most data analyses. The effects of wind direction were assessed using a subset of data from November 2006 through August 2007. The DustTrak analyzers only operated during April 2008 and from December 2008 through March 2009, and the relationships of GEM and PBM with DustTrak measurements were assessed using data from these periods.

Results and Discussion

Figure 4-2 shows a time series of GEM, GOM, PBM, and ozone in Reno from February 2007 through January 2009, and Table 4-1 shows summary data for this period. Concentrations of GEM in Reno were higher than the mean background concentration given for the Northern Hemisphere of 1.5 ± 0.2 ng m^{-3} (Lindberg et al., 2007) , PBM concentrations were lower than many rural sites (range of 6 to 42 pg m^{-3} given in Valente et al., 2007), and GOM concentrations were greater than has been reported for rural sites (range of 2 to 24 pg m^{-3} given in Valente et al., 2007) but in the range of urban or impacted sites (range of 6 to 121 pg m^{-3} given in Valente et al., 2007).

Also, GEM concentrations in this study were generally lower than those reported by Lyman and Gustin (2008) for a region of mercury enrichment in rural northern Nevada (3.0 ± 1.7 ng m^{-3} reported for Paradise Valley, Nevada; 2.5 ± 3.1 ng m^{-3} reported for Wells, Nevada), but they were similar to total gaseous mercury (TGM) concentrations reported by Stamenkovic et al. (2007) for the site in north Reno 169 m higher in elevation than the location of this study (2.3 ± 0.6 ng m^{-3}), and higher than GEM measured atop a 20 m tower at the same north Reno location (Table 4-1; Figure 4-3).

In addition, at the higher elevation location an increase in GEM or TGM concentration was observed each morning with sunrise and attributed to light-induced release of mercury deposited during the night or from naturally enriched substrates (Stamenkovic et al., 2007; Peterson et al., 2009). Alternatively, movement of GEM-rich air up from the underlying nocturnal boundary layer was suggested (Peterson et al., 2009).

In contrast, at the study location of this work GEM concentrations declined with first light (Figure 4-4), most likely due to dilution during the breakup of the nocturnal boundary layer.

Concentrations of GOM in this study were higher than those obtained in rural northern Nevada (13 ± 18 ng m^{-3} reported for Paradise Valley, 7 ± 8 ng m^{-3} reported for Wells; Lyman and Gustin, 2008), and lower than those measured at the higher elevation site in north Reno, especially during spring and summer (Table 4-1). Mean GOM concentrations in this work and in north Reno were higher in the summer and lowest in the winter with intermediate spring and fall values. No strong seasonal trends in PBM concentrations existed in this data, nor were reported by Peterson et al. (2009) for north Reno (Table 4-1).

Predictors of GEM Concentrations. For the 2 h dataset, concentrations of GEM tended to be higher when wind speed and temperature were lower and dew point was higher (Table 4-2), indicating stagnant conditions with strong surface influence. The 24 h dataset (Table 4-3) showed similar results, except that no correlation with temperature was observed when data were separated by season. The Reno-Sparks area contains natural and anthropogenic mercury sources, and GEM likely builds up in the valley when processes to dilute emitted GEM are less active, and GEM concentrations likely decrease in high winds because they flush clean air through the valley. GEM measurements reported by Peterson et al. (2009) at the higher elevation site in Reno were often lower than those in this study (Table 4-1, Figure 4-3), providing further evidence for local, ground-based GEM sources.

Since wind speed and atmospheric mixing are usually higher during daytime, this phenomenon likely explains much of the diurnal variation in GEM concentrations observable in Figure 4-4. Similar results have been reported for the site in north Reno (Stamenkovic et al., 2007; Peterson et al., 2009; Weis-Penzias et al., 2009), and in other locations (e.g. Kim and Kim, 2001; Liu et al., 2002; Kock et al., 2005; Temme et al., 2007). The stronger diel trend of GEM in summer relative to winter likely reflects a consistent summertime cycle between a deep daytime mixed layer and a shallow nighttime surface layer, in contrast to winter conditions wherein convective mixing is typically weak. Oxidation of GEM to GOM may also be responsible for some of the daytime decrease in GEM concentrations, but the relative importance of this phenomenon could not be determined from this research.

Predictors of GOM Concentrations. Concentrations of GOM tended to be higher when temperature was higher and dew point was lower, and this relationship was consistent across all seasons for the 2 h and 24 h datasets (Tables 4-2 and 4-3). Weiss-Penzias et al. (2009) showed the same trends at three sites in Nevada in the summer of 2007 and suggested that this was due to subsidence of warm, dry, GOM-rich free-tropospheric air. In this work, GOM concentrations in summer 2007 were higher than in summer 2008 (Figure 4-2). Peterson et al. (2009) noted that summer 2007 had higher GOM concentrations than previous years and attributed this difference to abnormally warm and dry conditions in the region. Weiss-Penzias et al. (2009) further attributed inter-annual differences in GOM concentrations and differences among sites in the region to variations in the amount of transport of air from a high altitude source region.

While some laboratory evidence indicates that ozone may be a significant oxidizer of GEM, producing GOM (c.f. Pal and Ariya, 2004a), ozone was a poor predictor of GOM concentrations in the multiple regression analyses (Tables 4-2 and 4-3). Furthermore, temperature, solar radiation, dew point, and wind speed were all important predictors of ozone concentrations in the 2 h dataset, but only solar radiation and wind speed were important at the 24 h time scale, except in summer when none of these variables were significant. In contrast, dew point and temperature were strong predictors of GOM for both the 2 h and 24 h datasets, and solar radiation was not a consistent predictor in either dataset. This difference between GOM and ozone indicates that while their hourly-scale patterns were similar (i.e. both tended to be higher during daytime), their concentrations were likely driven by different processes.

The highest concentrations and strongest diel cycle of GOM occurred in the summer, when concentrations peaked at noon and then decreased fairly rapidly (Figure 4-4). This peak time was out of phase relative to the observed pattern for ozone and more similar to the expected trend for OH and other peroxy radicals (Monks, 2005), as was observed by Peterson et al. (2009) for the higher elevation site in Reno. However, the weak predictive value of solar radiation on GOM concentrations in both the 2 h and 24 h datasets suggests that local oxidation by photooxidants may not be a dominant factor driving GOM concentrations.

The strong negative predictive value of dew point with GOM (Tables 2 and 3; also see Weiss-Penzias et al., 2009) and the coincidence of diel GOM highs with dew point lows provide evidence that observed GOM concentrations were related to boundary layer dynamics, since convective mixing is expected to bring dry air from the free

troposphere to the surface. Moreover, ozone concentrations on the valley floor were higher than those at the higher elevation site, while GOM concentrations showed the opposite trend, especially in summer and fall (Table 4-1; Figure 4-3). Higher ozone concentrations on the valley floor indicate surface-level production, while higher GOM concentrations aloft further implicate the free troposphere as a GOM source.

An additional driver of the strong relationship between GOM and temperature may be that since GOM compounds are semivolatile they are more likely to exist in the gas phase at higher temperatures, and tend to partition into the particulate phase at lower temperatures (Finlayson-Pitts and Pitts, 1999; Rutter and Schauer, 2007). However, GOM and PBM were not anticorrelated ($r = 0.01$, $p = 0.34$), and the relationship between PBM and temperature was positive or insignificant, depending on the season and dataset used (Tables 2 and 3), providing evidence against this hypothesis. Even so, only the fine fraction of PBM was measured, and the complete picture of PBM in the Reno atmosphere is unknown.

These lines of evidence point to subsidence of GOM-rich air from aloft as a source of GOM to the atmosphere in Reno. Other mechanisms, such as local oxidation of GEM to GOM, are likely also contributors to observed GOM concentrations, but this analysis was unable to produce strong evidence for them. Also, while the predictors of GOM concentrations were consistent across all seasons, GOM concentrations were greatest in summer. Weiss-Penzias et al. (2009) showed that, even in summer, air masses which experienced rain were not associated with high concentrations of GOM, and a modeling study by Sillman et al. (2007) showed that high GOM concentrations tended to build up aloft only in cloud-free air. Winter and spring are relatively wet along the

central Pacific Coast and in western Nevada, and cloudy or rainy conditions may inhibit the buildup of GOM, effectively shutting off the free-tropospheric GOM source.

Predictors of PBM Concentrations. The dominant predictor of PBM concentrations for both 2 and 24 h averages was GEM, and this trend was consistent across all seasons. Though there may have been some causal relationship between GEM and PBM (i.e. GEM sorbs onto particles and becomes PBM), the authors hypothesize that the relationship was due primarily to GEM and PBM being emitted together from valley sources. When multiple regression equations were computed for PBM without GEM as an independent variable (data not shown), the only consistently significant (negative) predictor of PBM concentrations was wind speed, providing further support for this hypothesis. Concentrations of PBM at the valley floor site and the higher elevation site were similar.

Analysis of Wind Direction. Multiple regression equations with wind direction variables included were computed for a subset of the 2 h dataset. In this analysis, larger standardized regression coefficients would indicate a stronger influence of winds from a particular direction on observed concentrations. However, no strong source direction was found for any of the three measured atmospheric mercury fractions. Winds from the north and east were weak negative predictors of GOM concentrations (standardized regression coefficients of -0.15 and -0.12, respectively), while winds from all directions were weak negative predictors of PBM concentrations relative to periods with wind less than 0.5 m s^{-1} (standardized regression coefficients ranging from -0.15 to -0.18), indicating that no particular direction was a source of higher or lower PBM concentrations, but instead concentrations were highest when wind speeds were low.

Winds from the north had a slight negative effect on GEM concentrations (standardized regression coefficient of -0.12).

Relationships of GEM and PBM with Particulate Matter. GEM was correlated with <1 μm and <10 μm particulate matter measured with Dusttrak analyzers (r^2 = 0.31 and 0.30, respectively), as was PBM (r^2 = 0.26 and 0.32, respectively), and particulate matter measured with Dusttraks was included as an independent variable in multiple regression analyses. Since <1 μm and <10 μm particulate matter were well correlated with each other (r^2 = 0.80), multiple regression results were similar regardless of which size mode was used. For GEM, the standardized regression coefficient of <1 μm particulate matter (0.41) was slightly stronger than that for wind speed (-0.33). Particulate matter <1 μm was the strongest predictor of PBM concentrations also, with a standardized regression coefficient of 0.54. These correlations suggest that GEM and particulate matter were emitted together from valley sources and controlled by similar meteorological phenomena.

GEM and PBM concentrations were relatively low and stable during the summer of 2007, but were higher with higher variability in June and July 2008 (Figure 4-2). Extensive wildfires in northeastern California highly impacted the Reno airshed during the summer of 2008 (Arnott et al., 2008), and may have been sources of GEM and PBM (Friedli et al., 2003). The Dusttrak analyzers were not operating during either summer, but 24 h PM2.5 samples were collected at a site nearby. Concentrations of PM2.5 were only weakly correlated with 24 h average GEM concentrations (r^2 = 0.20 and 0.22 for the summers of 2007 and 2008, respectively), but they were well correlated with PBM concentrations, especially during the summer of 2008 (Figure 4-5; r^2 = 0.49 and 0.71 in

2007 and 2008, respectively). Peterson et al. (2009) compared PBM concentrations during wildfire events with concentrations in normal conditions and were unable to determine an effect of wildfires on PBM concentrations in Reno. However, PBM concentrations measured in this study in the summer of 2008 (12 ± 12 pg m^{-3}) were 104% higher than in the summer of 2007 (6 ± 4 pg m^{-3}), and concentrations in July 2008 (16 ± 15 pg m^{-3}) were 163% higher than in July 2007 (6 ± 5 pg m^{-3}; differences were significant at $\alpha = 0.001$).

Conclusions

Concentrations of GEM and PBM measured in Reno were impacted primarily by atmospheric pollution from local sources and by meteorological conditions that trapped pollution in the valley. No strong sources or source directions were detected for GEM or PBM except wildfires in summer 2008. Emissions of GEM and PBM were likely mostly from area-wide anthropogenic and natural sources. Statistical relationships developed in this study suggest that the processes controlling GOM concentrations and ozone concentrations were different and that GOM concentrations were influenced by downwelling of GOM-rich air from the free troposphere. Other processes likely also contributed to observed GOM concentrations, but this work was unable to produce strong evidence for them.

Acknowledgements

This research was funded by an EPA Local-Scale Air Toxics Ambient Monitoring Grant. The authors thank University of Nevada, Reno students Coty Weaver, Ben Sedinger, Melissa Markee, Joel Donalson, Christianna Peterson, and Zach Johnson for help maintaining the monitoring site in Reno, Patrick Arnott of the University of Nevada, Reno for loaning the DustTrak analyzers, Lauri Mendoza at the Washoe County Health District for providing PM2.5 data, and Jonathan Kelley of the University of Nevada, Reno for instruction in statistical methodology.

Tables and Figures

Table 4-1. Seasonal summary statistics for atmospheric mercury and ozone concentrations and select meteorological parameters from February 2007 through January 2009. Values from Peterson et al. (2009) are from a higher elevation site in north Reno, and represent data collected from November 2004 to November 2007.

						Temp-	Dew-	Wind	Peterson et al. (2009)			
		GEM	GOM	PBM	Ozone	erature	point	Speed	GEM	GOM	PBM	Ozone
		ng m^{-3}	pg m^{-3}	pg m^{-3}	ppb	℃	℃	m s^{-1}	ng m^{-3}	pg m^{-3}	pg m^{-3}	ppb
SPRING	**Mean**	1.8	16	5	38	10.7	-4.2	2.6	1.6	15	8	33
Mar-May	**Median**	1.8	10	5	41	9.9	-4.1	1.9	1.5	13	7	33
	St. Dev.	0.5	18	5	18	7.6	4.7	2.3	0.3	14	4	9
	Max.	4.4	177	75	84	33.3	8.4	13.8				
SUMMER	**Mean**	2.0	36	9	41	22.4	1.6	2.3	1.3	51	8	39
Jun-Aug	**Median**	1.7	29	7	41	22.8	1.8	1.6	1.3	52	6	40
	St. Dev.	0.8	26	9	19	7.0	4.3	1.9	0.3	29	6	7
	Max.	9.8	157	161	102	39.4	15.7	10.7				
FALL	**Mean**	2.2	15	7	25	11.3	-1.8	2.0	1.6	31	10	20
Sep-Nov	**Median**	2.0	10	7	24	10.7	-1.7	1.2	1.6	27	9	18
	St. Dev.	0.7	17	5	17	8.4	4.5	1.8	0.3	24	6	11
	Max.	5.4	138	83	72	33.9	12.8	10.2				
WINTER	**Mean**	2.2	4	7	20	1.0	-5.6	2.0	1.8	7	9	13
Dec-Feb	**Median**	2.1	2	5	19	0.2	-5.8	1.2	1.7	5	7	11
	St. Dev.	0.6	6	5	16	5.6	3.9	2.0	0.5	7	8	10
	Max.	6.2	68	69	56	19.1	6.9	13.0				
ANNUAL	**Mean**	2.0	18	7	31	11.5	-2.5	2.2	1.6	26	9	26
	Median	1.9	10	6	32	10.7	-2.5	1.4	1.5	11	7	26
	St. Dev.	0.7	22	7	19	10.5	5.2	2.0	0.5	35	10	20
	Max.	9.8	177	161	102	39.4	15.7	13.8	6.4	401	180	99

Table 4-2. Pearson correlation coefficients (for the entire dataset) and r^2 values and standardized regression coefficients for multiple linear regression (for the entire dataset and for each season) for 2 h average data. Statistically insignificant regression coefficients ($\alpha = 0.01$) are denoted as "insig."

2 HOUR AVERAGED DATASET

			M.L.R. r^2	Temp.	Dewpt.	Sol. Rd.	Wnd. Sp.	GEM	Ozone
GEM		**Correlations**		-0.32	0.24	-0.30	-0.47		
	Multiple Lin. Regression	**All Data**	0.36	-0.40	0.39	insig.	-0.30		
		Spring	0.26	-0.29	0.14	insig.	-0.31		
		Summer	0.51	-0.34	0.45	insig.	-0.21		
		Fall	0.37	-0.32	0.29	insig.	-0.31		
		Winter	0.25	-0.11	0.24	insig.	-0.42		
GOM		**Correlations**		0.69	0.17	0.43	0.15	-0.24	0.47
	Multiple Lin. Regression	**All Data**	0.52	0.82	-0.23	0.05	-0.11	insig.	insig.
		Spring	0.44	0.73	-0.29	insig.	-0.19	-0.07	insig.
		Summer	0.35	0.45	-0.22	0.21	-0.13	insig.	insig.
		Fall	0.43	0.77	-0.23	insig.	insig.	0.26	insig.
		Winter	0.46	0.89	-0.53	-0.20	insig.	0.15	-0.19
PBM		**Correlations**		0.06	0.19	-0.05	-0.21	0.41	
	Multiple Lin. Regression	**All Data**	0.21	0.27	-0.06	insig.	-0.08	0.47	
		Spring	0.20	0.15	-0.13	insig.	0.10	0.51	
		Summer	0.22	0.15	insig.	-0.10	insig.	0.42	
		Fall	0.10	0.14	insig.	insig.	-0.21	0.22	
		Winter	0.44	0.18	-0.24	0.11	-0.19	0.59	
OZONE		**Correlations**		0.67	0.00	0.54	0.57		
	Multiple Lin. Regression	**All Data**	0.67	0.60	-0.23	0.15	0.33		
		Spring	0.64	0.44	-0.25	0.11	0.41		
		Summer	0.65	0.59	-0.24	0.14	0.08		
		Fall	0.71	0.58	-0.14	0.11	0.34		
		Winter	0.59	0.24	-0.12	0.20	0.59		

Table 4-3. Pearson correlation coefficients (for the entire dataset) and r^2 values and standardized regression coefficients for multiple linear regression (for the entire dataset and for each season) for 24 h average data. Statistically insignificant regression coefficients ($\alpha = 0.01$) are denoted as "insig."

24 HOUR AVERAGED DATASET

			M.L.R. r^2	Temp.	Dewpt.	Sol. Rd.	Wnd. Sp.	GEM	Ozone
GEM		**Correlations**		-0.10	0.16	-0.23	-0.43		
	Multiple Lin. Regression	**All Data**	0.27	-0.28	0.38	insig	-0.38		
		Spring	0.05	insig	insig	insig	-0.22		
		Summer	0.33	insig	0.47	insig	-0.30		
		Fall	0.30	insig	0.42	insig	-0.43		
		Winter	0.36	insig	0.25	insig	-0.54		
GOM		**Correlations**		0.76	0.39	0.61	0.05	-0.15	0.46
	Multiple Lin. Regression	**All Data**	0.64	1.11	-0.37	insig	insig	insig	insig
		Spring	0.62	1.04	-0.53	-0.31	-0.24	-0.16	insig
		Summer	0.39	0.73	-0.47	insig	insig	-0.21	insig
		Fall	0.52	0.82	-0.34	insig	insig	0.31	insig
		Winter	0.65	1.02	-0.72	insig	insig	insig	insig
PBM		**Correlations**		0.23	0.22	0.11	-0.26	0.52	
	Multiple Lin. Regression	**All Data**	0.37	0.46	-0.20	insig	insig	0.57	
		Spring	0.43	insig	-0.25	insig	0.21	0.62	
		Summer	0.36	insig	insig	insig	insig	0.54	
		Fall	0.28	0.58	insig	insig	-0.38	insig	
		Winter	0.73	0.30	-0.45	insig	-0.21	0.74	
OZONE		**Correlations**		0.58	0.26	0.69	0.50		
	Multiple Lin. Regression	**All Data**	0.64	0.20	insig	0.48	0.40		
		Spring	0.54	insig	insig	0.32	0.56		
		Summer	0.09	insig	insig	insig	insig		
		Fall	0.60	insig	insig	0.44	0.47		
		Winter	0.64	-0.20	insig	0.16	0.82		

Figure 4-1. Map of the Reno-Sparks area, including the study site from this work and the site in north Reno (Peterson et al., 2009). Lighter shading indicates higher elevation.

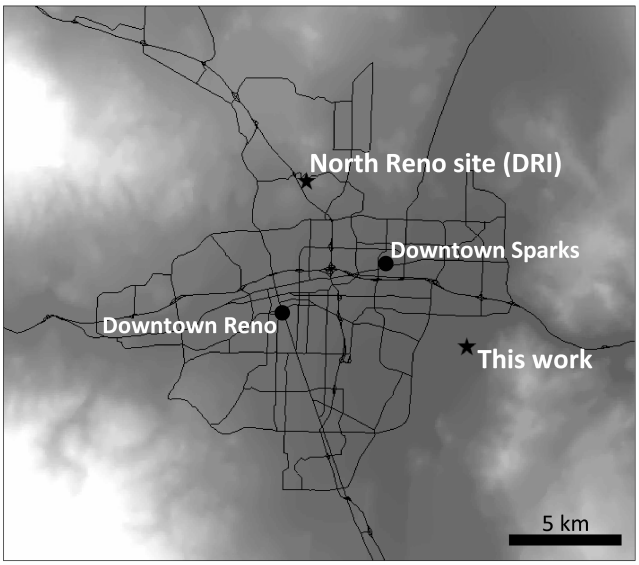

Figure 4-2. Time series of GEM, PBM, GOM, and ozone using 24 h averages.

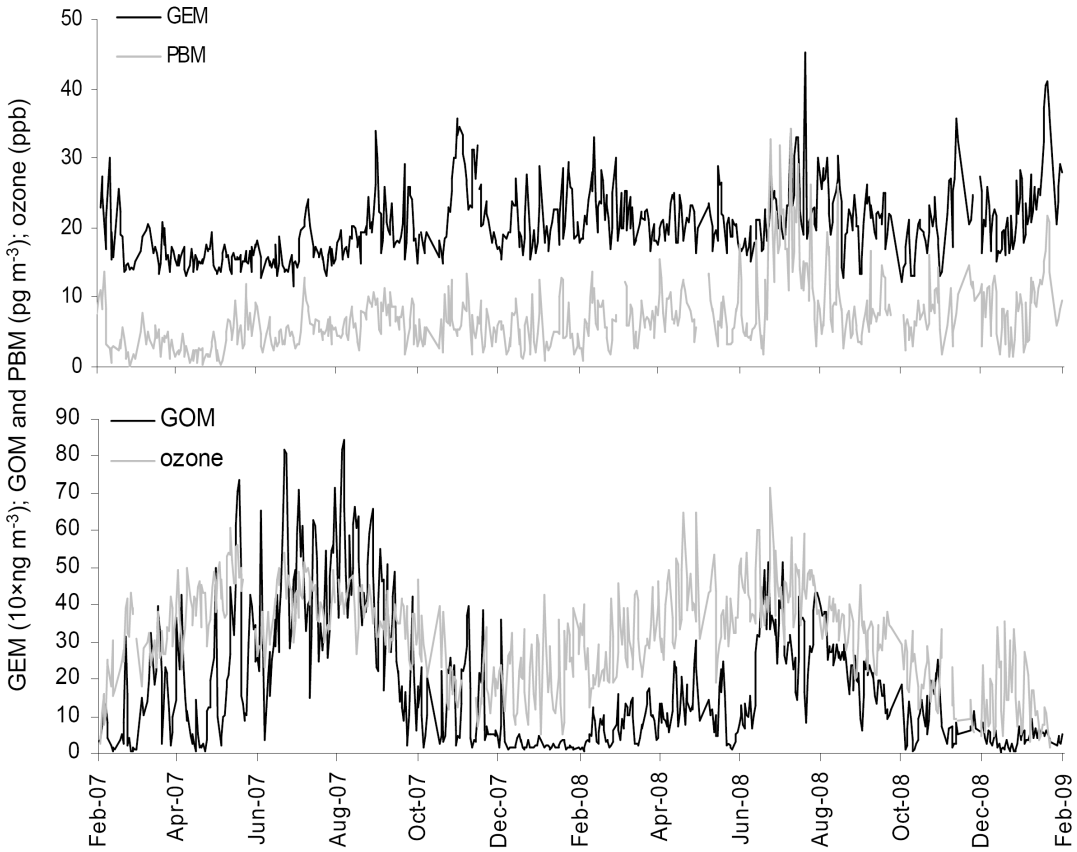

Figure 4-3. Time series of GEM and GOM in 2007 at the Reno valley floor and at the higher elevation site from Peterson et al. (2009).

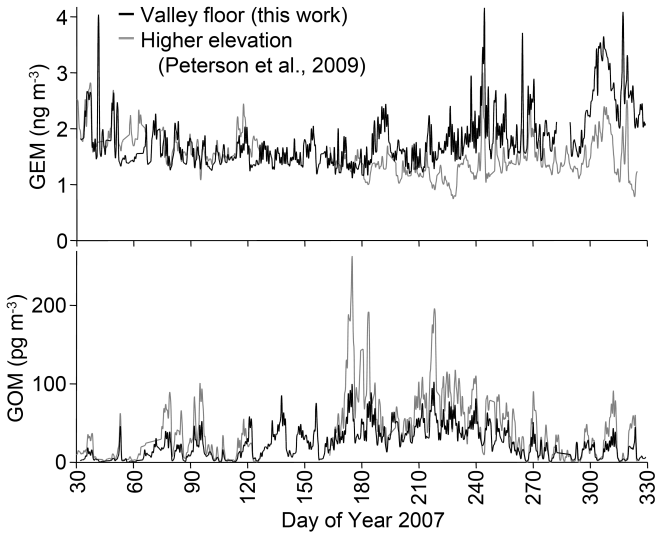

Figure 4-4. Seasonal mean hour-of-day plots of GEM, GOM, PBM, and ozone concentrations and dew point derived from 2 h average data. Whiskers represent standard error.

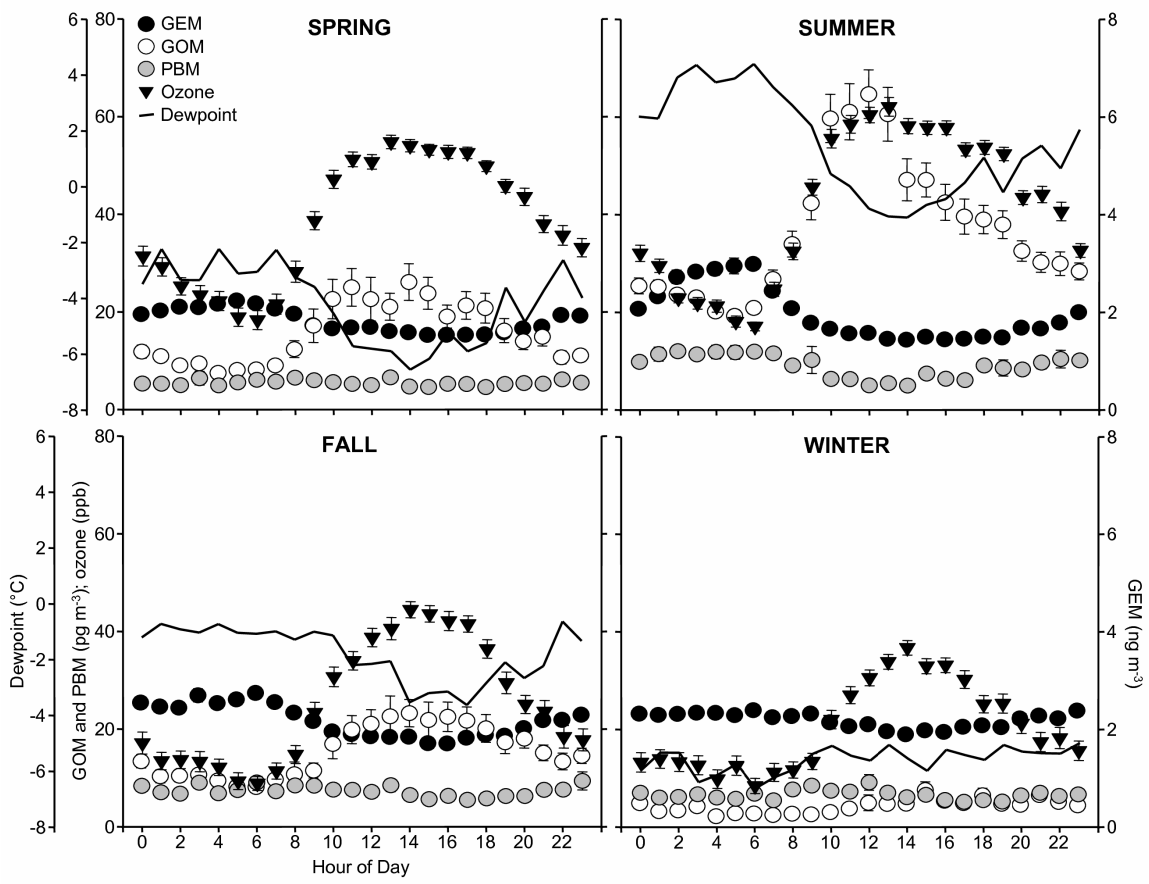

Figure 4-5. Concentrations of PM2.5 versus PBM concentrations during the summers of 2007 and 2008.

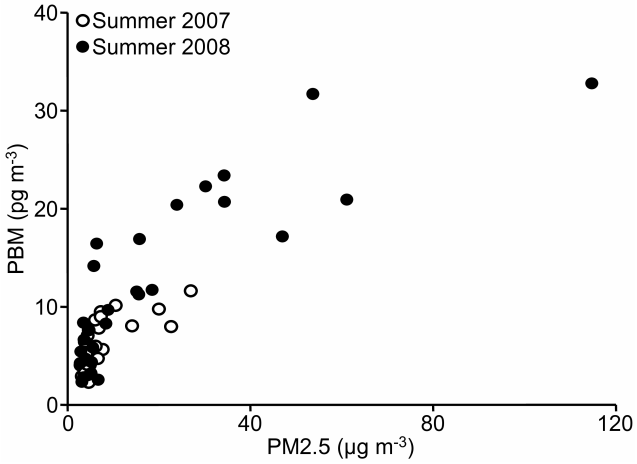

Chapter 5: Cation-exchange membranes as surrogate surfaces for gaseous oxidized mercury dry deposition

Seth N. Lyman[†], Mae S. Gustin[†], Eric M. Prestbo[‡α], Philip I. Kilner[‡α], Eric Edgerton[§], and Ben Hartsell[§]

†University of Nevada, Reno, Department of Natural Resources and Environmental Science/MS 370, 1664 North Virginia Street, Reno, Nevada, 89557

‡Frontier Geosciences, 414 Pontius Avenue North, Seattle, Washington, 98109

§Atmospheric Research & Analysis, Inc., 730 Avenue F, Suite 220, Plano, Texas, 75074

αNow with Tekran Instruments Corporation

(Submitted to *Environmental Science and Technology* in April 2009)

Abstract. This paper describes the development and application of a surrogate surface for estimating gaseous oxidized mercury dry deposition. The response of surfaces to gaseous oxidized mercury exposures and environmental conditions was tested in laboratory chambers and in diverse field environments. Deposition of mercury to surfaces in the field was well correlated with gaseous oxidized mercury concentrations ($r^2 = 0.84$, $p < 0.01$, $n = 326$) and not with gaseous elemental or particulate-bound mercury concentrations. Laboratory tests showed that the surfaces collected $HgCl_2$, $HgBr_2$, and HgO with equal efficiency, and deposition to the surfaces was not significantly influenced by temperature, humidity, or ozone concentrations. Since deposition of gaseous oxidized mercury to surrogate surfaces is uniform and consistent, measured

deposition is an oversimplification of expected deposition to complex natural surfaces. However, the surrogate surface method is useful for determining the spatial and temporal variability and maximum potential of gaseous oxidized mercury dry deposition.

Introduction

Deposition of mercury from the atmosphere can lead to contamination of water bodies and fish, posing a health risk to humans and wildlife that consume fish (Fitzgerald et al., 1998; Mergler et al., 2007). Methods for measurement of mercury deposition in precipitation are relatively straightforward, and measurements are made routinely at many sites throughout North America (c.f. http://nadp.sws.uiuc.edu/mdn/). However, methods for measurement of mercury dry deposition are not well developed and scientific understanding of dry deposition rates and trends is limited.

Atmospheric mercury is typically measured as three fractions: gaseous elemental mercury (GEM), gaseous oxidized mercury (GOM, a.k.a. RGM), and particulate-bound mercury (PBM) (Landis et al, 2002). Among these, GOM is thought to be of particular importance as a component of total mercury dry deposition because of its high solubility and reactivity (Lindberg et al., 2007). However, because of low concentrations and the relatively low precision of GOM measurement methods, micrometeorological methods to measure GOM surface flux have proven difficult and have only been carried out in a few studies (Lindberg and Stratton, 1998; Poissant et al., 2004; Skov et al., 2006; deposition velocities ranging from 0.4 to 7.6 cm s^{-1}). Surrogate surfaces have been applied to measure mercury dry deposition, including water surfaces (Sakata and Marumoto, 2005; Marsik et al., 2007) and cation-exchange membranes (Caldwell et al., 2006; Lyman et al., 2007). Surrogate surfaces are attractive because they do not have the strict siting, precision, and measurement frequency requirements of micrometeorological methods, and they are cheaper and less labor intensive. However, the depositional behavior of a gas to a surrogate surface cannot be assumed to be the same as depositional behavior to a

natural surface (Wesely and Hicks, 2000), and surrogate surface results must be weighed in light of this uncertainty.

In this study, the cation-exchange membrane surface applied by Lyman et al. (2007), and first used by Prestbo et al. (2005), was tested extensively with the intent to answer the following questions: (1) What are optimal procedures for deployment and collection of the surface? (2) How consistently does the surface perform in different climatological and geographical settings? (3) How well does deposition to the surface compare to expected GOM deposition to natural surfaces? (4) How much statistical and logical uncertainty exist in the surrogate surface measurements? To answer these questions, long-term (1 yr) and short-term (3 months) deployment campaigns were carried out at four locations in the United States, and surfaces were subjected to varying chemical and climatological conditions in two controlled laboratory chambers.

Methods

Surrogate Surface. Supported I.C.E. 450 membrane (Pall Corporation, P/N ICE45S3R), an acidic, negatively-charged polysulfone cation-exchange membrane, was used as the surrogate surface. The supported membrane, which has a fibrous polyester backing, was used because unsupported I.C.E. 450 membrane, which consists of an activated polyethersulfone material, was more fragile and tended to have much higher mercury concentrations in blanks.

Two types of mounts were used to hold membranes when deployed. The first was a simple rectangular acrylic plate with an acrylic fastener to hold the membrane against the plate (107 cm^2 surface area). This mount was not aerodynamic and was not resistant

to contamination from precipitation (Lyman et al., 2007). The second mount was an aerodynamic polyoxymethylene disc (104 cm^2 surface area) which, when sealed on top with petroleum jelly, shielded the deployed membrane against precipitation except during heavy, windy rain events. Both mounts were deployed with the exposed surface facing downward in field deployments except as otherwise noted. Data from rain-contaminated surfaces were not used. Rectangular mounts were scrubbed with soap and soaked in a 5% HNO_3 bath for at least 12 h between each use, and aerodynamic mounts were scrubbed with soap and soaked in a 10% HCl bath for 12-24 h between each use.

Membranes were loaded into mounts on site in unfiltered ambient air and were only handled with PTFE-coated tweezers. After deployment, membranes were collected into trace-clean 125 mL I-Chem jars and stored at -20°C until analysis. Also, three or four membranes from the same lot deployed were collected and used as method blanks. Data were blank corrected using method blanks. Field blanks were collected by placing surfaces in clean mounts and then immediately collecting them, and field blanks were not different from method blanks ($p = 0.80$). Membrane analytical procedures and deposition rate and deposition velocity calculations were as in Lyman et al. (2007).

Field Deployments. Samples were deployed at Mercury Deposition Network (MDN) site NV98 in Reno, Nevada (39.51°N, 119.72°W, elevation 1340 m); MDN site NV02 in Paradise Valley, Nevada (41.50°N, 117.50°W, elevation 1388 m); Southeastern Aerosol Research and Characterization (SEARCH) network site OLF in Pensacola, Florida (30.55°N, 87.38°W, elevation 44 m); and SEARCH network site YRK near Yorkville, Georgia (33.93°N, 85.05°W, elevation 394 m).

All field deployments occurred between October 2006 and October 2008. All deployments were carried out as sets of three or four samples, and deployments were for one week unless otherwise noted. Regular deployments of surfaces in aerodynamic mounts were carried out for 64 weeks in Reno and 49 weeks in Pensacola and Yorkville. Regular deployments in rectangular mounts were carried out for 66 weeks in Reno and 11 weeks in Paradise Valley, and all method and surface comparison deployments were carried out in Reno. Surrogate surfaces were also deployed in rectangular mounts for eight weeks in a network deployment effort in summer 2008 in Reno, Paradise Valley, Wells, and Ruby Valley, Nevada.

A suite of ancillary data was collected at all field sites during surrogate surface deployments except during the Nevada network deployment. Ancillary data included GEM, GOM, and PBM concentrations measured with Tekran 2537A/1130/1135 mercury speciation systems (Landis et al., 2002) and standard meteorological data. Ozone concentrations were measured in Reno. More information about field sites and field data collection is available in the Supporting Information.

Comparisons of Different Surfaces and Deployment Methods. To compare mercury deposition rates to different surfaces, cation-exchange membrane surfaces were deployed simultaneously with PTFE filters (n = 1 deployment), KCl-impregnated quartz fiber filters (n = 3), the unsupported version of the cation-exchange membrane (n = 4), and the cation-exchange membrane deployed with the backing side out (n = 8).

To determine the effect of deployment time on deposition rates, the total amount of mercury deposited to surfaces in rectangular mounts in two consecutive one-week sample sets was compared against the total amount of mercury deposited to a sample set

deployed for the entire two weeks. Also, the total amount of mercury deposited to surfaces in two consecutive two-day sample sets and one consecutive three-day sample set was compared against the total amount of mercury deposited to a sample set deployed for the entire one week. Each of these deployment time tests was replicated.

To determine the influence of surface orientation on deposition, surfaces in acrylic mounts deployed down-facing were compared against surfaces deployed up-facing (n = 31). To determine the difference between mount types, surfaces deployed in rectangular mounts and aerodynamic mounts were compared (n = 25). Tests to determine the influence of deployment location on deposition were also carried out, and information about these tests is available in the Supporting Information. All comparison tests and method tests were carried out during periods with average GOM concentrations greater than 5 pg m^{-3}.

Controlled Chamber Experiments. Surrogate surfaces were deployed in two different chambers to determine whether air chemistry and/or environmental factors influenced deposition. In Chamber 1, GEM concentrations were manipulated in ambient air (n = 10 deployments) or in air scrubbed of all mercury with an activated carbon cansiter (n = 13) to determine whether the surfaces collect GEM. Chamber 2 was used to determine how deposition of GOM to surfaces varied with GOM concentration, GOM species ($HgCl_2$, $HgBr_2$, and HgO), humidity, temperature, and ozone concentration (n = 3 or more deployments for each unique chamber condition). More information about chamber experiments is available in the Supporting Information.

Data Analysis and Model. Data processing and summary statistics were carried out in Microsoft Excel 2003. Correlation and linear regression routines were carried out in

SPSS 16.0, and Student t-tests (used to test the similarity of two datasets) were carried out in Kaleidagraph 4.02. Unless otherwise specified, all statistical values and comparisons were significant at $\alpha = 0.01$. A dry deposition model (Lyman et al., 2007; Zhang et al., 2003; constructed in Microsoft Excel 2003) was used to estimate GOM deposition at field sites during surrogate surface deployments. More information about this model is available in the Supporting Information.

Results

Detection Limit and Blank Correction. The detection limit for seven day deployments, calculated as three times the standard deviation of blanks, was 0.05 ± 0.05 ng m^{-2} h^{-1} (mean ± standard deviation) or 0.9 ± 0.8 pg m^{-3} of GOM (derived from the mean deposition velocity of GOM to surfaces deployed in aerodynamic mounts). Calculating the detection limit as three times the standard deviation of samples deployed during weeks with GOM concentrations less than 1 pg m^{-3} yielded a value of 0.07 ± 0.04 ng m^{-2} h^{-1} or 1.2 ± 0.7 pg m^{-3} of GOM. In addition to method blanks, field samples were blank corrected using the deposition rate from deployment periods that had average GOM concentrations less than 1 pg m^{-3} (0.20 ng m^{-2} h^{-1}) to account for sampler contamination. More information about blank corrections is available in the Supporting Information.

Comparisons of Different Surfaces. The PTFE filters collected 84% less mercury than cation-exchange membranes ($p = 0.02$). Quartz fiber filters impregnated with KCl collected 97 ± 0% less mercury than cation-exchange membranes. Unsupported membranes collected 15 ± 8% less mercury than supported membranes ($p = 0.11$). In Lyman et al. (2007), supported cation-exchange membranes were incorrectly deployed

with the polyester backing side exposed. Membranes with the backing exposed collected 53 ± 8% less mercury than correctly deployed membranes, and the surrogate surface results of Lyman et al. (2007) are biased by this amount.

Comparisons of Different Deployment Methods. Surfaces deployed for two weeks collected 10 ± 1% less mercury than the sum of two corresponding sets of surfaces deployed consecutively for one week each. Surfaces deployed for one week were not different than the sum of three corresponding sets of surfaces deployed for shorter periods ($p = 0.70$). The deposition velocity of GOM to up-facing surfaces was 9% higher than to down-facing surfaces ($p = 0.06$). Deposition rates for surfaces deployed in either direction were not correlated with concentrations of GEM and PBM, but solar radiation was a significant negative predictor for deposition to up-facing surfaces when added with GOM as an independent variable in a multiple regression routine. The mean deposition velocity of GOM to surfaces deployed in rectangular mounts (1.8 ± 0.8 cm s^{-1}) was 60% higher than to surfaces in aerodynamic mounts (1.1 ± 0.5 cm s^{-1}). Deposition to surfaces deployed in both mounts were well correlated with GOM concentration ($r^2 = 0.90$ and 0.91, respectively).

Field Results. At all sites, deposition of mercury to surfaces was correlated with average GOM concentration and was not well correlated with GEM or PBM concentrations (Table 5-1, Figure 5-1). The correlation of deposition in Yorkville with GEM and PBM reflects the fact that GOM in Yorkville was correlated with GEM and PBM ($r^2 = 0.41$ and 0.33, respectively). Deposition of mercury to surfaces was correlated with modeled GOM dry deposition, but the strength of this correlation varied with location (Table 5-1). The deposition velocity of GOM to surfaces in aerodynamic mounts was 564 ± 258%

greater than modeled GOM deposition velocity in Reno and 182 ± 173% and 112 ± 149% greater than modeled deposition velocity in Pensacola and Yorkville, respectively (Table 5-1).

To assess whether wind speed, temperature, or humidity influenced deposition rates, each of these variables was added with GOM as an independent variable to predict deposition to surfaces in multiple linear regression analyses. All of these variables were significant co-predictors of deposition in Reno, but temperature (positive relationship) and humidity (negative relationship) each only increased r^2 by 1%, and wind speed (positive relationship) increased r^2 by 3%. Wind speed wasn't a significant co-predictor in Pensacola or Yorkville ($p = 0.32$ and 0.48, respectively), but temperature and humidity were; adding temperature increased r^2 by 8 and 7% in Pensacola and Yorkville, respectively (positive relationship), and adding relative humidity increased r^2 by 14% in Yorkville (negative relationship). In Reno, ozone was not a significant co-predictor of mercury deposition to surfaces.

The deposition velocity of GOM to surfaces in rectangular mounts deployed in Paradise Valley (3.7 ± 0.9 cm s^{-1}) was 84% higher than the deposition velocity to surfaces in rectangular mounts in Reno during the same period (2.0 ± 0.4 cm s^{-1}). The average GOM concentration in Paradise Valley (25 ± 10 pg m^{-3}) was 47% lower than in Reno (48 ± 8 pg m^{-3}), and the amounts of mercury deposited to surfaces (i.e. deposition rates) at the two sites were not different ($p = 0.12$). The 2008 network deployment also showed that sites across northern Nevada had similar deposition rates, especially Reno and Paradise (Figure 5-2).

Chamber Results. Surrogate surface deployments in Chamber 1 showed that deposition to surfaces was dependent on the amount of GEM added to the chamber if inlet air was scrubbed of mercury via an activated carbon canister ($r^2 = 0.70$; TGM concentrations ranged from 0.0 to 10.4 ng m^{-3}), but deposition was not dependent on the amount of GEM added if inlet air was particulate-filtered ambient air ($r^2 = 0.06$, p= 0.20; TGM concentrations ranged from 2.2 to 12.7 ng m^{-3}).

Deposition of mercury to surfaces in Chamber 2 was linearly dependent on GOM concentration within the chamber (Figure 5-3, $r^2 = 0.95$ for deployments with $HgCl_2$ permeated and constant temperature and humidity), and not dependent on GEM concentration ($r^2 = 0.07$, p = 0.25). The deposition velocity to surfaces exposed to HgO (0.43 ± 0.08 cm s^{-1}) and $HgBr_2$ (0.37 ± 0.04 cm s^{-1}) was not different from the deposition velocity of surfaces exposed to $HgCl_2$ (0.39 ± 0.05 cm s^{-1}; p = 0.29 and 0.24 for HgO and $HgBr_2$ respectively). Deposition to surfaces in high relative humidity (0.42 ± 0.06 cm s^{-1}, 76 ± 7% humidity) and high ozone concentrations (0.48 ± 0.16 cm s^{-1}, 135 ± 6 ppb ozone) were not different from deposition in normal chamber conditions ($HgCl_2$ permeated, 22 ± 6% relative humidity, 3 ± 2 ppb ozone; p = 0.33 and 0.15, respectively).

The deposition velocity to surfaces deployed in Chamber 2 at low temperature (0.88 ± 0.25 cm s^{-1}, -1.4 ± 1.6°C) was higher than in normal chamber conditions (24.0 ± 1.2°C). This negative relationship between deposition velocity and temperature is in contrast to field results, which showed a slight positive relationship. Moreover, surfaces deployed in Chamber 2 with an average temperature that was slightly above freezing (2.4°C) yielded deposition velocities that were not different (0.40 ± 0.12 cm s^{-1}, p = 0.98) from those under normal chamber conditions, indicating that the chamber temperature

effect was not linear. Surrogate surfaces were deployed close to the chamber air inlet, while GOM measurements were taken from the outlet on the other side of the chamber (see diagram in Supporting Information), and the authors hypothesize that GOM deposited on the cold, frosty chamber walls while traveling from the inlet to the outlet, biasing GOM measurements low and giving surrogate surface deposition velocities the appearance of being biased high.

The deposition velocity of GOM to surfaces deployed in the chamber was 72% lower than to surfaces deployed in rectangular mounts at the Reno field site, and this difference is thought to be due to differences in turbulent dynamics between the chamber and field sites.

Surrogate Surface Resistance. The Lyman et al. model (2007) calculates deposition velocity (V_d) as

$V_d = 1/(R_a + R_b + R_c)$,

where R_a and R_b are the aerodynamic and quasi-laminar sublayer resistances, respectively, and R_c is the surface resistance. R_a and R_b are dependent on atmospheric turbulence, while R_c is influenced by a variety of meteorological and surface conditions. Since R_a and R_b are not surface-dependent and the deposition velocity to surrogate surfaces is known, the surface resistance (R_c) of surrogate surfaces was calculated as

$R_c = 1/V_d - R_a - R_b$.

This resulted in a calculated surface resistance value of 0 ± 113 s m^{-1} for surrogate surfaces deployed at field sites in aerodynamic mounts, compared with modeled natural surface resistances of 614 ± 214 s m^{-1} in Reno, 147 ± 44 s m^{-1} in Pensacola, and 173 ± 45 s m^{-1} in Yorkville.

When modeled surface resistance was set to a constant low value of 10 s m^{-1} as recommended by Wesely (1989) for highly soluble and reactive compounds, the model more closely approximated the magnitude of measured deposition to surfaces (deposition to surfaces was 14 ± 49% higher than modeled deposition in Reno ($p = 0.04$) and 8 ± 82% and 11 ± 75% lower in Pensacola and Yorkville, respectively ($p = 0.12$ in Pensacola)). What is more, the deposition velocity of GOM to surrogate surfaces correlated much better with modeled GOM deposition velocity when R_c was set to 10 s m^{-1} ($r^2 = 0.83$ for all sites combined) than if R_c was calculated normally ($r^2 = 0.47$).

Trends in Deposition. Annual dry deposition of GOM to surrogate surfaces was 6.8 μg m^{-2} in Reno (missing weeks were given seasonal average values), 0.7 μg m^{-2} in Pensacola (90% less than Reno), and 1.9 μg m^{-2} in Yorkville (73% less than Reno; Table 5-2). Annual dry deposition of GOM to surrogate surfaces in Reno was 342% greater than wet deposition measured at the site as part of the MDN network (1.5 μg m^{-2}). An MDN site, GA40, exists in Yorkville, but data through September 2008 are not yet available. Using the average annual wet deposition for 2005, 2006, and 2007, annual dry deposition of GOM to surrogate surfaces in Yorkville was 83% less than annual wet deposition (10.7 μg m^{-2}). Using average annual wet deposition for 2005, 2006, and 2007 from MDN site AL24 (122 km from Pensacola), annual dry deposition of GOM to surrogate surfaces in Pensacola was 95% less than wet deposition (13.6 μg m^{-2}).

At all sites in the northern Nevada network deployment, deposition to surfaces was correlated to GOM concentrations measured in Reno ($r^2 = 0.48$ to 0.73; Figure 5-2). Also, the deposition rate at each northern Nevada site was correlated with deposition rates at other sites ($r^2 = 0.81$-0.92). Similarly, deposition rates in Pensacola and

Yorkville were correlated ($r^2 = 0.38$) during 49 weeks of simultaneous deployment. Deposition in Pensacola and Yorkville peaked in late winter and spring (Figure 5-4; Table 5-2), whereas deposition in Reno showed a peak in spring followed by a greater peak in mid-summer. As expected, the seasons with the highest deposition rates also had the highest GOM concentrations. However, the deposition velocity of GOM to surfaces in Reno was also higher in spring and summer relative to other seasons (Table 5-2), which enhanced the effect of increased GOM concentration on the deposition rate.

Discussion

This work shows that the cation-exchange membrane surface is a useful surrogate for characterizing GOM dry deposition. Mercury deposition to surrogate surfaces was correlated with GOM concentration and with modeled GOM dry deposition at sites with very different conditions. Surface resistance calculations showed that the surrogate surface is extremely efficient at collecting GOM. Chamber and field data showed that the effects of temperature, humidity, and GEM concentrations on deposition to surfaces were likely small or non-existent. The observed influence of temperature and humidity on deposition of GOM to surfaces in Pensacola and Yorkville were likely statistical artifacts, given that GOM concentration was well correlated with those parameters at those sites (data not shown). Moreover, deposition to surfaces was not dependent on natural surface variability (i.e. with variability of R_c in the dry deposition model), and differences in GOM deposition to surfaces were largely explained by differences in turbulent transfer rates (represented by R_a and R_b in the model).

The weaker correlation between GOM concentration and deposition to surfaces in Pensacola and Yorkville relative to Reno may have been due to limitations of the method used to collect GOM data. Measurements of GOM made by the Tekran system are not continuous, and the systems in Pensacola and Yorkville utilized a 1 h sampling period and a 1 h desorption period, measuring only 50% of the GOM experienced by surrogate surfaces during each deployment period. The system in Reno utilized a 2 h sampling period and a 1 h desorption period, measuring GOM for 67% of each deployment period. Additionally, GOM in Reno exhibited relatively predictable, regular diel cycles with periodic synoptic-scale enhancements (Weiss-Penzias et al., 2009), and the missing 33% of data in Reno was probably fairly well represented by the collected data. In Pensacola and Yorkville GOM concentrations tended to be strongly influenced by plumes from nearby point sources (Edgerton et al., 2006), making the GOM datasets at these sites more skewed (i.e. less predictable; Pensacola and Yorkville weekly GOM datasets had Pearson's skewness coefficients that were 51% and 32% higher, respectively, than in Reno). Median GOM concentrations predicted deposition more poorly than mean concentrations in Pensacola and Yorkville, showing that the surfaces detect mean GOM deposition. Also, integrating the area under the curve for GOM concentrations did not predict deposition to surfaces better than mean GOM concentration.

Limitations. The down-facing orientation of surfaces was designed to minimize deposition of coarse particles, but coarse PBM was not measured at field sites (the Tekran system measures only fine mode PBM), so this study could not definitively determine whether coarse PBM influenced deposition of mercury to surfaces. Fine PBM did not correlate with deposition to surfaces, but all sites had low average PBM

concentrations (5 ± 4 pg m^{-3} for all deployments at all sites), so it is unknown whether high concentrations of fine PBM would influence deposition.

While the uniform surface resistance of the surrogate surface allows for easy comparison of results among sites and across time, it is likely unrepresentative of GOM deposition in the real world. Deposition of GOM to natural surfaces will vary not just with variations in turbulence (i.e. variations in R_a and R_b), but with variations in leaf area, vegetation, soil type, humidity, temperature, surface wetness, etc. (i.e. variations in R_c). Thus, surrogate surfaces likely oversimplify reality. This problem may be able to be partially overcome by scaling surrogate surface results to leaf area or "calibrating" results using micrometeorological measurements or models.

It is impossible for surface resistance to any surface to be less than the calculated surrogate surface resistance of 0 s m^{-1}, but very few direct measurements of GOM dry deposition to natural surfaces have been published for comparison, so the extent to which deposition to the surrogate surface over-represents reality is unknown. Nonetheless, it is safe to regard the surrogate surface as an upper limit of possible GOM dry deposition.

The higher deposition rate to surfaces in rectangular mounts relative to aerodynamic mounts was likely due to artificial turbulence created by the rectangular mounts. However, even the aerodynamic mounts should not be expected to have turbulent properties similar to natural surfaces such as leaves, soil, or tree bark, so this presents another deviation from real conditions. Finally, the surfaces measure only GOM dry deposition, not total mercury dry deposition (i.e. GOM + GEM + PBM). Because some collected mercury appears to be re-volatilized from the surrogate surfaces if they

are deployed face up and exposed to high solar radiation, the surfaces should not be deployed face up to collect PBM in addition to GOM.

Applications. While the surrogate surface is unable to capture the influence of natural surface variability, it can detect variability in GOM concentration and atmospheric turbulence. Thus, it has utility for tracking changes in GOM deposition over time and for assessing regional or global trends in GOM dry deposition.

The data collected in this study showed that, even considering the uncertainty inherent in surrogate surfaces, dry deposition of GOM in Reno is an extremely important part of total mercury deposition. In contrast, deposition of GOM in Pensacola and Yorkville is a small component of total mercury deposition, especially since the surrogate surfaces may over-represent real GOM deposition. Correlations among different sites in northern Nevada and in the Southeast showed that the processes leading to GOM deposition are regional in scale. In future studies, long-term surrogate surface deployments like those conducted in this work could be used in tandem with periodic micrometeorological measurements to efficiently assess both the spatial and temporal variability *and* the magnitude of GOM dry deposition.

Acknowledgements

Funding for this research was provided by a Local-Scale Air Toxics Ambient Monitoring Grant from the U.S. Environmental Protection Agency and by the Electric Power Research Institute. The authors wish to thank Bill and Lana Gibbs (MDN site NV99); Anthony Lesperance and Andy Peterson (MDN site NV02); Lowell Lui (Gallagher State

Fish Hatchery); Dwain Shiflett and Jill Franke (Atmospheric Research and Analysis, Inc.); and Coty Weaver, Ben Sedinger, Christianna Peterson, Zach Johnson, and Travis Lyman (University of Nevada, Reno) for deploying surrogate surfaces at field sites. The authors thank Brian Hanson, Tyler Ellis, and Coty Weaver (University of Nevada, Reno) for analyzing thousands of surrogate surface samples in the laboratory. The authors also appreciate insightful comments by Che-Jen Lin (Lamar University).

Tables and Figures

Table 5-1. Summary data for all sites. Regression coefficients shown indicate correlation with deposition of mercury to surrogate surfaces. "insig." means that a value is not significant at $\alpha = 0.05$. Surrogate surface deposition velocities and deposition rates are for surfaces deployed in aerodynamic mounts, except for Paradise, where values from surfaces in rectangular mounts were adjusted down based on comparisons of surfaces deployed in aerodynamic mounts and rectangular mounts.

	Weeks	GOM Corr. r^2	GEM Corr. r^2	PBM Corr. r^2	Model Dep. Corr. r^2	GOM Conc. pg m^{-3}	Surrogate Surf. Dep. Rate ng m^{-2} h^{-1}	Surrogate Surf. Dep. Velocity cm s^{-1}	Model Dep. Velocity cm s^{-1}	$R_c = 10$ Model dep. Velocity cm s^{-1}
Reno	64	0.84	0.04	insig.	0.91	22 ± 16	1.0 ± 0.8	1.4 ± 0.5	0.2 ± 0.1	1.1 ± 0.2
Paradise	5	0.49	insig.	insig.	0.61	25 ± 10	2.0 ± 0.4	2.2 ± 0.5	0.3 ± 0.0	1.5 ± 0.1
Pensacola	49	0.53	insig.	insig.	0.38	3 ± 2	0.1 ± 0.1	1.1 ± 0.7	0.5 ± 0.2	0.9 ± 0.3
Yorkville	49	0.53	0.10	0.26	0.25	7 ± 5	0.2 ± 0.2	0.9 ± 0.5	0.5 ± 0.1	0.9 ± 0.2

Table 5-2. Seasonal data summaries for Reno, Pensacola, and Yorkville. Values with asterisks are three-year means from 2005-2007 data at MDN sites AL24 and GA40 for Pensacola and Yorkville, respectively.

		Surrogate Surf. Dep.	**Mercury Wet Dep.**	**Precip.**	**GOM**	**Surg. Surf. Dep. Veloc.**
		μg m^{-2} $season^{-1}$		mm $season^{-1}$	pg m^{-3}	cm s^{-1}
Spring	Reno	1.3	0.4	17	11 ± 5	1.6 ± 0.4
Mar-May	Pensacola	0.4	3.6*	233	4 ± 2	1.1 ± 0.5
	Yorkville	0.7	2.7*	331	10 ± 6	0.9 ± 0.4
Summer	Reno	3.5	0.3	11	28 ± 9	1.7 ± 0.4
Jun-Aug	Pensacola	0.2	5.5*	423	3 ± 2	1.2 ± 0.7
	Yorkville	0.3	4.2*	350	4 ± 2	0.9 ± 0.7
Fall	Reno	1.8	0.6	1	21 ± 10	1.1 ± 0.3
Sep-Nov	Pensacola	0.0	2.4*	681	1 ± 1	0.6
	Yorkville	0.4	1.9*	198	4 ± 3	1.1 ± 0.1
Winter	Reno	0.2	0.3	30	4 ± 3	0.7 ± 0.7
Dec-Feb	Pensacola	0.1	2.1*	454	4 ± 3	1.1 ± 1.0
	Yorkville	0.4	1.9*	296	9 ± 3	0.5 ± 0.3

Figure 5-1. GOM concentration versus deposition of mercury to surrogate surfaces in aerodynamic mounts at all field sites. Deposition rates for Paradise were adjusted down based on comparisons of surfaces deployed in aerodynamic mounts and rectangular mounts.

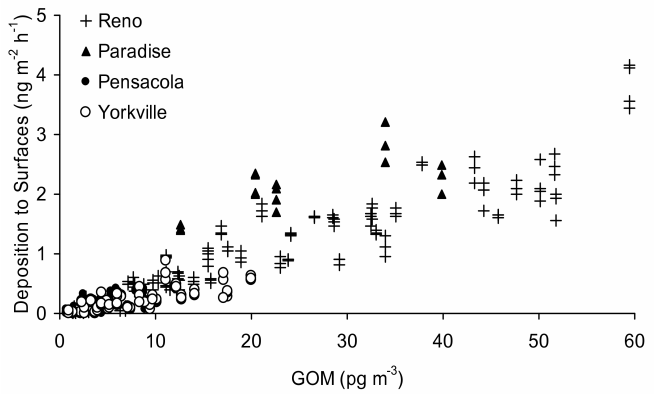

Figure 5-2. Time series and map of network deployment of surrogate surfaces at four sites in Nevada. Error bars show standard deviation.

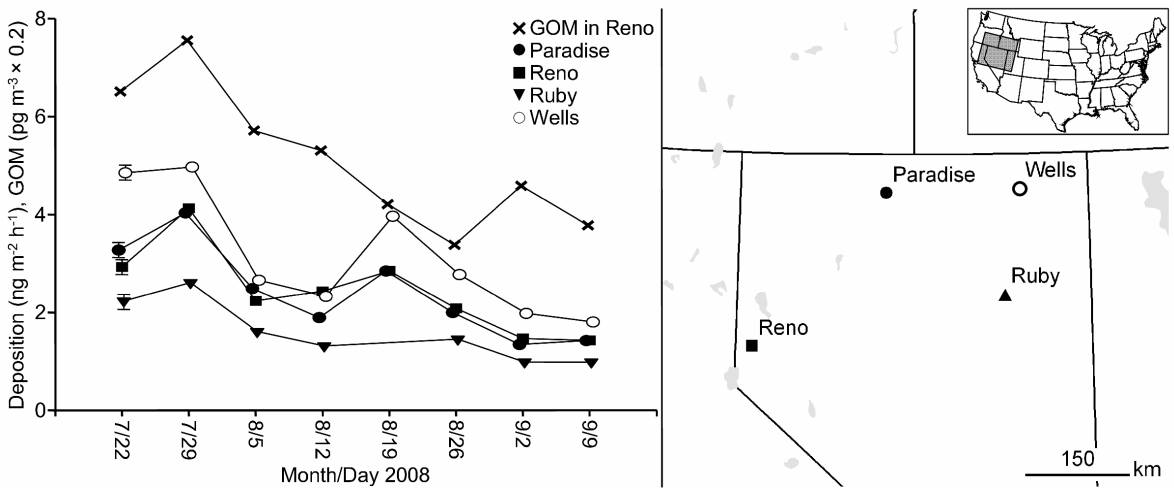

Figure 5-3. GOM concentration versus mercury deposition to surrogate surfaces in Chamber 2. Base case is 22 ± 6% relative humidity, 3 ± 2 ppb ozone, and 24.0 ± 1.2°C.

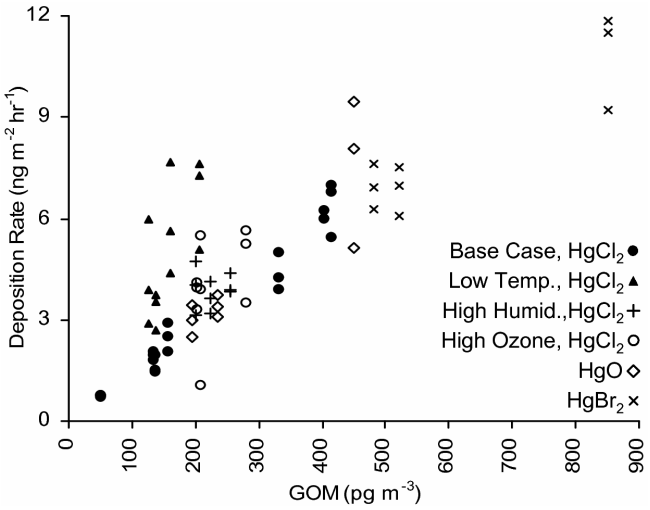

Figure 5-4. Time series of deposition of mercury to surrogate surfaces in Reno, Pensacola and Yorkville and wet mercury deposition in Reno. Error bars show standard deviation.

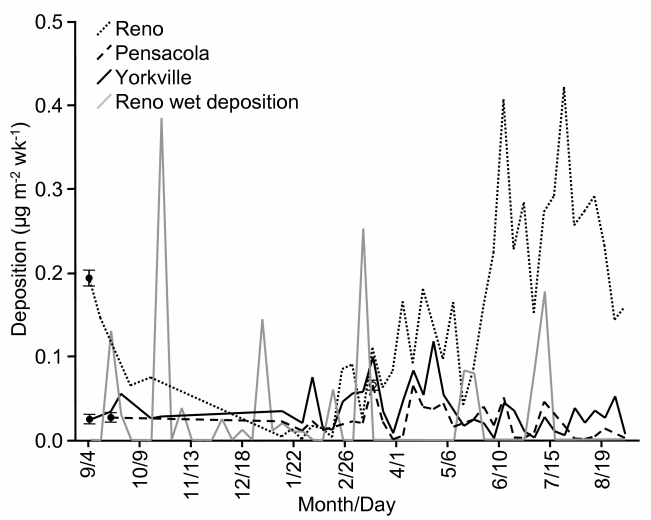

Supporting Information

Field Sites and Methods. The Reno field site is about 9 km from downtown Reno, Nevada in an urban desert valley just east of the Sierra Nevada Mountains. The Paradise Valley site is in a rural desert valley surrounded by mountains on three sides. The Pensacola site is in a suburban area 20 km north of the Gulf of Mexico. The Yorkville site is a rural site 40 km west of Atlanta, Georgia. Surfaces were deployed at 3 m at all Nevada sites and 5 m in Pensacola and Yorkville. Surfaces in Reno and Paradise Valley were deployed on independent sampling poles several meters from any buildings, and deployments in Pensacola and Yorkville were on sampling booms that extended 2 m from a building.

At all sites the accuracy of Tekran systems was checked regularly by injection of a known quantity of mercury vapor into air being sampled by the 2537A (weekly into ambient air in Reno and Paradise Valley, quarterly into zero air in Pensacola and Yorkville). Ozone was measured in Reno with a Teledyne-API 400E, and calibration checks were performed weekly. Temperature, humidity, wind speed and direction, solar radiation, precipitation, and leaf wetness were measured in Reno, Paradise, Pensacola, and Yorkville.

Descriptions of Laboratory Chambers. Air entering all chambers was filtered with 0.2 μm particulate filters, the chambers were covered from light during deployment, and chamber deployments were typically for 72 h. Chamber 1 was a 50 × 36 × 36 cm acrylic chamber with a flow rate of 7 L min^{-1}. GEM was permeated (Dynacal HE-SR permeation tube) into chamber inlet air to manipulate GEM concentrations. Temperature, humidity, solar radiation, and total gaseous mercury (TGM) concentration were measured

within the chamber. Total gaseous mercury was measured with a Tekran 2537A. Surfaces in Chamber 1 were deployed in rectangular mounts.

Chamber 2 was a 57 × 44 × 32 cm acrylic chamber, and it was housed in a chest freezer to allow temperature manipulation. A subset of inlet (filtered ambient) air was passed over a heated ultra-pure (18.2 MΩ cm^{-1}) water bath to manipulate humidity. A subset of inlet air was passed through a temperature-controlled vial containing $HgCl_2$, $HgBr_2$, or HgO to manipulate GOM concentrations. Before switching between different GOM species, the chamber was heated and flushed with air until residual GOM concentrations were no more than 10-20% of concentrations during GOM permeations. The flow rate through the chamber was 7.5 L min^{-1}. GOM and GEM were measured with a Tekran 2537A/1130 system. A 1.3 cm (diameter) × 40 cm (length) PTFE tube heated to 50°C connected the chamber to the Tekran 1130. Ozone was generated with a Teledyne-API model 700E and measured with a Teledyne-API model 400E. Surfaces in Chamber 2 were deployed in rectangular mounts.

Dry Deposition Model. Details of model construction are available in Lyman et al. (2007). The evergreen broadleaf shrubs land use category was used for Reno and Paradise Valley, and the short grass and forbs category was used for Pensacola and Yorkville. Comparison of the Lyman et al. model (2007) with the original Zhang et al. (2003) FORTRAN code showed that the Lyman et al. model produced deposition velocities that were not significantly different from the Zhang et al. model when no precipitation occurred but were 11 ± 0% lower than the Zhang et al. model when precipitation did occur. The discrepancy during precipitation was due to a difference in the way soil and cuticle resistance were calculated during rain and dew events.

Deployment Location Tests. To test whether proximity to a building affected deposition, sets of surfaces were deployed in three deployments in Reno using aerodynamic mounts on a free-standing sampling pole and on a 2 m boom projecting from a building (9 m from the pole; all surfaces were 3 m above ground level). The deposition rate of GOM to surfaces deployed on the free-standing pole was not different from deposition to surfaces deployed on the boom that projected from a building ($p = 0.35$-0.95).

Blank Correction. Surfaces deployed in aerodynamic mounts during weeks when average GOM concentration was less than 1 pg m^{-3} had a deposition rate of 0.20 ± 0.04 ng m^{-2} h^{-1}, three times higher than could be explained by GOM deposition alone (based on mean deposition velocity of GOM to surfaces deployed in aerodynamic mounts), providing evidence that contamination influenced the deposition rate. Deposition to surfaces deployed during low GOM periods did not correlate with GEM or PBM concentration, so it is unlikely that GEM or PBM were major contributors to contamination. The authors hypothesize that contamination occurred as residual mercury in mounts migrated to surrogate surfaces. Such contamination would not have been detected in field blanks, since field blanks were inserted into mounts and then immediately removed. All field samples were blank corrected using 0.20 ng m^{-2} h^{-1}, and samples with deposition rates less than this were given a value of zero (9% of data). Before blank correction, the slope of the regression line with deposition to surfaces as the dependent variable and GOM concentration as the independent variable was 0.050, and the y-intercept was 0.161 (significantly different from zero; $p < 0.01$). After blank correction, the slope was the same but the y-intercept was -0.033 (slightly different from

zero; p = 0.06). Since the y-intecepts for surfaces in aerodynamic mounts and rectangular mounts were not significantly different (p = 0.75), surfaces deployed in rectangular mounts at field sites were also blank corrected using the same method.

Figure 5-5. Diagram of Chamber 2.

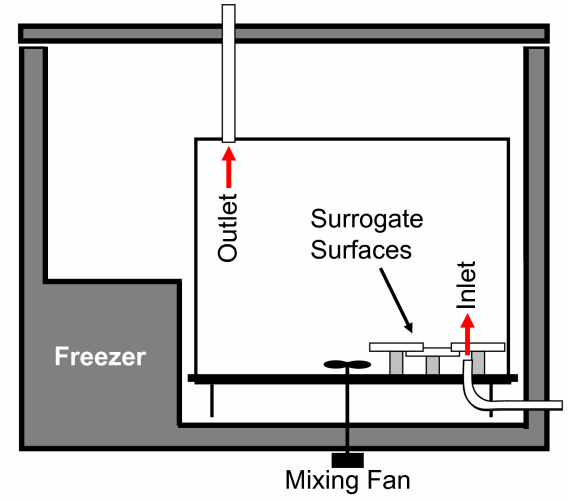

Figure 5-6. Surrogate surfaces in an aerodynamic mount (A), and a rectangular mount (B).

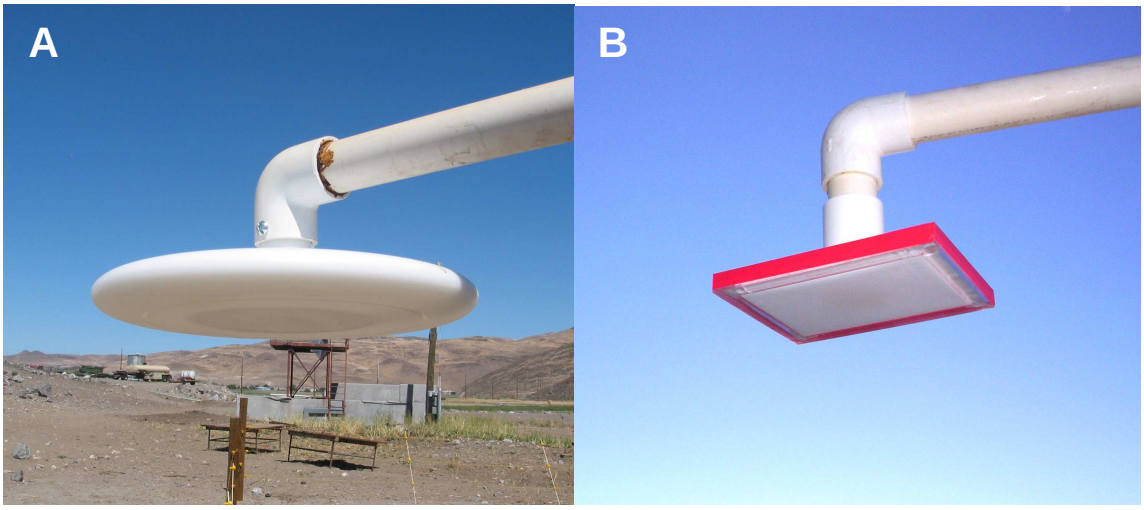

Chapter 6: A Passive Concentration Sampler for Gaseous Oxidized Mercury

Seth N. Lyman[†], Mae S. Gustin[†], Eric M. Prestbo[‡§]

†University of Nevada, Reno, Department of Natural Resources and Environmental Science/MS 370, 1664 North Virginia Street, Reno, Nevada, 89557

‡Frontier Geosciences, 414 Pontius Avenue North, Seattle, Washington, 98109

§ Now with Tekran Instruments Corporation

Abstract. This paper reports on the development of a passive (diffusive) concentration sampler for gaseous oxidized mercury and the testing of this sampler in controlled laboratory and field conditions. Atmospheric gaseous oxidized mercury concentrations calculated from passive sampler data were correlated with those obtained using an automated analyzer ($r^2 = 0.71$, $p < 0.01$, $n = 110$ for one-week deployments; $r^2 = 0.89$, $p < 0.01$, $n = 22$ for two-week deployments). Sampler uptake was not significantly affected by changes in temperature, humidity, or ozone concentration in field deployments, but was slightly dependent on wind speed. As such, passive sampler measurements were corrected based on this factor. The detection limit for two-week sampler deployments was ~5 pg m^{-3}. Field data showed these samplers are useful for investigating spatial and temporal variability in gaseous oxidized mercury concentrations.

Introduction

Although mercury contamination is most often associated with aquatic systems, the atmosphere is a global reservoir for mercury and a major source of mercury to ecosystems (Lindberg et al., 2007). As such, understanding the spatial and temporal variability in atmospheric mercury concentrations at different scales is necessary to fully understand potential impacts. Atmospheric mercury is typically measured as three fractions; gaseous elemental mercury (GEM), gaseous oxidized mercury (GOM; a.k.a. RGM; thought to consist of a variety of Hg(II) species such as $HgCl_2$, $HgBr_2$, HgO, etc.), and particulate-bound mercury (PBM). It is important to measure these three fractions, since each have different physical and chemical properties and different transport, transformation, and deposition dynamics (Schroeder and Munthe, 1998).

The Tekran® 2537A/1130/1135 system (Landis et al., 2002) is a commercially available, automated instrument for measurement of GEM, GOM, and PBM in the ambient atmosphere. Since its development early this decade, this system has dramatically increased scientific understanding of atmospheric mercury behavior (e.g. Lindberg et al., 2002; Hedgecock et al., 2003; Swartzendruber et al., 2006; and others). It provides automated high-quality, high-resolution (one hour or less) measurements. However, because the Tekran system is expensive and operation is labor-intensive, few long-term datasets exist for atmospheric mercury fractions (though the number is growing), and the spatial coverage of measurements is poor, especially outside of North America and Europe (Valente et al., 2007).

This paper describes efforts to develop a passive (diffusive) sampler for gaseous oxidized mercury. A passive sampler typically consists of a collection surface that has a

high affinity for the gas of interest and a barrier that eliminates turbulence and creates a region of stagnant air between the barrier and the collection surface where only diffusion occurs. Gas molecules are collected on passive samplers by passing through the barrier, diffusing through the region of stagnant air, and sorbing to the collection surface (Namiesnik et al., 2005). After deployment, the sampler is disassembled and the collection surface is analyzed to determine the mass of the compound of interest. This value can then be used to calculate the concentration of the gas of interest in the sampled atmosphere.

Passive samplers require no electric power, are simple to deploy, and are usually cheaper than automated analyzers, but they require longer minimum sampling times (hours to months, depending on the sampler and the gas of interest) and often have poorer precision (Harper and Purnell, 1987). Several passive samplers for ambient GEM or total gaseous mercury (i.e. GEM + GOM) have been developed (Kvletkus and Sakalys, 1994; Masataka et al., 1999; Brumbaugh et al., 2000; Skov et al., 2007), but the authors of this work are not aware of any attempts to develop a passive sampler for GOM. This work describes the performance of a novel GOM passive sampler in diverse field and laboratory settings, including its effectiveness relative to other sampler designs and its accuracy relative to automated measurements.

Methods

Sampler Design. The final sampler design consisted of an activated polysulfone cation-exchange membrane collection surface, a series of acrylic plates as barriers to turbulence (Figure 1), and a polycarbonate container as a protective housing and additional

turbulence barrier. Lyman et al. (2009) showed that the cation-exchange membrane used is an extremely efficient uptake surface for GOM and is not influenced by GEM concentrations. The main barrier to turbulence was a 1.2 cm thick acrylic plate situated over the collection surface. This plate had 126 holes of 0.32 cm diameter through which air passed from the atmosphere to the collection surface. Placed over this plate was a solid acrylic plate (i.e. external shield; 0.6 cm thick) that served as an additional turbulence barrier. A gap of 0.6 cm existed between the plate with holes and the external shield, allowing air to flow between the two parts and into the holes. To reduce contamination from the sampler body, thin PTFE sheeting (1 mm thick) was placed between the collection surface and the acrylic plates. The assembled sampler was 14.9 × 11.1 × 4.2 cm, and the exposed membrane surface area was 107 cm^2. This design melded the principles of a Palmes tube sampler (Palmes et al., 1976; Plaisance et al., 2004) and a badge-type sampler (e.g. Tang et al., 1997; Rabaud et al., 2001), maximizing the collection surface area and minimizing potential deposition to the sampler body and gas diffusion distance within the sampler.

During deployment, samplers were housed in 20 cm diameter × 19 cm deep cylindrical polycarbonate containers painted with opaque, light colored paint, providing a shield from precipitation, wind, and sun. Containers were positioned with the opening facing down, and the samplers inside were aligned parallel to the container top with the collection surface facing down. Velcro® straps secured the samplers to the tops of containers.

Sampler Preparation, Deployment, and Analysis. Acrylic sampler parts were immersed in a 5% HNO_3 bath for at least 12 hours between each use. The PTFE liners

were immersed for at least 12 hours in a 5% HNO_3 bath followed by 48 hours in a 90°C 50% HNO_3 bath between each use. Samplers were assembled in a HEPA filtered positive pressure hood, and sampler parts were held together using Fisherbrand® label tape. The gaps between the diffusive barrier and the external shield (see Figure 1) were sealed first with PTFE tape and then with Fisherbrand® label tape, and remained sealed except during deployment. Samplers were stored in double Ziploc® bags when not in use and were only handled with gloved hands.

All sampler deployments were for one week except for a subset of field deployments in Reno that were for two weeks (n = 5 deployments), and wind tunnel tests, which were for between one and two weeks. Prepared samplers were shipped between field sites and the UNR laboratory each week, and site operators followed a written standard operating procedure for sampler deployment and collection. Two or more samples and one to three matrix blanks were deployed during each sampling interval. Blanks were prepared and deployed exactly as samples, but their sampler openings were kept sealed with tape during deployment. Sampler concentrations were corrected using simultaneously collected blank data.

After deployment, samplers were disassembled in a HEPA filtered positive pressure hood and cation-exchange membranes were placed into individual 125 mL I-Chem jars and stored at -20°C until analysis. Cation exchange membranes were digested in 100 mL of 1% HCl solution and 6 mL of BrCl solution and then analyzed according to EPA Method 1631 (USEPA, 2002).

Blank Tests. Tests were performed to determine whether holding time and holding temperature influenced blank values. For the holding time test, twelve samplers were

prepared and sealed in double Ziploc® bags. Four samplers were immediately disassembled and their collection surfaces placed into jars and frozen, while the other eight samplers in the Ziploc® bag were placed in a laboratory drawer. After two and four weeks, four samplers were disassembled and collected. For the holding temperature test, four samplers were placed for two weeks in an oven at 40°C, four were placed in a lab drawer (~24°C), and four were placed in a refrigerator (~2°C). **Other Sampler Designs.** *KCl-Impregnated Quartz Fiber Filters*- KCl-impregnated quartz fiber filters were tested as collection surfaces. These were prepared by pipetting 7 mL of a 2.4 M KCl solution onto the filters so the entire filter was saturated, drying the filters, then heating the filters at 500°C for 3 hours to remove residual mercury. Filters were loaded into samplers immediately after heating. After deployment samplers were immediately disassembled and filters analyzed by placing in a quartz tube within a Lindberg tube furnace and heating to 500°C in a mercury-free air stream. Desorbed mercury was quantified using a Tekran® 2537A. The Tekran® 2537A was calibrated external to the Tekran® software by injecting known amounts of mercury vapor into sample air and creating a four-point calibration curve from the peak area output of the instrument.

Preliminary Sampler Body Experiments- To develop a sampler body that shielded the membrane from wind, potential designs were deployed in wind tunnels described below. These included n = 4 deployments using 4 wind tunnels each time with the final sampler including the cylindrical polycarbonate container, n = 2 deployments for the final sampler without the external shield but with the polycarbonate container, and n = 1 deployment using a diffusive canister modified from Wania et al. (2003). The diffusive canister was an enclosed cylindrical polycarbonate housing with a series of 1 cm holes drilled along

the top edge and through the bottom, and the holes were shielded to restrict direct air flow through the holes and into the canister. Collection surfaces were directly exposed to air within the canister.

Field Deployments. Passive samplers were deployed for 37 weeks at Mercury Deposition Network (MDN) site NV98 in Reno, Nevada (Figure 2; 39.51°N, 119.72°W); for eight simultaneous weeks at MDN NV02 in Paradise Valley, Nevada (41.50°N, 117.50°W), MDN NV99 near Wells, Nevada (41.55°N, 115.21°W), Ruby Valley, Nevada (40.20°N, 115.50°W), and Southeastern Aerosol Research and Characterization (SEARCH) network sites OLF in Pensacola, Florida (30.55°N, 87.38°W) and YRK near Yorkville, Georgia (33.93°N, 85.05°W); and for four weeks in Dixboro, Michigan (42.30°N, 83.66°W). Deployments in Reno were carried out between May 2008 and April 2009, and deployments at all other sites were carried out between July and September 2008.

Atmospheric mercury fractions (GEM, GOM, and PBM <2.5 μm) were measured simultaneously with sampler deployments in Reno, Pensacola, Yorkville, and Dixboro with Tekran® 2537A/1130/1135 systems. Tekran systems were cleaned and calibrated according to established standard operating procedures for each site, and external calibration checks were performed regularly by injecting known quantities of mercury vapor into sample air streams (in ambient air in Reno and Dixboro, in mercury-free air in Pensacola and Yorkville). Ozone was measured in Reno with a T-API® Model 400E ozone analyzer that was calibrated weekly with a NIST-traceable ozone standard. Samplers at instrumented sites were deployed at the height of Tekran® system inlets (4 m

in Reno and Dixboro, 5 m in Pensacola and Yorkville), and samplers at other sites were deployed at 3 m.

Temperature, humidity, wind speed and direction, solar radiation, precipitation, and leaf wetness were measured in Reno, Pensacola, Yorkville, and Dixboro. Meteorological data for Paradise Valley, Wells, and Ruby Valley were obtained from the Remote Automated Weather Station (RAWS) Climate Archive (www.raws.dri.edu). RAWS data includes air temperature, relative humidity, wind speed and direction, precipitation, and solar radiation. The Morey Creek RAWS site was used for Paradise (12 km away from field site), Stag Mountain was used for Wells (16 km away), and Ruby Lake was used for Ruby Valley (1 km away).

Chamber Deployments. Samplers (without polycarbonate containers) were deployed in a 57 × 44 × 32 cm acrylic laboratory chamber to determine whether GOM concentration, GOM species ($HgCl_2$, $HgBr_2$, and HgO), GEM concentration, temperature, humidity, or ozone concentration affected uptake rates. Chamber inlet air was filtered with a 0.2 μm filter, and the chamber flow rate was 7.5 L min^{-1}. The chamber was housed in a chest freezer, providing for manipulation of temperature. To add humidity a component of the inlet air stream was passed over a temperature controlled water bath. Ozone generated with a T-API® Model 700E was added to the inlet air for some exposures and measured in outlet air with a T-API® Model 400E. To add specific GOM compounds to the chamber a component of the inlet air was passed over a temperature-controlled PTFE permeation tube containing $HgCl_2$, $HgBr_2$, or HgO. A Tekran® 2537A/1130 system connected to the chamber using a heated PTFE tube was used to measure GEM and GOM concentrations. Five deployments were carried out with $HgCl_2$ permeated (varying

concentrations), temperature at about 25°C, no water vapor added, and no ozone added. Three deployments each were carried out with low temperature, high humidity, $HgBr_2$ permeated, HgO permeated, and ozone added.

Wind Tunnel Tests. Samplers were deployed in polycarbonate containers 0.5 m downwind of variable speed fans inside 46 cm diameter × 3 m PVC pipes that served as wind tunnels (n = 3 deployments for the final sampler design). Wind speed in each tunnel was measured with a Young® 05103 wind meter at the beginning, midpoint, and end of each deployment period.

Data Analyses. Data were processed using Microsoft Excel 2003, Correlation and regression analyses were performed using SPSS 16.0, t-tests were performed in Kaleidagraph 4.02, and wind direction analyses were performed in Kaleidagraph 4.02. All statistics were considered significant at $\alpha = 0.01$ unless otherwise noted. Where applicable, values are reported as mean ± standard deviation.

The uptake rate of mercury by passive samplers (units of pg h^{-1}) was calculated as the mass of mercury collected on cation-exchange membranes (blank-corrected) divided by the length of the deployment. The empirically-derived theoretical flow rate of GOM into samplers (units of L min^{-1} or m^3 h^{-1}) was calculated as the uptake rate divided by the average GOM concentration measured by the Tekran® system during the deployment period.

Relative standard deviation (RSD) was calculated as

$$RSD = 100 \times SD/M$$

where SD is the standard deviation and M is the mean. Relative percent difference (RPD) was calculated as

$RPD = 100 \times |P - A|/A$

where P is the GOM concentration calculated from a passive sampler and A is the GOM concentration measured with the Tekran® system.

Results and Discussion

KCl-impregnated Filters as Collection Surfaces. Blanks for the KCl filters were relatively low (60 ± 8 pg per filter), and the analysis method for KCl filters was more simple and direct than that for cation-exchange membranes. However, uptake of mercury by samplers with KCl filters as collection surfaces was not correlated with GOM concentration ($r^2 = 0.00$, $p = 0.94$). This is in contrast to the work of Rutter et al. (2008), which showed that KCl filters were effective as an active collection surface for GOM. The authors hypothesize that the KCl surface is viable as a short-term collection surface (for example, Landis et al. (2002) showed breakthrough on KCl denuders after 12 hours), but not for the relatively long exposure period of passive sampler deployments.

Wind Tunnel Tests of Other Sampler Bodies. Wind tunnel tests allowed for development of a sampler that minimized wind effects but maximized GOM collection. The slope of the relationship between tunnel wind speed ($m\ s^{-1}$) and sampler flow rate ($m^3\ h^{-1}$) was 0.081 for the diffusive canister and 0.079 for the final sampler without an external shield, 260% and 249% greater, respectively, than the slope for a prototype version of the final sampler (0.023). Thus, the final sampler as described above was used as the optimum design.

Blank Tests. The amount of mercury in blanks was linearly related to holding time ($r^2 = 0.97$) and holding temperature ($r^2 = 0.75$) indicating that collection surfaces received

contamination from the sampler body over time and in warmer temperatures. Collection surfaces from blanks contained 0.28 ± 0.02 ng mercury immediately after assembly, and gained 0.10 ng per week of storage at room temperature. Blanks stored at 40°C and 2°C had 18% more and 20% less mercury, respectively, than samplers stored at room temperature. To correct for these effects, blanks were deployed, stored, and analyzed with all samples and blank concentrations were used to correct all sampler data. The relative standard deviation of replicate blanks was not correlated with temperature or holding time ($p = 0.73$ and 0.69, respectively), indicating that these factors did not affect the precision of sampler results.

Chamber and Wind Tunnel Results. The uptake rate of mercury by passive samplers deployed in the laboratory chamber was correlated with average GOM concentration ($r^2 = 0.80$) and not correlated with GEM concentration ($r^2 = 0.06$, $p = 0.48$). The theoretical flow rate under typical chamber conditions (22.9 ± 1.4°C, 23 ± 6% humidity, 3 ± 2 ppb ozone, $HgCl_2$ permeated) was 0.34 ± 0.15 L min^{-1}. This was not different from the flow rate when $HgBr_2$ was permeated ($p = 0.29$; 0.28 ± 0.06 L min^{-1}) or when HgO was permeated ($p = 0.23$; 0.27 ± 0.05 L min^{-1}). Though the flow rate in high ozone conditions was not statistically significantly different from typical conditions ($p = 0.18$; 0.74 ± 0.63 L min^{-1}; 166 ± 3 ppb ozone), it was more variable. This may have been due to an interaction of the cation exchange membrane surface with ozone, since Lyman et al. (2009) showed similar results for membranes exposed directly to chamber air (i.e. without a turbulence barrier), or this effect may have been due to a change in the performance of the Tekran® system in high ozone conditions.

The flow rate was significantly lower when the temperature was low (0.13 ± 0.06 L min^{-1}; -1.7 ± 1.8°C), which may have been due to a GOM measurement bias caused by enhanced GOM wall loss in cold conditions. Lyman et al. (2009) reported higher than expected uptake of GOM to cation-exchange membranes deployed in the same chamber used in this study when the chamber temperature was below 0°C. They hypothesized that this was due to wall loss of GOM as it traveled through the chamber (chamber walls were frosty during cold temperature deployments), which biased GOM measurements at the chamber outlet low relative to the GOM experienced by the membranes, which were positioned near the chamber inlet. The passive samplers in this work were deployed on the opposite side of the chamber relative to Lyman et al. (2009; see Figure 3), and the finding in this work that passive samplers deployed in the chamber in cold conditions collected significantly less mercury than those deployed in typical conditions supports the hypothesis of Lyman et al. (2009). Also, the flow rate to samplers deployed in high humidity was slightly lower than in typical conditions ($p = 0.06$; 0.23 ± 0.12 L min^{-1}; 74 ± 6% humidity), and since condensation formed on chamber walls during high humidity deployments, the same wall-loss hypothesis may explain this difference as well.

The flow rate for samplers deployed in wind tunnels was linearly dependent on wind speed (Figure 4).

Field Results. Automated measurements of GOM were correlated with the uptake rate of mercury to samplers in one-week deployments (Figure 5; $r^2 = 0.70$) and were even better correlated with the average uptake rate of replicate samplers ($r^2 = 0.78$) and the uptake rate of samplers deployed for two weeks ($r^2 = 0.84$). Unfortunately, only the Reno site had a large enough range of GOM concentrations to adequately show the linearity of

this relationship. No significant correlation existed between GOM concentration and uptake rate when data from Pensacola, Yorkville, or Dixboro were considered individually (p = 0.44, 0.73, and 0.48, respectively). The Tekran® systems at Pensacola, Yorkville, and Dixboro alternated between 1 h sampling periods and 1 h analysis periods, allowing them to measure GOM only 50% of the time, while the passive samplers measured GOM continuously, and this difference may account for some of the scatter in the dataset (see Lyman et al., 2009 for more discussion of this problem).

The theoretical flow rate for all samplers deployed at field sites with automated measurements was 1.21 ± 2.41 L min^{-1}. The flow rate of samplers deployed at field sites was not correlated with GEM, PBM, or ozone concentration (p = 0.40, 0.96, and 0.57, respectively), nor was it correlated with temperature, humidity, or solar radiation (p = 0.97, 0.75, and 0.73, respectively). The flow rate was weakly linearly dependent on wind speed when the entire dataset was used (r^2 = 0.05), and more strongly dependent on wind speed if one-week samplers deployed during periods with average GOM concentration less than 10 pg m^{-3} were removed (Figure 4; r^2 = 0.40).

Calculating GOM Concentrations from Passive Samplers. Concentrations of GOM were calculated as

$$GOM = U/F$$

where U is the uptake rate (in pg h^{-1}), and F is the calculated flow rate of air to the sampler (in m^3 h^{-1}). Since the flow rate for passive samplers was linearly dependent on wind speed, the relationship of wind speed with the empirically-derived flow rate was used to calculate a wind-dependent F for the above equation as

$$F = 0.0362 \times WS \qquad (r^2 = 0.54)$$

where WS is the wind speed in m s^{-1}. The y-intercept (0.017 m^3 h^{-1}) for this equation was not different from zero (p = 0.31). Samplers deployed for two weeks and samplers deployed in wind tunnels were used to establish this equation.

The regression slope of flow rate versus wind speed derived from wind tunnel deployments was not different from that derived from two-week deployments (p = 0.99). However, the slopes for these two data sets were slightly different from the slope for one-week deployments, even if the data from deployments with GOM concentrations less than 10 pg m^{-3} were excluded (slope of 0.056, p = 0.03 and 0.14, respectively). The one-week deployment data set included outliers that influenced the slope, and it under-predicted GOM concentrations relative to automated measurements (slope of 0.89; p = 0.07). Because of this, these data were not used to calculate flow rate.

Flow rates calculated based on wind speed were not different from empirically-derived flow rates of GOM to samplers (Table 1; p = 0.36, 0.68, and 0.75 for all one-week samples, one-week samples with GOM greater than 10 pg m^{-3}, and two-week samples, respectively). Also, concentrations of GOM derived from passive samplers (with wind correction) were well correlated with GOM concentrations derived from automated measurements (Table 1; Figure 6). The slopes for this relationship were not significantly different from one (p = 0.82, 0.98, and 0.99 for all one-week samples, one-week samples with GOM greater than 10 pg m^{-3}, and two-week samples, respectively), and y-intercepts were not significantly different from zero (p = 0.43, 0.94, and 0.85 for all one-week samples, one-week samples with GOM greater than 10 pg m^{-3}, and two-week samples, respectively).

When GOM concentrations were calculated from passive samplers using a flow rate that wasn't dependent on wind speed (i.e. the average empirically-derived flow rate of GOM to samplers), the slope between calculated GOM and GOM measured by the Tekran® system was still not different from one ($p = 0.42$ and 0.72 for one-week and two-week samples, respectively), but r^2 values were weaker (0.70 and 0.84 for one-week and two-week samples, respectively), and, more importantly, GOM concentrations calculated this way were non-randomly biased.

Detection Limits, Precision, and Accuracy. Because the theoretical flow rate for samplers was dependent on wind speed, the detection limit also depended on wind speed. Calculated from three times the standard deviation of blanks, the detection limit for two-week samples was 7 pg m^{-3} if the average wind speed during deployment was 1 m s^{-1}, and 2 pg m^{-3} if the average wind speed during deployment was 3 m s^{-1}. The detection limit was twice as high for one-week samples.

For both the one-week and two-week data sets, the relative percent difference between automated and passive measurements increased with decreasing GOM concentration (Figure 7). Samplers deployed for one week had a lower relative percent difference and relative standard deviation if data collected during weeks when the average GOM concentration was less than 10 pg m^{-3} were excluded (Table 1). Data collected from two-week deployments had a similar relative percent difference and relative standard deviation compared to one-week data with GOM concentration greater than 10 pg m^{-3}.

Analysis of GOM Concentrations. Passive measurements of GOM at field sites showed that the passive sampler was able to resolve regional and continental-scale

variation in GOM concentrations (Figure 8). Concentrations of GOM in the eastern United States were mostly below the passive sampler's detection limit during the summer of 2008, while GOM concentrations in Nevada were considerably higher. Neither temperature, dew point, solar radiation, nor wind speed was a consistent predictor of GOM at field sites in Nevada.

Samplers deployed in Nevada showed a declining trend of GOM concentrations over the 8 weeks of deployment, and automated measurements of GOM in Reno showed a similar trend. In addition, surrogate surfaces used to measure GOM dry deposition (using the same cation exchange membrane collection surface as in this study) showed the same trends as the GOM passive samplers (Lyman et al., 2009).

Concentrations of GOM in Wells were high relative to the other sites in Nevada, contrary to the findings of Lyman and Gustin (2008), which reported GOM concentrations of 10 ± 8 pg m^{-3} at the same site in the summer of 2005. This discrepancy may be due to different sample locations between the studies, since the data in Lyman and Gustin (2008) were collected in a narrow river valley, whereas measurements in this work were collected on a hilltop 2.4 km away from and 75 m higher than the previous site. Weiss-Penzias et al. (2009) showed that GOM concentrations were higher in Reno at a location about 150 m above the valley floor relative to a location on the valley floor. Such a GOM elevation gradient may be evidence of an upper-atmospheric source of GOM, as has been postulated by others (Swartzendruber et al., 2006; Selin et al., 2007; Sillman et al., 2007; Weiss-Penzias et al., 2009). An alternative explanation is that the environmental conditions during sampling in this study were significantly different than those during which the previous study occurred. The Lyman and Gustin (2008) study

occurred during a relatively rainy period, while in this work precipitation only occurred on the first day of the eight week study. This could have impacted formation, availability and perhaps input of GOM to the area.

The Wells site is downwind of gold ore processing facilities that are known to emit GOM to the atmosphere (Lyman and Gustin, 2008). However the nearest such facility, the Jerritt Canyon Mine (70 km west-southwest of the Wells site), ended operation August 8 to 12, 2008, and remained off line into 2009 (McMurdo, 2008; Harding, 2009). Based on this the higher GOM cannot be attributed to this source. Other potential GOM point sources are located more than 120 km southwest of the Wells site, including ore processing facilities and a coal fired power plant (see map of area mercury sources in Lyman and Gustin, 2008). The highest GOM concentrations in Wells were associated with average weekly surface winds from the southwest (Figure 9). This could indicate influence from anthropogenic point sources in that area or could be due to transport from a non-anthropogenic source region southwest of the site in the upper atmosphere (c.f. Weiss-Penzias et al., 2009). A much more detailed analyses of air masses interacting with each site, as well as additional sampler deployments, would likely be necessary to definitively determine the source of elevated GOM at the Wells site.

Conclusions

Field results showed that passive samplers collected GOM uniformly regardless of temperature, humidity, or ozone concentration, but uptake of GOM by the sampler did depend on wind speed, a common problem for passive samplers (e.g. Koutrakis et al.,

1993; Plaisance et al., 2004), including other passive samplers for semivolatiles (Pozo et al., 2004; Sderstrm et al., 2004; Harner et al., 2003; Tuduri et al., 2006). Wind turbulence increases the theoretical flow rate by decreasing the depth of the diffusive layer surrounding the sampler (Wania et al., 2003; Plaisance et al., 2004), and this effect may be amplified for reactive compounds such as GOM, since a deeper diffusive layer would allow more time for these compounds to be sorbed to the sampler body. Even though wind speed had only a minor effect on the correlation between passive and automated measurements, the effect was important because it imparted non-random bias, resulting in higher estimated GOM concentrations at higher wind speeds. Also, the wind effect may not be linear below the range of wind speeds measured in this study (as in Plaisance et al., 2004 and Skov et al., 2007).

The detection limit for one-week deployments appears to be too high to yield meaningful data at some sites, but two-week samples and one-week samples had similar theoretical sampling rates and regression slopes (Table 1), indicating no loss from or saturation of the collection surface over a two week period, and a minimum deployment period of two weeks is advised. The feasibility of longer sampler deployments should be investigated.

In spite of some limitations, this sampler appears able to yield meaningful measurements of GOM in real field conditions. The relative percent difference between passive and automated measurements was within the range found by Lyman et al. (2007) for GOM measurements from two collocated automated systems, and the deployment time for the passive sampler is shorter than minimum deployment times for passive samplers for other compounds with concentrations similar to GOM (Shen et al., 2005;

Santiago and Cayetano, 2008; Pozo et al., 2009). The sampler was able to resolve spatial and temporal trends in GOM concentrations, and was simple enough to be deployed by site operators with minimal training.

Acknowledgements

A Local-Scale Air Toxics Ambient Monitoring Grant from the U.S. Environmental Protection Agency and a grant from the Electric Power Research Institute provided funding for this work. The authors thank Bill and Lana Gibbs, Anthony Lesperance, Andy Peterson, Lowell Lui, Dwain Shiflett, Jill Franke, Frank Marsik, Coty Weaver, Christianna Peterson, and Travis Lyman for deploying samples at field sites. They also thank Tyler Ellis, Travis Lyman, Musheng Alishahi, Coty Weaver, and Casandra Woodward for help with cleaning, assembly, and analysis of samplers.

Tables and Figures

Table 6-1. Summary of sampler performance. Slopes and r^2 values are for linear regression between GOM concentrations from the automated Tekran® system and GOM concentrations derived from passive samplers. Relative percent differences are comparisons of passive and automated measurements. Relative percent differences were computed for all individual samples, but relative standard deviations were only computed for sample sets with three or more replicate samples.

	1 Week All Data	1 Week GOM>10	2 Week
# of Samples	110	41	22
Emperical Flow Rate	1.40 ± 2.32	1.24 ± 0.63	1.46 ± 0.63
Calc. Flow Rate	1.19 ± 0.43	1.19 ± 0.27	1.41 ± 0.32
Slope	0.98	1.00	1.00
r^2	0.71	0.59	0.89
Rel. % Difference	95 ± 181%	28 ± 22%	31 ± 23%
# of Sample Sets	16	4	5
Rel. Standard Dev.	83 ± 60%	25 ± 15%	27 ± 19%

Figure 6-1. Expanded view of GOM passive sampler.

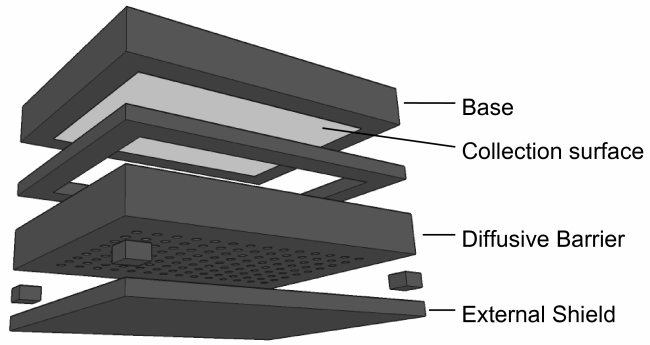

Figure 6-2. Map of field sites

Figure 6-3. Schematic of chamber (modified from Supplemental Information in Lyman et al., *submitted*).

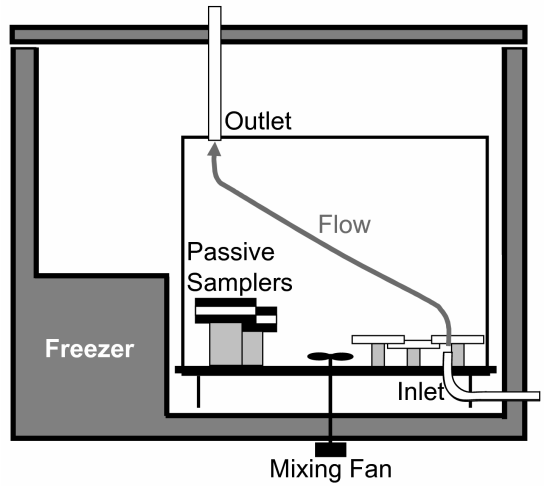

Figure 6-4. Wind speed versus theoretical flow rate of passive samplers at all field sites. For the samplers deployed for one week, only those deployed in periods with average GOM concentration greater than 10 pg m^{-3} are shown.

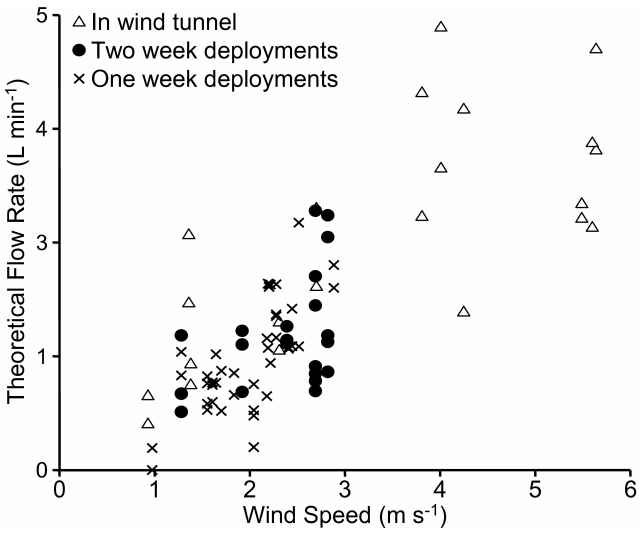

Figure 6-5. Uptake rate of mercury to passive samplers versus GOM concentration. Deployments for two weeks were carried out in Reno.

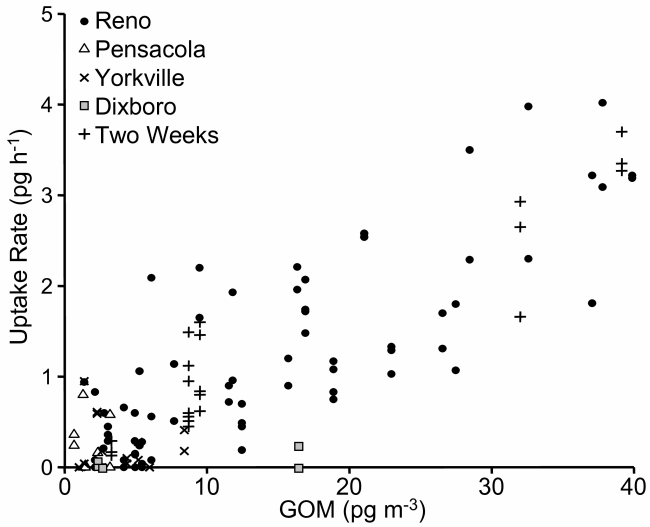

Figure 6-6. Concentrations of GOM measured with automated Tekran® system versus GOM concentrations derived from passive samplers (with wind speed correction). The line with long dashes indicates the detection limit for two-week samples, and the line with short dashes indicates the detection limit for one-week samples (at 2 m s^{-1} wind speed).

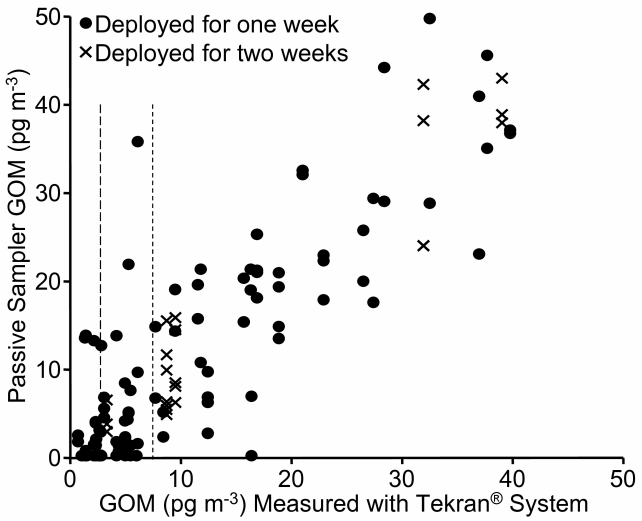

Figure 6-7. Concentration of GOM (measured with Tekran® system) versus relative percent difference between GOM concentrations calculated from passive samplers and automated GOM measurements.

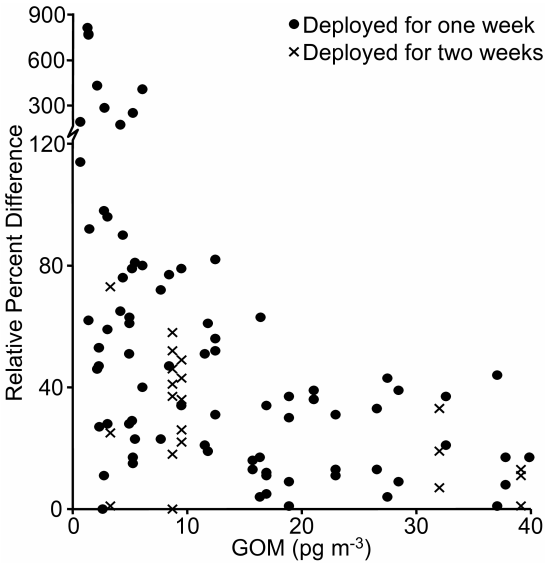

Figure 6-8. Concentrations of GOM from all field sites. Values shown are averages of duplicate samplers, and vertical bars show the average standard deviation for each site.

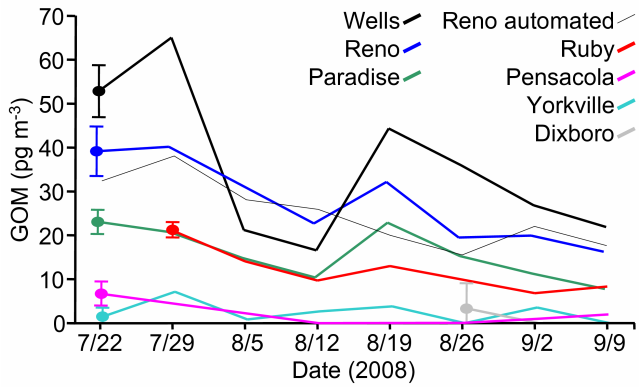

Figure 6-9. Wind rose diagram showing relationship between wind direction (degrees) and GOM concentrations measured with passive samplers.

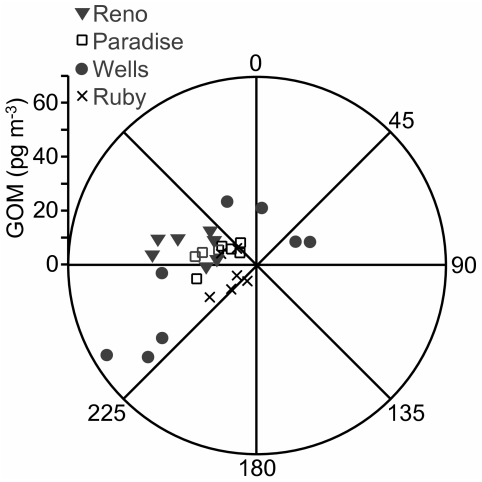

Chapter 7: Conclusions

New Methods. The cation-exchange membrane surrogate surface and the passive sampler for GOM concentrations are simple, relatively low-cost methods that can increase understanding of GOM in the atmosphere. These methods are unique tools that are well suited for particular applications, and should not be considered replacements for automated measurements.

As discussed in Chapter 5, since GOM deposition to the surrogate surface can't be assumed to be similar to natural surfaces, surrogate surface measurements may not be representative of the magnitude of GOM deposition to natural surfaces. In Chapter 3 deposition to surrogate surfaces was not well correlated with deposition to leaf surfaces, but this discrepancy may have simply been due to high and variabile pre-existing mercury concentrations in leaves that made the leaf surface methods unable to detect GOM dry deposition on a weekly time step.

Because of the uncertainties associated with surrogate surfaces, they should be viewed as a secondary or supplemental method to more established micrometeorological methods such as modified Bowen ratio or relaxed eddy accumulation. Micrometeorological methods are direct measurements of the transport of gases from the atmosphere to the surface, so they can more accurately determine the magnitude of dry deposition. What is more, these methods generally have much better temporal resolution than surrogate surfaces, allowing them to better assess short-term temporal variability in dry deposition. However, because of their low cost and ease of use, the surrogate surfaces may be more able than traditional micrometeorological methods to assess long-

term temporal variability or spatial variability of GOM dry deposition. Side-by-side comparisons of micrometeorological measurements and surrogate surface measurements in a variety of settings are needed to better establish the effectiveness and accuracy of the surrogate surfaces.

The passive concentration sampler for GOM has similar advantages – and similar disadvantages – to the surrogate surface. Though relatively simple to use, passive samplers tend to carry more uncertainty than automated measurements (Chapter 6; Krupa and Legge, 2000; Partyka et al., 2007). Passive measurements are most useful in settings or studies where automated measurements are not feasible or affordable, such as studies requiring simultaneous measurements in many different locations. Shen et al. (2005) used passive samplers at 40 locations throughout North and Central America to assess the prevalence of gas-phase persistent organic pollutants in the Western Hemisphere. This number of study sites would have been prohibitive using automated samplers, and the protracted sampling time required for passive measurements (1 yr in the Shen et al., 2005 study) can be seen as an advantage when assessing broad spatial trends because it reduces the influence of short-time scale phenomena. The Global Atmospheric Passive Sampling (GAPS) network is another example of the unique applicability of passive samplers for assessing broad-scale spatial variability (Pozo et al., 2009).

Surrogate surfaces and passive concentration samplers may also prove useful for characterizing spatial variability at the local scale. In fact, the first use of cation-exchange membranes as surrogate surfaces was to characterize local mercury dry deposition around a coal-fired power plant (Prestbo et al, 2005). Also, since micrometeorological measurements of dry deposition in hilly or mountainous terrain are

problematic because of theoretical limitations of the method (Stull, 2004), and dry deposition models are less reliable in mountainous terrain (Wesely and Hicks, 2000), surrogate surfaces may be useful in such terrains for they have no such limitations. Since GOM concentrations appear to increase with altitude (Swartzendruber et al., 2006), mountains may be subject to disproportionately high GOM dry deposition rates, and deployment of passive samplers and surrogate surfaces in mountain environments may yield valuable data.

Atmospheric Mercury Concentrations. This work showed that GEM concentrations in northern Nevada were strongly influenced by emissions from local or regional natural and anthropogenic sources (Chapters 2 and 4). This was true for rural sites, where high mercury concentrations depended on transport from discrete natural and anthropogenic source regions, on meteorological conditions such as precipitation and sunlight (which control the rate of mercury release from substrates), and on wind conditions, which control the amount of atmospheric mixing and determine the rate of dilution of GEM-rich air. This was also true for the urban Reno site, where GEM concentrations were higher when atmospheric mixing was low and locally emitted pollutants built up in near-surface air. In Chapter 4, whether the emitted GEM in Reno was the result of emissions from soil surfaces or direct anthropogenic sources was unable to be determined.

Though stack tests have shown that a large percentage of mercury emissions from northern Nevada gold processing facilities is GOM (Nevada, 2007), Chapter 2 showed that the ratio of GOM to GEM in air in northern Nevada was extremely low, even when air arrived from mine locations. Edgerton et al. (2006) reported lower-than-expected GOM concentrations in plumes downwind of coal fired power plants, and hypothesized

that either stack emissions from power plants overestimated GOM concentrations or that GOM was reduced to GEM within plumes. This same phenomenon may occur in Nevada.

Chapters 2 and 4 presented little evidence that GOM concentrations in northern Nevada were influenced by anthropogenic sources, and instead supported the findings of Weiss-Penzias et al. (2009) that GOM concentrations in northern Nevada are influenced by down-welling of GOM-rich air from the free troposphere. Although more work needs to be done to confirm this hypothesis, it has implications for high elevation sites and deserts throughout the world (Selin et al., 2007) and may be an important component of the global mercury cycle. Though this work did not provide strong evidence for local, surface-level oxidation of GOM, this phenomenon likely occurs in northern Nevada, and is superimposed by the influence of down-welling of GOM-rich air from the free troposphere.

Fires occurring in the summer of 2008 may have influenced GOM concentrations, but any influence is difficult to elucidate since summer is the time of year when elevated concentrations occur. Elemental and particulate Hg concentrations both increased during this time and would be influenced by biomass burning (Freidli et al., 2003). Ozone concentrations would also be expected to increase due to biomass burning because fires emit ozone precursors, but similar to GOM, ozone concentrations were high during the summer of 2007 also, and the direct impact of fires on concentrations is not clear. The fact that GOM concentrations in Reno rapidly increased in June 2008 at the start of fire activity (Figure 4-3), suggests that wildfires may have contributed to observed GOM concentrations in Reno.

Mercury Dry Deposition. Chapter 3 showed that dry deposition contributed potentially 50 ± 25% of total deposition (wet + dry) in rural northern Nevada. Although deposition to surrogate surfaces is most likely different than that occurring to natural surfaces, this is a significant estimate because it is the first to use direct measurements. Chapter 5 showed that estimated dry deposition in Nevada was much higher than at two sites in the southeastern United States, due to higher GOM concentrations in Nevada, but higher wet mercury deposition inputs at the southeastern sites resulted in higher total deposition for latter. This highlights the need to better understand the processes that control dry deposition on regional and local scales.

Since total mercury dry deposition may depend strongly on GOM concentrations, a better understanding of regional GOM concentrations is needed to accurately assess mercury loading from the atmosphere. In Chapter 3 PBM was not a major component of total dry deposition, but PBM may play a larger role at urban locations with high PBM concentrations. Also, since coarse-mode PBM wasn't measured in this work, its contribution to total dry deposition is not known.

Though GEM concentrations were orders of magnitude higher than GOM concentrations, GEM surface fluxes were small at northern Nevada sites, and GEM dry deposition (based on soil flux measurements) was less important than GOM dry deposition (based on the GOM dry deposition model or surrogate surfaces). Since GOM at northern Nevada sites is not thought to be of local origin, despite the fact that there are natural and anthropogenic sources of atmospheric mercury in the region, dry deposition in Nevada is a function of the availability of GOM-rich air from aloft (as well as some surface-level oxidation of GEM). If, as hypothesized by Selin and Jacob (2008), wet

mercury deposition is also influenced strongly by cloud absorption and rainout of high-altitude GOM, it may be that most of the total mercury deposition in Nevada, not just dry deposition, is of distant origin, and locally emitted mercury has little regional effect.

Mercury models are often validated against wet deposition measurements (Bullock and Brehme, 2002; Selin and Jacob, 2008), but this work shows that dry deposition can be a major component of total deposition, especially in arid regions, and the performance of the dry deposition modules of mercury models needs to be compared against direct dry deposition measurements.

References

Arnott W., Gyawali M., Arnold I., 2008. Aerosol Extinction and Single Scattering Albedo Downwind of the Summer 2008 California Wildfires Measured With Photoacoustic Spectrometers and Sunphotometers From 355 nm to 1047 nm. Eos 89, AGU Fall Meeting Supplement, Abstract A11D-0169.

Bloom N.S., Watras C.J., 1989. Observations of methylmercury in precipitation. Science of the Total Environment 87/88, 199-207.

Brumbaugh W.G., Petty J.D., May T.W., Huckins J.N., 2000. A passive integrative sampler for mercury vapor in air and neutral mercury species in water. Chemosphere Global Change Science 2, 1-9.

Bullock R.O., 2000. Current methods and research strategies for modeling atmospheric mercury. Fuel Processing Technology 65-66, 459-471.

Bullock R.O., Brehme K.A., 2002. Atmospheric mercury simulation using the CMAQ model: formulation description and analysis of wet deposition results. Atmospheric Environment 36, 2135-2146.

Caldwell C.A., Swartzendruber P., Prestbo E., 2006. Concentration and dry deposition of mercury species in arid south central New Mexico (2001-2002). Environmental Science and Technology 40, 7535-7540.

Calvert J.G., Lindberg S.E., 2005. Mechanisms of mercury removal by O_3 and OH in the atmosphere. Atmospheric Environment 39, 3355-3367.

Carpi A., 1997. Mercury from combustion sources: a review of the chemical species emitted and their transport in the atmosphere. Water, Air, and Soil Pollution 98, 1573-2932.

Carpi A., Lindberg S.E., 1998. Application of a Teflon dynamic flux chamber for quantifying soil mercury flux: tests and results over background soil. Atmospheric Environment 32, 873-882.

Chiou C.T., Shoup T.D., 1985. Soil sorption of organic vapors and effects of humidity on sorptive mechanism and capacity. Environmental Science and Technology 19, 1196-1200.

Chow, J.C., Watson, J.G., 2006. Guideline on Speciated Particulate Monitoring, Draft 3. Accessed 12/1/2006 from the Bureau of Air Pollution Control website at hhttp://www.epa.gov/ttn/amtic/files/ambient/pm25/spec/drispec.pdf.

Chu P., Porcella D.B., 1995. Mercury stack emissions from U.S. electric utility power plants. Water, Air, and Soil Pollution 80, 135-144.

Clarkson T.W., Magos L., 2006. The toxicology of mercury and its chemical compounds. Critical Reviews in Toxicology 36, 609-662.

Clesceri L.S., Greenberg A.E., Eaton A.D., Eds., 1998. Standard Methods for the Examination of Water and Wastewater, 20th Edition. United Book Press, Baltimore, Maryland.

Coolbaugh M.F., Gustin M.S., Rytuba J.J., 2002. Annual emissions of mercury to the atmosphere from natural sources in Nevada and California. Environmental Geology 42, 338-349.

Darby L.S., Banta R.M., Brewer W.A., Neff W.D., Marchbanks R.D., McCarty B.J., Senff C.J., White A.B., Angevine W.M., Williams E.J., 2002. Vertical variations in O_3 concentrations before and after a gust front passage. Journal of Geophysical Research 107, D13, doi: 10.1029/2001JD000996.

DCNR, 2006. Nevada Natural Resources Council Report. Accessed 12/6/2006 from the Nevada Department of Conservation and Natural Resources websites at http://dcnr.nv.gov/nrp01/climate.htm.

Drever J.I., 1997. The Geochemistry of Natural Waters: Surface and Groundwater Environments, 3 ed. Prentice-Hall, Upper Saddle River, New Jersey.

Duyzer J.H., Verhagen H.L.M., Weststrate J.H., Bosveld F.C., 1992. Measurement of the Dry Deposition Flux of NH_3 on to Coniferous Forest. Environmental Pollution 75, 3-13.

Ebinghaus R., Jennings S.G., Schroeder W.H., Berg T., Donaghy T., Guentzel J., Kenny C., Kock H.H., Kvietkus K., Landing W., Muhleck T., Munthe J., Prestbo E.M., Scheeberger D., Slemr F., Sommar J., Urba A., Wallschlager D., Xiao Z., 1999. International field intercomparison measurements of atmospheric mercury species at Mace Head, Ireland. Atmospheric Environment 33, 3063-3073.

Ebinghaus R., Kock H., Temme C., Einax J.W., Lowe A.G., Richter A., Burrows J.P., Schroeder W.H., 2002. Antarctic springtime depletion of atmospheric mercury. Environmental Science and Technology 36, 1238-1244.

Edgerton E.S., Hartsell B.E., Jansen J.J., 2006. Mercury speciation in coal-fired power plant plumes observed at three surface sites in the Southeastern U.S. Environmental Science and Technology 40, 4563-4570.

Engle M.A., Gustin M.S., 2002. Scaling of atmospheric mercury emissions from three naturally enriched areas: Flowery Peak, Nevada; Peavine Peak, Nevada; and Long Valley Caldera, California. The Science of the Total Environment 290, 91-104.

Engle M.A., Gustin M.S., Goff F., Counce D.A., Janik C.J., Bergfeld D., Rytuba J.J., 2006. Atmospheric mercury emissions from substrates and fumaroles associated with

three hydrothermal systems in the western United States. Journal of Geophysical Research 111, D17304, doi:10.1029/2005JD006563.

Engle M.A., Gustin M.S., Johnson D.W., Murphy J.F., Miller W.W., Walker R.F., Wright J., Markee M., 2006. Mercury distribution in two Sierran forest and one desert sagebrush steppe ecosystems and the effects of fire. Science of the Total Environment 367, 222-233.

Engle M.A., Gustin M.S., Lindberg S.E., Gertler A.W., Ariya P.A., 2005. The influence of ozone on atmospheric emissions of gaseous elemental mercury and reactive gaseous mercury from substrates. Atmospheric Environment 39, 7506-7517.

Engle M.A., Gustin M.S., Zhang H., 2001. Quantifying natural source mercury emissions from the Ivanhoe Mining District, north-central Nevada, USA. Atmospheric Environment 35, 3987-3997.

Engle M.A., Tate M.T., Krabbenhoft D.P., Kolker A., Olson M.L., Edgerton E.S., DeWild J.F., McPherson A.K., 2008. Characterization and cycling of atmospheric mercury along the central U.S. Gulf Coast. Applied Geochemistry 23, 419-433.

Ericksen J.A., Gustin M.S., Lindberg S.E., Olund S.D., Krabbenhoft D.P., 2005. Assessing the potential for re-emission of mercury deposited in precipitation from arid soils using a stable isotope. Environmental Science and Technology 39, 8001-8007.

Ericksen J.A., Gustin M.S., Schorran D.E., Johnson D.E., Lindberg S.E., Coleman J.S., 2003. Accumulation of atmospheric mercury in forest foliage. Atmospheric Environment 37, 1613-1622.

Ericksen J.A., Gustin M.S., Xin M., Weisberg P.J., Fernandez G.C.J., 2006. Air-soil exchange of mercury from background soils in the United States. Science of the Total Environment 366, 851-863.

Feng X., Lu J.Y., Conrad D., Hao G.Y., Banic C.M., Schroeder W.H., 2004. Analysis of inorganic mercury species associated with airborne particulate matter/aerosols: method development. Analytical and Bioanalytical Chemistry 380, 683-689.

Ferrara R., Maserti B., Petrosino A., Bargagli R., 1986. Mercury levels in rain and air and the subsequent washout mechanism in a central Italian region. Atmospheric Environment 20, 125-128.

Finlayson-Pitts B.J., Pitts J.N., 1999. Chemistry of the Upper and Lower Atmosphere. Academic Press: San Francisco.

Fitzgerald W.F., Engstrom D.R., Mason R.P., Nater E.A., 1998. The case for atmospheric mercury contamination in remote areas. Environmental Science and Technology 32, 1-7.

Fitzgerald W.F., Gill G.A., Kim J.P., 1984. An equatorial Pacific Ocean source of atmospheric mercury. Science 224, 597-599.

Foster J., Barkus E., Yavorsky C., 2006. Understanding and Using Advanced Statistics. SAGE Publications, Thousand Oaks, California.

Frescholtz T.F., Gustin M.S., 2004. Soil and foliar mercury emission as a function of soil concentration. Water, Air, and Soil Pollution 155, 223-237.

Friedli H.R., Radke L.F., Lu J.Y., Banic C.M., Leaitch W.R., MacPherson J.I., 2003. Mercury emissions from burning of biomass from temperate North American forests: laboratory and airborne measurements. Atmospheric Environment 37, 253-267.

Gabriel M.C., Williamson D.G., Brooks S., Lindberg S., 2005. Atmospheric speciation of mercury in two contrasting Southeastern US airsheds. Atmospheric Environment 39, 4947-4958.

Gardfeldt K., Sommar J., Ferrara R., Ceccarini C., Lanzillotta E., Munthe J., Wangberg I., Lindqvist O., Pirrone N., Sprovieri F., Pesenti E., Stromberg D., 2003. Evasion of mercury from coastal and open waters of the Atlantic Ocean and the Mediterranean Sea. Atmospheric Environment 37, 73-84.

Gillis A.A., Miller D.R., 2000. Some local environmental effects on mercury emission and absorption at a soil surface. Science of the Total Environment 260, 191-200.

Gilmour C.C., Henry E.A., Mitchell R., 1992. Sulfate stimulation of mercury methylation in freshwater sediments. Environmental Pollution 26, 2281-2287.

Glass G.E., Sorensen J.A., Schmidt K.W., Rapp G.R., Yap D., Fraser D., 1991. Mercury deposition and sources for the upper Great Lakes region. Water, Air, and Soil pollution 56, 235-249.

Goss K., 1993. Effects of temperature and relative humidity on the sorption of organic vapors on clay minerals. Environmental Science and Technology 27, 2127-2132.

Grigal D.F., 2002. Inputs and outputs of mercury from terrestrial watersheds: a review. Environmental Reviews 10, 1-39.

Gustin M.S., 2003. Are mercury emissions from geologic sources significant? A status report. The Science of the Total Environment 304, 153-167.

Gustin M.S., Coolbaugh M.F., Engle M.A., Fitzgerald B.C., Keislar R.E., Lindberg S.E., Nacht D.M., Quashnick J., Rytuba J.J., Sladek C., Zhang H., Zehner R.E., 2003. Atmospheric mercury emissions from mine wastes and surrounding geologically enriched terrains. Environmental Geology 43, 339-351.

Gustin M.S., Engle M., Ericksen J., Lyman S., Stamenkovic J., Xin M., 2006. Mercury exchange between the atmosphere and low mercury containing substrates. Applied Geochemistry 21, 1913-1923.

Gustin M.S., Lindberg S.E., Weisberg P.J., 2008. An update on the natural sources and sinks of atmospheric mercury. Applied Geochemistry 23, 482-493.

Gustin M., Stamenkovic J., 2005. Effect of watering and soil moisture on mercury emissions from soils. Biogeochemistry 76, 215-232.

Gustin M.S., Taylor G.E., Leonard T.L., 1996. Atmospheric mercury concentrations associated with geologically and anthropogenically enriched sites in central western Nevada. Environmental Science and Technology 30, 2572-2579.

Hall B.D., Olson M.L., Rutter A.P., Frontiera R.R., Krabbenhoft D.P., Gross D.S., Yuen M., Rudolph T.M., Schauer J.J., 2006. Atmospheric mercury speciation in Yellowstone National Park. Science of the Total Environment 367, 354-366.

Harding A., 2009. Jerritt Canyon mill restarting: Yukon-Nevada plans gold pour next week; employment impact unknown. Elko Daily Free Press, 25 March.

Harner T., Farrar N.J., Shoeib M., Jones K.C., Gobas F., 2003. Characterization of polymer-coated glass as a passive air sampler for persistent organic pollutants. Environmental Science and Technology 37, 2486-2493.

Harper M., Purnell C.J., 1987. Diffusive sampling – a review. Journal of the American Industrial Hygiene Association 48, 214-218.

Hedgecock I.M., Pirrone N., 2004. Chasing quicksilver: modeling the atmospheric lifetime of $Hg^0_{(g)}$ in the marine boundary layer at various latitudes. Environmental Science and Technology 38, 69-76.

Hedgecock I.M., Pirrone N., Sprovieri F., Pesenti E., 2003. Reactive gaseous mercury in the marine boundary layer: modeling and experimental evidence of its formation in the Mediterranean region. Atmospheric Environment 37, 41-49.

Hicks B.B., Baldocchi D.D., Meyers T.P., Hosker R.P., Matt D.R., 1987. A preliminary multiple resistance routine for deriving dry deposition velocities from measured quantities. Water, Air, and Soil Pollution 36, 311-330.

Hintelmann H., Harris R., Heyes A., Hurley J.P., Kelly C.A., Krabbenhoft D.P., Lindberg S., Rudd J.W.M., Scott K.J., St. Louis V.L., 2002. Reactivity and mobility of new and old mercury deposition in a boreal forest ecosystem during the first year of the METAALICUS study. Environmental Science and Technology 36, 5034-5040.

Holmes C.D., Jacob D.J., Mason R.P., Jaffe D.A., 2009. Sources and deposition of reactive gaseous mercury in the marine atmosphere. Atmospheric Environment 43, 2278-2285.

Holmes C.D., Jacob D.J., Yang X., 2006. Global lifetime of elemental mercury against oxidation by atomic bromine in the free troposphere. Geophysical Research Letters 33, L20808, doi:10.1029/2006GL027176.

Joensuu O.I., 1971. Fossil Fuels as a source of mercury pollution. Science 172, 1027-1028.

Johnson D.W., Benesch J.A., Gustin M.S., Schorran D.S., Lindberg S.E., Coleman J.S., 2003. Experimental evidence against diffusion control of Hg evasion from soils. Science of the Total Environment 304, 175-184.

Keeler G., Glinsorn G., Pirrone N., 1995. Particulate mercury in the atmosphere: significance, transport, transformation and sources. Water, Air, and Soil Pollution 80, 159-168.

Kim K.H., Kim M.Y., 2001. Some insights into short-term variability of total gaseous mercury in urban air. Atmospheric Environment 35, 49-59.

Kim K.H., Mishra V.K., Hong S., 2006. The rapid and continuous monitoring of gaseous elemental mercury (GEM) behavior in ambient air. Atmospheric Environment 40, 3281-3293.

Kirk J.L., St. Louis V.L., Hintelmann H., Lehnherr I., Else B., Poissant L., 2008. Methylated mercury species in marine waters of the Canadian high and sub Arctic. Environmental Science and Technology 42, 8367-8373.

Kock H.H., Bieber E., Ebinghaus R., Spain T.G., Thees B., 2005. Comparison of long-term trends and seasonal variations of atmospheric mercury concentrations at the two European coastal monitoring stations Mace Head, Ireland, and Zingst, Germany. Atmospheric Environment 39, 7549-7556.

Koutrakis P., Wolfson J.M., Bunyaviroch A., Froehlich S.E., Hirano K., Mulik J.D., 1993. Measurement of ambient ozone using a nitrite-coated filter. Analytical Chemistry 65, 209-214.

Krupa S.V., Legge A.H., 2000. Passive sampling of ambient, gaseous air pollutants: an assessment from an ecological perspective. Environmental Pollution 107, 31-45.

Kutner M.H., Nachtsheim C.J., Neter J., 2004. Applied Linear Regression Models, 4th ed. McGraw-Hill, Boston.

Kvletkus K., Sakalys J., 1994. A passive sampler for the monitoring of gaseous mercury amounts in the atmosphere. In Watras, C. J and Huckabee, J. W. (Eds.), Mercury Pollution: Integration and Synthesis; CRC Press: Boca Raton, FL, pp 553-556.

Lamborg C.H., Fitzgerald W.F., Vandal G.M., Rolfhus K.R., 1995. Atmospheric mercury in northern Wisconsin: sources and species. Water, Air, and Soil Pollution 80, 189-198.

Landis M.S., Stevens R.K., Schaedlich F., Prestbo E.M., 2002. Development and characterization of annular denuder methodology for the measurement of divalent inorganic reactive gaseous mercury in ambient air. Environmental Science and Technology 36, 3000-3009.

Lin C., Pehkonen S.O., 1999. The chemistry of atmospheric mercury: a review. Atmospheric Environment 33, 2067-2079.

Lin C.J., Pongprueksa P., Lindberg S.E., Pehkonen S.O., Byun D., Jang C., 2006. Scientific uncertainties in atmospheric mercury models I: model science evaluation. Atmospheric Environment 40, 2911-2928.

Lindberg S.E., Brooks S., Lin C.J., Scott K.J., Landis M.S., Stevens R.K, Goodsite M., Richter A., 2002. Dynamic oxidation of gaseous mercury in the Arctic troposphere at polar sunrise. Environmental Science and Technology 36, 1245-1256.

Lindberg S., Bullock R., Ebinghaus R., Engstrom D., Feng X., Fitzgerald W., Pirrone N., Prestbo E., Seigneur C., 2007. A synthesis of progress and uncertainties in attributing the sources of mercury in deposition. Ambio 36, 19-32.

Lindberg S.E., Hanson P.J., Meyers T.P., Kim K.H., 1998. Air/surface exchange of mercury vapor over forests – the need for a reassessment of continental biogenic emissions. Atmospheric Environment 32, 895-908.

Lindberg S.E., Kim K., Meyers T.P., Owens J.G., 1995. Micrometeorological gradient approach for quantifying air/surface exchange of mercury vapor: tests over contaminated soils. Environmental Science and Technology 29, 126-135.

Lindberg S.E., Meyers T.P., 2001. Development of an automated micrometeorological method for measuring the emission of mercury vapor from wetland vegetation. Wetlands Ecology and Management 9, 333-347.

Lindberg S.E., Meyers T.P., Taylor G.E., Turner R.R., Schroeder W.H., 1992. Atmosphere-surface exchange of mercury in a forest: results of modeling and gradient approaches. Journal of Geophysical Research 97(D2), 2519-2528.

Lindberg S.E., Stratton W.J., 1998. Atmospheric mercury speciation: concentrations and behavior of reactive gaseous mercury in ambient air. Environmental Science and Technology 32, 49-57.

Lindberg S.E., Zhang H., Gustin M., Vette A., Marsik F., Owens J., Casimir A., Ebinghaus R., Edwards G., Fitzgerald C., Kemp J., Kock H.H., London J., Majewski M., Poissant L., Pilote M., Rasmussen P., Schaedlich F., Schneeberger D., Sommar J., Turner R., Wallschlaeger D., Xiao Z., 1999. Increases in mercury emissions from desert soils in response to rainfall and irrigation. Journal of Geophysical Research 104, 21879-21888.

Liu B., Keeler G.J., Dvonch J.T., Barres J.A., Lynam M.M., Marsik F.J., Morgan J.T., 2007. Temporal variability of mercury speciation in urban air. Atmospheric Environment 41, 1911-1923.

Lohman, K., Seigneur, C., Edgerton, E., Jansen, J., 2006. Modeling mercury in power plant plumes. Environmental Science and Technology 40, 3848-3854.

Lyman S.N., Gustin M.S., 2008. Speciation of atmospheric mercury at two sites in northern Nevada, USA. Atmospheric Environment 42, 927-939.

Lyman S.N., Gustin M.S., Prestbo E.M., Kilner P.I., Edgerton E., Hartsell, B., 2009. Cation-exchange membranes as surrogate surfaces for gaseous oxidized mercury dry deposition. Environmental Science and Technology, *submitted*.

Lyman S.N., Gustin M.S., Prestbo E.M., Marsik F.J., 2007. Estimation of dry deposition of mercury in Nevada by direct and indirect methods. Environmental Science and Technology 41, 1970-1976.

Lynam M.M., Keeler G.J., 2005. Automated speciated mercury measurements in Michigan. Environmental Science and Technology 39, 9253-9262.

Manolopoulos H., Schauer J.J., Purcell M.D., Rudolph T.M., Olson M.L., Rodger B., Krabbenhoft D.P., 2007. Local and regional factors affecting atmospheric mercury speciation at a remote location. Journal of Environmental Engineering and Science 6, 491-501.

Marsik F.J., Keeler G.J., Landis M.S., 2007. The dry-deposition of speciated mercury to the Florida Everglades: measurements and modeling. Atmospheric Environment 41, 136-149.

Masataka N., Hiroaki S., Ryuji Y., Koji T., 1999. Examination of an improved passive sampler for gaseous mercury on the landfill site. Journal of Environmental Chemistry 9, 681-684.

Mason R.P., Lawson N.M., Sullivan K.A., 1997. The concentration, speciation and sources of mercury in Chesapeake Bay precipitation. Atmospheric Environment 31, 3541-3550.

Mason R.P., Sheu G.R., 2002. Role of the ocean in the global mercury cycle. Global Biogeochemical Cycles 16, 40-41.

McMurdo D.A., 2008. Mine shuts down – Jerritt Canyon deserted after layoffs: state, local officials surprised. Elko Daily Free Press, 15 August.

Mergler D., Anderson H.A., Chan L.H.M., Mahaffey K.R., Murray M., Sakamoto M., Stern A.H., 2007. Methylmercury exposure and health effects in humans: worldwide concern. Ambio 36, 3-11.

Meyers T.P., Finkelstein P., Clarke J., Ellestad T.G., Sims P.F., 1998. A multilayer model for inferring dry deposition using standard meteorological measurements. Journal of Geophysical Research 103(D17), 22645-22661.

Monks PS. Gas-phase radical chemistry in the troposphere. Chem Soc Rev 2005; 34: 376-395.

Morel F.M.M., Kraepiel A.M.L., Amyot M., 1998. The chemical cycle and bioaccumulation of mercury. Annual Review of Ecology and Systematics 29, 543-566.

Munthe J., Wangberg I., Pirrone N., Iverfeldt A., Ferrara R., Ebinghaus R., Feng X., Gardfeldt K., Keeler G., Lanzillotta E., Lindberg S.E., Lu J., Mamane Y., Prestbo E., Schmolke S., Schroeder W.H., Sommar J., Sprovieri F., Stevens R.K., Stratton W., Tuncel G., Urba A., 2001. Intercomparison of methods for sampling and analysis of atmospheric mercury species. Atmospheric Environment 35, 3007-3017.

Myers G.J., Davidson P.W., Cox C., Shamlaye C., Cernichiari E., Clarkson T.W., 2000. Twenty-seven years studying the human neurotoxicity of methylmercury exposure. Environmental Research 83, 275-285.

Myers G.J., Davidson P.W., Cox C., Shamlaye C.F., Palumbo D., Cernichiari E., Sloane-Reeves J., Wilding G.E., Kost J., Huang L., Clarkson T.W., 2003. Prenatal methylmercury exposure from ocean fish consumption in the Seychelles child development study. Lancet 361, 1686-1692.

Nacht D.M., Gustin M.S., 2004. Mercury emissions from background and altered geologic units throughout Nevada. Water, Air, & Soil Pollution 151, 179-193.

Namiesnik J., Zabiegala B., Kot-Wasik A., Partyka M., Wasik A., 2005. Passive sampling and/or extraction techniques in environmental analysis: a review. Analytical and Bioanalytical Chemistry 381, 279-301.

NASA, 2006. NASA Earth Observatory, Leaf Area Index January 2004. Accessed 4/15/2006 from the NASA Earth Observatory website at http://earthobservatory.nasa.gov/Observatory/Datasets/lai.modis.html.

Nevada, 2007. Nevada Division of Environmental Protection Bureau of Air Pollution Control. 2006 OHM Test Data for Tier-1 Units. Accessed 7/2/2007 from the Bureau of Air Pollution Control website at http://ndep.nv.gov/bapc/mercury/.

Nriagu J., Becker C., 2003. Volcanic emissions of mercury to the atmosphere: global and regional inventories. The Science of the Total Environment 304, 3-12.

Pacyna E.G., Pacyna J.M., 2002. Global emission of mercury from anthropogenic sources in 1995. Water, Air, and Soil Pollution 137, 149-165.

Pacyna E.G., Pacyna J.M., Pirrone N., 2001. European emissions of atmospheric mercury from anthropogenic sources in 1995. Atmospheric Environment 35, 2987-2996.

Pacyna E.G., Pacyna J.M., Steenhuisen F., Wilson S., 2006. Global anthropogenic mercury emission inventory for 2000. Atmospheric Environment 40, 4048-4063.

Pal B., Ariya P.A., 2004a. Studies of ozone initiated reactions of gaseous mercury: kinetics, product studies, and atmospheric implications. Physical Chemistry Chemical Physics 6, 572-579.

Pal B., Ariya P.A., 2004b. Gas-phase HO-initiated reactions of elemental mercury: kinetics, product studies, and atmospheric implications. Environmental Science and Technology 38, 5555-5566.

Palmes E.D., Gunnison A.F., DiMattio J., Tomczyk C., 1976. Personal sampler for nitrogen dioxide. Journal of the American Industrial Hygiene Association 37, 570-577.

Partyka M., Zabiegala B., Namiesnik J., Przyjazny A., 2007. Application of passive samplers in monitoring of organic constituents in air. Critical Reviews in Analytical Chemistry 37, 51-78.

Peterson C., Gustin M., Lyman S., 2009. Atmospheric mercury concentrations and speciation measured from 2004 to 2007 in Reno, Nevada, USA, Atmospheric Environment, doi:10.1016/j.atmosenv.2009.04.053.

Plaisance H., Piechocki-Minguy A., Garcia-Fouque S., Galloo J. C., 2004. Influence of meteorological factors on the NO_2 measurements by passive diffusion tube. Atmospheric Environment 38, 573-580.

Poissant L., Pilote M., 1998. Mercury concentrations in single event precipitation in southern Quebec. Science of the Total Environment 213, 65-72.

Poissant L., Pilote M., Beauvais C., Constant P., Zhang H., 2005. A year of continuous measurements of three atmospheric mercury species (GEM, RGM, and Hg_p) in southern Quebec, Canada. Atmospheric Environment 39, 1275-1287.

Poissant L., Pilote M., Xu X., Zhang H., Beauvais C., 2004. Atmospheric mercury speciation and deposition in the Bay St. Francois wetlands. Journal of Geophysical Research 109, D11301, doi:10.1029/2003JD004364.

Pozo K., Harner T., Lee S.C., Wania F., Muir D.C.G., Jones K.C., 2009. Seasonally resolved concentrations of persistent organic pollutants in the global atmosphere from the first year of the GAPS study. Environmental Science and Technology 43, 796-803.

Pozo K., Harner T., Shoeib M., Urrutia R., Barra R., Parra O., Focardi S., 2004. Passive-sampler derived air concentrations of persistent organic pollutants on a north-south transect in Chile. Environmental Science and Technology 38, 6529-6537.

Prestbo E., Calhoun J., Mason R., Baines A., 2005. Mercury in power plant and municipal waste combustion plumes: phase II – ambient mercury sampling, document number DNR 12-10212005-71, Maryland Department of Natural Resources, Annapolis, Maryland.

Rabaud N.E., James T.A., Ashbaugh L.L., Flocchini R.G., 2001. A passive sampler for the determination of airborne ammonia concentrations near large-scale animal facilities. Environmental Science and Technology 35, 1190-1196.

Rea A.W., Lindberg S.E., Keeler G.J., 2000. Assessment of dry deposition and foliar leaching of mercury and selected trace elements based on washed foliar and surrogate surfaces. Environmental Science and Technology 34, 2418-2425.

Rutter A.P., Hanford K.L., Zwers J.T., Perillo-Nicholas A.L., Schauer J.J., 2008. Evaluation of an offline method for the analysis of atmospheric reactive gaseous mercury and particulate mercury. Journal of the Air and Waste Management Association 58, 377-383.

Rutter A.P., Schauer J.J., 2007. The effect of temperature on the gas-particle partitioning of reactive mercury on atmospheric aerosols. Atmospheric Environment 41, 8647-8657.

Rytuba J.J., 2003. Mercury from mineral deposits and potential environmental impact. Environmental Geology 43, 326-338.

Sakata M., Marumoto K., 2005 Wet and dry deposition fluxes of mercury in Japan. Atmospheric Environment 39, 3139-3146.

Santiago E.C., Cayetano M.G., 2007. Polycyclic aromatic hydrocarbons in ambient air in the Philippines derived from passive sampler with polyurethane foam disk. Atmospheric Environment 41, 4138-4147.

Schroeder W., Lindqvist O., Munthe J., Xiao Z., 1992. Volatilization of mercury from lake surfaces. Science of the Total Environment 125, 47-66.

Schroeder W.H., Munthe J., 1998. Atmospheric mercury – an overview. Atmospheric Environment 32, 809-822.

Sderstrm H.S., Bergqvist P.A., 2004. Passive air sampling using semipermeable membrane devices at different wind-speeds in situ calibrated by performance reference compounds. Environmental Science and Technology 38, 4828-4834.

Seigneur C., Vijayaraghavan K., Lohman K., Karamchandani P., Scott C., 2004. Global source attribution for mercury deposition in the United States. Environmental Science and Technology 38, 555-569.

Seigneur C., Wrobel J., Constantinou E., 1994. A chemical kinetic mechanism for atmospheric inorganic mercury. Environmental Science and Technology 28, 1589-1597.

Seinfeld J.H., Pandis S.N., 1998. Atmosphepheric Chemistry and Physics. Wiley and Sons: New York, New York.

Selin N.E., Jacob D.J., 2008. Seasonal and spatial patterns of mercury wet deposition in the United States: constraints on the contribution from North American anthropogenic sources. Atmospheric Environment 42, 5193-5204.

Selin N.E., Jacob D.J., Park R.J., Yantosca R.M., Strode S., Jaegle L., Jaffe D., 2007. Chemical cycling and deposition of atmospheric mercury: global constraints from observations. Journal of Geophysical Research 112, D02308, doi: 10.1029/2006JD007450.

Senior C.L., Sarofim A.F., Zeng T., Helble J.J., Mamani-Paco R., 2000. Gas-phase transformations of mercury in coal-fired power plants. Fuel Processing Technology 63, 197-213.

Shen L., Wania F., Lei Y.D., Teixeira C., Muir D.C.G., Bidleman T.F., 2005. Atmospheric distribution and long-range transport behavior of organochlorine pesticides in North America. Environmental Science and Technology 39, 409-419.

Sillman S., Marsik F.J., Al-Wali K.I., Keeler G.J., Landis M.S., 2007. Reactive mercury in the troposphere: Model formation and results for Florida, the northeastern United States, and the Atlantic Ocean. Journal of Geophysical Research 112, D23305, doi: 10.1029/2006JD008227.

Skov H., Brooks S.B., Goodsite M.E., Lindberg S.E., Meyers T.P., Landis M.S., Larsen, M.R.B., Jensen B., McConville G., Christensen J., 2006. Fluxes of reactive gaseous mercury measured with a newly developed method using relaxed eddy accumulation. Atmospheric Environment 40, 5452-5463.

Skov H., Sorensen B.T., Landis M.S., Johnson M.S., Sacco P., Goodsite M.E., Lohse C., Christiansen K.S., 2007. Performance of a new diffusive sampler for Hg^0 determination in the troposphere. Environmental Chemistry 4, 75-80.

Sommar J., Gardfeldt K., Stromberg D., Feng X., 2001. A kinetic study of the gas-phase reaction between the hydroxyl radical and atomic mercury. Atmospheric Environment 35, 3049-3054.

Stamenkovic J., Gustin M.S., 2009. Nonstomatal versus stomatal uptake of atmospheric mercury. Environmental Science and Technology 43, 1367-1372.

Stamenkovic J., Lyman S., Gustin M.S., 2007. Seasonal and diel variation of atmospheric mercury concentrations in the Reno (Nevada, USA) airshed. Atmospheric Environment, 41, 6662-6672.

Stevens E.R., 1978. Nonanthropogenic ozone in California urban areas. In Air Quality Meteorology and Atmospheric Ozone, ASTM STP 653, Morris, A. L. and Barras, R. C., Eds. American Society for Testing and Materials, West Conshohocken, Pennsylvania.

Stull R.B., 1988. An Introduction to Boundary Layer Meteorology. Kluwer Academic Publishers, Boston, Massachusetts.

Stumm W., Morgan J.J., 1996. Aquatic Chemistry: Chemical Equilibria and Rates in Natural Waters, 3 ed. Wiley and Sons, New York.

Swartzendruber P.C., Jaffe D.A., Prestbo E.M., Weiss-Penzias P., Selin N.E., Park R., Jacob D.J., Strode S., Jaegle L., 2006. Observations of reactive gaseous mercury in the free troposphere at the mount bachelor observatory. Journal of Geophysical Research 111, D24301, doi:10.1029/2006JD007415.

Tang H., Brassard B., Brassard R., Peake E., 1997. A new passive sampling system for monitoring SO_2 in the atmosphere. Field Analytical Chemistry and Technology 1, 307-314.

Tekran Model 2537A Mercury Vapour Analyzer User Manual. 2002. Tekran, Inc: Toronto, Canada.

Temme C., Blanchard P., Steffen A., Banic C., Beauchamp S., Poissant L., Tordon R., Wiens B., 2007. Trend, seasonal and multivariate analysis study of total gaseous mercury data from the Canadian atmospheric mercury measurement network (CAMNet). Atmospheric Environment 41, 5423-5441.

Temme C., Einax J.W., Ebinghaus R., Schroeder W.H., 2003. Measurements of atmospheric mercury species at a coastal site in the Antarctic and over the south Atlantic Ocean during polar summer. Environmental Science and Technology 37, 22-31.

Tuduri L., Harner T., Hung H., 2006. Polyurethane foam (PUF) disks passive air samplers: wind effect on sampling rates. Environmental Pollution 144, 377-383.

Turetsky M.R., Harden J.W., Friedli H.R., Flannigan M., Payne N., Crock J., Radke L., 2006. Wildfires threaten mercury stocks in northern soils. Geophysical Research Letters 3, L16403, doi:10.1029/2005GL025595.

Ullrich S.M., Tanton T.W., Abdrashitova S.A., 2001. Mercury in the aquatic environment: a review of factors affecting methylation. Critical Reviews in Environmental Science ant Technology 31, 241-293.

USEPA Method 1631, Revision E., 2002. Mercury in water by oxidation, purge and trap, and cold vapor atomic fluorescence spectrometry. U. S. Environmental Protection Agency, Office of Water (4303), Washington, D. C.

Valente R.J., Shea C., Humes K.L., Tanner R.L., 2007. Atmospheric mercury in the Great Smoky Mountains compared to regional and global levels. Atmospheric Environment 41, 1861-1873.

Varekamp J.C., Buseck P.R., 1986. Global mercury flux from volcanic and geothermal sources. Applied Geochemistry 1, 65-73.

Venkatram, A., Pleim, J., 1999. The electrical analogy does not apply to modeling dry deposition of particles. Atmospheric Environment 33, 3075-3076.

Vermette S., Lindberg S., Bloom N., 1995. Field tests for a regional mercury deposition network-sampling design and preliminary test results. Atmospheric Environment 29, 1247-1251.

Vette A.F., Landis M.S., Keeler G.J., 2002. Deposition and emission of gaseous mercury to and from Lake Michigan during the Lake Michigan Mass Balance Study (July, 1994-October, 1995). Environmental Science and Technology 36, 4525-4532.

Wania F., Shen L., Lei Y.D., Teixeira C., Muir D.C.G., 2003. Development and calibration of a resin-based passive sampling system for monitoring persistent organic pollutants in the atmosphere. Environmental Science and Technology 37, 1352-1359.

Watras C.J., Huckabee J.W., Eds., 1994. Mercury Pollution: Integration and Synthesis. CRC Press: Boca Raton, Florida.

Weiss-Penzias S., Gustin M.S., Lyman S.N., 2009. Observations of speciated atmospheric mercury at three sites in Nevada, USA: evidence for a free tropospheric source of reactive gaseous mercury. Journal of Geophysical Research, *in press*.

Weiss-Penzias P., Jaffe D.A., McClintick A., Prestbo E.M., Landis M.S., 2003. Gaseous elemental mercury in the marine boundary layer: evidence for rapid removal in anthropogenic pollution. Environmental Science and Technology 37, 3755-3763.

Wesely M.L., 1989. Parameterization of surface resistances to gaseous dry deposition in regional-scale numerical models. Atmospheric Environment 23, 1293-1304.

Wesely M.L., Hicks B.B., 2000. A review of the current status of knowledge on dry deposition. Atmospheric Environment 34, 2261-2282.

Western, 2007. Western Great Basin Incident Activity Report: 2005. Accessed 7/2/2007 from the Western Great Basin Coordination Center website at http://gacc.nifc.gov/wgbc/predictive/intelligence/paststatistics/EOY05.pdf.

WHO, 2005. Mercury in Drinking Water. WHO/SDE/WSH/05.08/10. World Health Organization.

Yamartino R.J., 1984. A comparison of several “single-pass” estimators of the standard deviation of wind direction. Journal of Climate and Applied Meteorology 23, 1362-1366.

Zehner R.E., Gustin M.S., 2002. Estimation of mercury vapor flux from natural substrate in Nevada. Environmental Science and Technology 36, 4039-4045.

Zhang L., Brook J.R., Vet R., 2003. A revised parameterization for gaseous dry deposition in air-quality models. Atmospheric Chemistry and Physics 3, 1777-1804.

Zhang L., Gong S., Padro J., Barrie L., 2001. A size-segregated particle dry deposition scheme for an atmospheric aerosol module. Atmospheric Environment 35, 549-560.

Zhang L., Moran M.D., Makar P.A., Brook J.R., Gong S., 2002. Modeling gaseous dry deposition in AURAMS: a unified regional air-quality modeling system. Atmospheric Environment 36, 537-560.